Simultaneous Correlative Light and Electron Microscopy of Samples in Liquid

Nalan LIV

The work presented in this thesis was performed at the Charged Particle Optics group (Department of Imaging Physics), Faculty of Applied Sciences, Delft University of Technology.

Financial support for the printing of this thesis was kindly provided by
Stichting tot Bevordering van de Elektronenmicroscopie in Nederland (SEN)

ISBN: 978-94-6186-362-1

Cover Design: Nalan Liv
Printed by: Ridderprint BV

An electronic version of this dissertation is available at
http://repository.tudelft.nl/

Simultaneous Correlative Light and Electron Microscopy of Samples in Liquid

Proefschrift

ter verkrijging van de graad van doctor
aan de Technische Universiteit Delft,
op gezag van de Rector Magnificus prof. ir. K. Ch. A. M. Luyben,
voorzitter van het College voor Promoties,
in het openbaar te verdedigen op
vrijdag, 03 oktober 2014 om 12:30 uur

door

Nalan LIV
Master of Science
geboren te Uzunköprü, Turkije.

Dit proefschrift is goedgekeurd door:

Promotor: Prof.dr.ir. P. Kruit

Copromotor: Dr.ir. J.P. Hoogenboom

Samenstelling promotiecommissie:

Rector Magnificus, voorzitter

Prof.dr.ir. P. Kruit, Technische Universiteit Delft, promotor

Dr.ir. J.P. Hoogenboom, Technische Universiteit Delft, copromotor

Prof. A.J. Koster, Leids Universitair Medisch Centrum

Prof. A.B. Houtsmuller, Erasmus Medisch Centrum

Prof. P.J. Peters, Technische Universiteit Delft en Universiteit Maastricht

Dr. B.N.G. Giepmans, Universitair Medisch Centrum Groningen

Dr. P. O'Toole, University of York

Prof. Dr. H.W. Zandbergen, Technische Universiteit Delft, reservelid

"Out beyond the ideas of wrongdoing and rightdoing,
there is a field. I'll meet you there."
– Rumi

Table of Contents

Chapter I

Introduction

"New directions in science are launched by new tools much more often than by new concepts. The effect of a concept-driven revolution is to explain old things in new ways. The effect of a tool-driven revolution is to discover new things that have to be explained."

– Imagined Worlds, Freeman Dyson

The challenges in bio-imaging

Just as the microchip fabrication and information technologies have shaped the last quarter of the 20th century, acquisition and analysis of biomedical information is projected to have a big impact on the 21st century. When the microscope was first invented in the 17th century, it initiated the accelerated knowledge accumulation in biological sciences and stimulated novel discoveries on structural biology. The invention of the microscope effectively contributed in the diagnosis of diseases and disease causing microorganisms like in the early cases of malaria and tuberculosis. Currently, bio-imaging is probably having its second spark in revolutionizing science, providing means for direct visualization of intra-cellular events and probing structure and function of bio-molecules. With the lately announced "big science" projects, like mapping the human brain during health and disorder, the current challenges and impact of bio-imaging are highlighted.

Instruments and protocols for microscopy are continuously progressing to provide further information, like improved resolution, 3-D imaging capabilities or temporal resolution with live-cell imaging. Cellular structures are complicated, complex and consists of many structural variations on a small scale. Many biomolecules, like nucleic acids, lipids and proteins, are involved all at the same time in many cellular processes. Whether or not a cellular function is performed correctly depends on which bio-molecules are present at a specific time, at a specific structural feature. Therefore, to get a comprehensive understanding of cellular processes many biomolecules need to be imaged at the same time, at a resolution comparable to their size, in reference to the detailed cellular ultrastructure, and all that with temporal resolution (dynamics). Unfortunately, current imaging techniques lack the capability to visualize all these required aspects simultaneously, and there is a growing desire for imaging methodologies that can bridge biomolecular imaging and/or dynamic live cell imaging with structural imaging techniques. A first approach in this direction is the correlation of data obtained with different microscopy techniques that each target a different aspect. Significantly interest in Correlated Light and Electron Microscopy (CLEM) has increased in the past few years: the Light Microscope (LM) can visualize biomolecules through the use of fluorescent labels and it can monitor live cell dynamics, the Electron Microscope (EM) can image the cellular ultrastructure at sub-nanometer resolution.

Fluorescence Microscopy

Fluorescence Microscopy (FM) is a widespread LM technique, especially in the biological and biomedical sciences, in which fluorescence emission from a specimen is viewed. In fluorescence, the sample absorbs incident photons and emits light (the fluorescence signal) at a distinct, wavelength longer than that of the incident photons. Thus it is particularly powerful because of its high specify and ability to contrast different parts of labelled samples. In particular, the development of genetically expressed fluorescent labels, such as green fluorescent protein (GFP) and its various variants has produced a step change for biomedical imaging [1,2]. This is being applied to label specific genes, molecular complexes, and proteins in order to study their localizations and interactions within live and fixed cells. Immuno-fluorescent labelling approaches, in which the specificity of antibodies to their antigen is employed, also had a profound effect on our

understanding the cellular structure and function. Additionally, other small molecule fluorescent probes have been engineered to provide information about the local environment of the fluorescent molecules, e.g. like in Ca^{+2} imaging [3].

Depth resolved 3-D fluorescence imaging of biological samples can be achieved with confocal FM, in which a point source of light is used for excitation and a confocal pinhole is used to reject out-of-focus light to realize optical sectioning [4]. Confocal FM has become the standard biomedical research tool, being routinely used to acquire 3-D fluorescent images of biological samples. Likewise, there are many other important advances in LM, like wide-field microscopes providing sectioning capability [5,6], multi-photon microscopy [7–9], and other nonlinear microscopy techniques exploiting second or third harmonic generations [10–12]. The ability to visualize molecular biology with accessible contrast in non-invasive FM has been driving the microscopy community to also develop techniques for improved spatial resolution. The resolving power of conventional LM is limited by diffraction, as reported by Abbe in 1873, to >0,5λ/NA, approximately to 212 nm at 488 nm wavelength which is the primary laser source on most confocal microscopes [13]. In the past decade, optical super-resolution techniques have been developed to achieve higher resolution than this diffraction limit, using deterministic and/or stochastic single-molecule strategies, such as STED, STORM, and PALM [14–16]. It should be noted that the optimal performance of super-resolution approaches depends on lengthy imaging procedures, and/or significant post data processing. To date, a spatial resolution of ~20 nm in the lateral dimensions and ~50 nm in the axial dimension have been achieved with super-resolution techniques [17].

However, for all fluorescence measurements it is only the labeled elements that can be visualized while the underlying cellular ultrastructure remains invisible. Only the labelled molecules of interest can be detected and visualized with FM, while the information on their size, shape and structural organization with respect to the rest of cellular architecture is missing. The possibility of imaging single fluorescent proteins in live cells with a resolution below 50 nm using super-resolution techniques even further necessitates mapping these localizations onto the ultra-structural information of the cells.

Electron Microscopy

Contrary to diffraction limited LM, electron microscopy (EM) has the highest resolution among the spectrum of imaging techniques. Since its first implementation by Ruska and Knoll in 1932 [18], it has served as the main tool for ultra-structural high resolution imaging in biological sciences as well as in physical sciences. Also differing from FM, EM provides a whole ultra-structural map of the sample, delivering comprehensive information on the sub-structure of intracellular compartments, but often with no protein specificity.

Transmission EM (TEM), in which a coherent electron beam is focused on the sample and the transmitted electrons through the sample are focused into a magnified image, has the highest resolution, in sub-nanometer scale. TEM imaging is done with fixed, embedded and ultrathin sectioned samples, as the final image formation is achieved by collecting the transmitted

electrons [19]. Also in scanning TEM (STEM), transmitted electrons are collected beneath the sample but after the sample is scanned by a narrow spot focused electron beam in a raster. On the other hand, in scanning EM (SEM), a focused electron beam is raster scanned over the sample and the generated electrons are collected with electron detectors located above the sample. The imaging in SEM is mostly done either by inelastically scattered secondary electrons or by elastically scattered back-scattered electrons, which would yield information on sample topography and Z-contrast of the sample, respectively [20]. Collection of different electron types with different detectors provides diverse kinds of information from the sample, and therefore the choice of EM technique to be used should be defined according to the sample and research question.

Although EM is a well-established methodology, new sample preparation procedures to provide best ultra-structural preservation and better staining of biological samples are progressively developed and reported [21–24]. Conventional staining in EM is mostly achieved with osmium tetroxide, uranyl acetate and lead citrate staining, which stain unsaturated lipid structures (e.g. membranes), phosphate and amino groups (e.g. DNA, RNA and some proteins) and negative ions, respectively. EM is exploited fully when its capability to visualize whole cellular architecture is complimented with molecular information, by labelling specific proteins. Immuno-EM labelling, in which traditionally antibodies are bound to colloidal 1 to 20 nm gold particles, is the most widely used technique to label specific proteins. Cryo-electron microscopy (CryoEM), in which frozen cells are directly imaged in EM, carries the intriguing promise to be the method of viewing cells in probably their most natural states [25]. Though, the benefit of preservation is unfortunately achieved at the expense of staining in cryo-specimens [26].

Electron tomography can be used to generate 3-D images of sub-cellular macro-molecular structures by imaging the sample at incremental degrees of rotation around its center in a TEM [27,28]. 3-D imaging can also be achieved in principle, by collecting serial ultrathin sections, imaging, and aligning the resulting micrographs to a 3D stack in any EM technique [29,30]. However, this procedure can be very cumbersome, time consuming and prone to errors with respect to sectioning and aligning steps. There are recent approaches for 3D EM, which utilize the combination SEM with focused ion beam (FIB) milling [31] or ultramicrotomy [32,33]. In these techniques, ultrathin slices, with a thickness of about 50 nm in ultramicrotomy and down to 1-2 nm in case of FIB, of the specimen are sequentially removed and images are recorded after each removal.

Additionally, since the initial development of electron optical imaging techniques, liquid-EM imaging has been one of the main objectives in this field. Several strategies of differential pumping approaches and enclosed cells have been utilized to adapt electron microscopy for observation of liquid samples. Environmental SEM (ESEM) was shown to be capable of imaging surfaces of uncoated, "wet" cells by introducing a gaseous environment (water vapor) in the specimen chamber [34–36]. However, ESEM imaging of biological specimen is quite limited, as most of the cells, especially eukaryotic cells, cannot withstand the osmotic pressure differences. On the other hand, the recent developments in production of thin membranes enabled the development of liquid enclosures not only for TEM and STEM [37–39] but also for SEM [40–42]. These membranes make it

possible to encapsulate cells fully hydrated environments and use the EM to investigate these fixed cells in near-native environments.

Despite the ultrastructural information and incomparable resolution that it provides in near-native state, EM procedures can only be applied to fixed biological specimen, unlike in non-invasive FM. Also, staining and labelling opportunities for simultaneous visualization of several different proteins are much narrower compared to labelling possibilities in FM. These facts represent EM and FM not as substitutive, but rather complimentary methods for bio-medical imaging studies.

Correlative Light and Electron Microscopy

Bridging strengths of both microscopy techniques, interest in CLEM, is increasing rapidly in recent years. This is reflected not only in an increasing number of scientific publications, but also in novel commercial products dedicated to CLEM investigation. In CLEM a specimen, preferably the same region, is first visualized by LM and next by EM. Typically FM is favored among other LM methods in CLEM studies as it can provide information about the localization of several proteins and cellular structures exploiting the widely available specific fluorescent labels and stains. Usually, FM inspection of the sample is done first, and then the sample is transferred to the electron microscope.

Correlative light electron microscopy workflow is presented in Figure 1, where Langerhans islets are visualized with correlative FM and SEM imaging. The fluorescence microscope (FM) can be employed to screen the sample for localization of a region of interest (ROI) or a rare occurrence in large and complex samples, based on the positions where particular fluorescently labeled proteins and/or structures are present. For instance, FM images in Figure 1.a and b are used to locate insulin positive Langerhans islets which will be imaged with high resolution in EM. These selected ROIs are then scanned in SEM with high resolution and ultra-structural information (Figure 1.c, d, and e.). Increasingly, CLEM can be also used to link live cell imaging with FM with the information on the underlying cellular environment [43–45]. The dynamic imaging of samples provides the crucial information to understand complex cellular events in all its dimensions, including the temporal information. Then the sample is fixed at a selected time point to comprehend these dynamic FM observations with the underlying cellular architectural information from EM imaging.

Despite its usefulness in targeting biologically relevant questions, wide- spread use of CLEM is hampered by the absence of optimized specimen preparation protocols, CLEM compatible labels, slow speed of data acquisition, the lack of FM-EM correlation accuracy, and the complexity of the experimental routines. There is a growing number of studies aimed at developing optimized protocols [46–52], better labels [53–58], and improved technologies [59,60] to facilitate extensive CLEM studies.

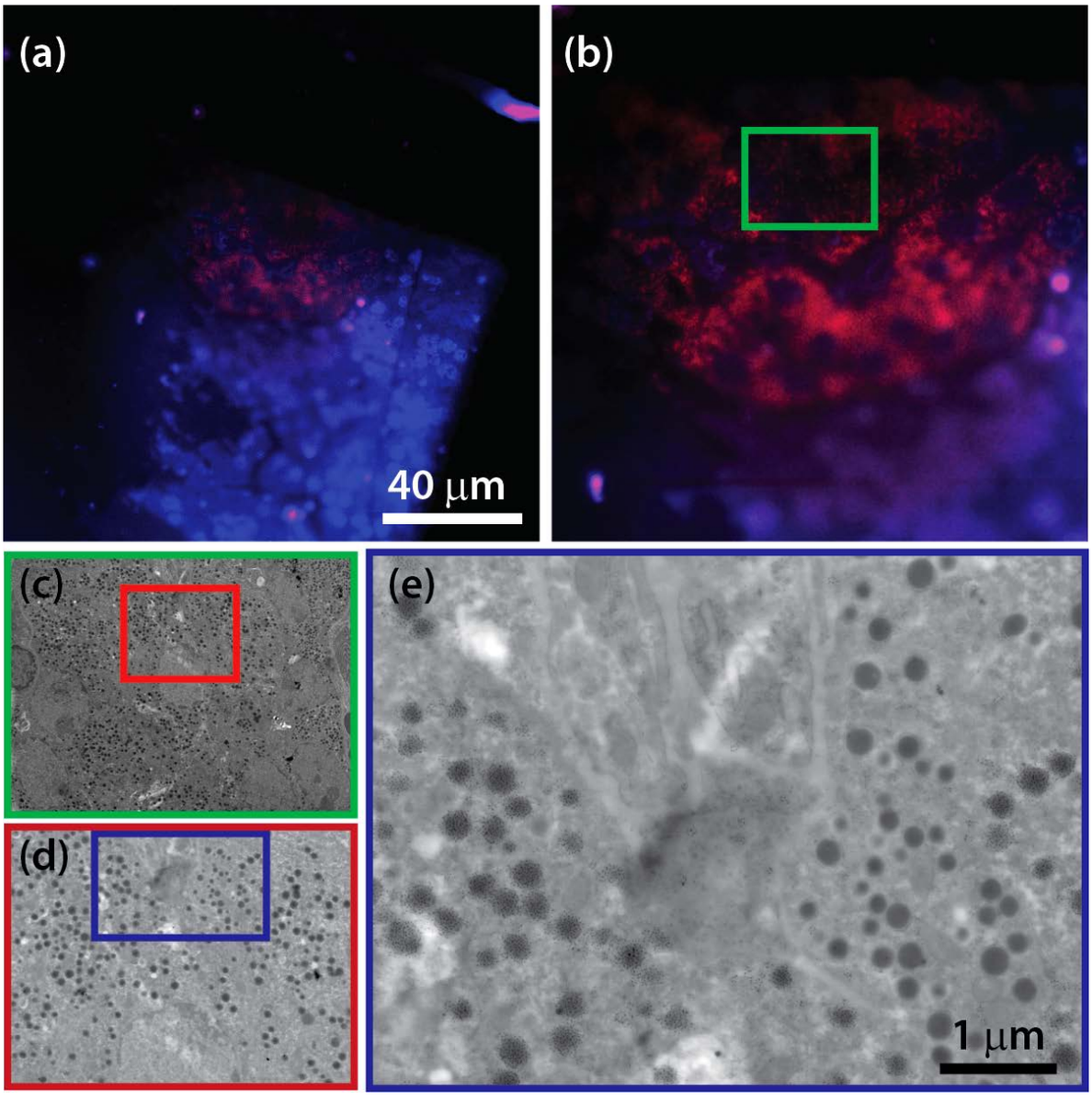

Figure 1. Correlative Imaging of Islets of Langerhans. (a) FM image of pancreatic tissue, fluorescently stained with Hoechst and immuno-labelled with QDot655 for insulin. EM staining is achieved with uranyl acetate and osmium tetroxide. **(b)** An enlarged image of the Langerhans islet present in (a). **(c)**SEM image of green boxed area in (b). SEM images provide ultrastructural information of the Langerhans islet. **(d)** SEM image of red boxed area in (c). Horizontal Full with of the images in (b), (c), and (d) are 56 μm, 30 μm, and 12 μm , respectively. **(e)** SEM image of the blue boxed area in (d). Only at this magnification, QDots that label insulin granules are visible.

Strategies for Integrated Correlative Microscopy

An approach to tackle the limitations in CLEM is integrating LM and EM in one microscope, (iCLEM). First, once the relative coordinate systems are defined between LM and EM modalities, all difficulties about relocating ROIs in LM or EM are removed and the experimental routine for CLEM is effectively shortened. Also, as there is no need for sample transfer in such a microscope, the risk of sample contamination or damage during transport is eliminated. Intermediate sample preparation steps to prepare the sample for EM after the FM observation may lead to additional damage or sample distortion. Finally, going back and forth between imaging modalities becomes much simpler in an integrated microscope. In order to fully profit from the analytical power of both LM and EM, it is desirable but not trivial to achieve an integration which does not compromise the capabilities of either the LM and/or the EM.

Currently, several strategies for iCLEM have been reported, which integrate a LM either in a TEM or in a SEM. In the 1980's by Wouters et al. initiated an integrated solution for SEM, in which the LM is operated with a 45° relative angle to the SEM axis [61]. However, an accurate alignment between the LM and SEM axes was not attainable and electron detection was partially interfered the optical components placed in the SEM chamber. For TEM, an integrated CLEM microscope known as iLEM was developed by Agronskaia et al. in 2008 [62]. In this system, a long working distance and low NA light objective lens is positioned perpendicular to the TEM axis. For LM inspection the sample is tilted 90°, and then tilted back to be imaged by TEM with a positioning accuracy of about 20 μm. Also recently, incorporation of a fluorescence light microscope inside a dedicated SEM column was reported by Kanemaru et al. [63], where the light objective lens shares the same axis with the SEM and the electron beam passes through an hole in the center of the light objective lens. Although this system provides a natural alignment between LM and SEM, the resolution it can provide for LM and SEM is limited. Another development for iCLEM, which is named as atmospheric scanning electron microscope (ASEM), have been reported by Nishiyama et al. in 2010 [42,64,65]. This system works with a dedicated inverted SEM column and a chamber that is separated from air with a thin membrane. In such a configuration, any light microscope can be positioned above the SEM and utilized to image the sample placed on the thin membrane. However, although this system even enables liquid-EM imaging as mentioned before, the size of the imaging area is quite limited and the achievable SEM resolution is intrinsically reduced as the imaging is done through the thin membrane.

Thus, an integrated solution for CLEM that incorporates a LM and an EM directly in a single apparatus without compromise on either modality and without the need for sample translation is still lacking. Nevertheless, such a solution may greatly facilitate CLEM inspection procedures, may enable quantitative CLEM and may ultimately enable the integration of super-resolution microscopy in a SEM.

Integration of a high-NA Light Microscope in a Scanning Electron Microscope

The iCLEM approach developed in our group incorporates an inverted LM into an SEM. The integration is performed in such a way that both microscopes can be used at their full, uncompromised capabilities [66]. The LM is mounted onto the door of the vacuum chamber, so that the SEM can be easily retrofitted with the LM but also returned to its original state by simply exchanging the doors (see Figure 2). Light is guided to and/or from the objective lens through an optical window in the door. Therefore, illumination and detection optics can be placed outside the vacuum in a desired, flexible configuration.

The inverted light microscope is positioned to fill the empty space below the sample stage in the SEM chamber. As all the electron optics are located above the sample stage, the LM and SEM are operated independently in a totally uncompromised state. The sample mounted on a transparent substrate is basically sandwiched between the light and the electron microscope The NA of the integrated LM can reach up to 0.95 with dry objectives or even up to 1.4 with oil-immersion objectives, with vacuum-compatible immersion oil. Illumination and detection optics of the integrated LM can be further enriched for an advanced microscopy set-up, for instance super resolution microscopy. Similarly, electron-beam induced deposition (EBID) processing and all of the SEM detectors, like back scatter electron detectors (BSED) and an energy dispersive x-ray (EDX) analysis, which are situated above the sample, can be utilized in the integrated microscope.

Additionally, the same region in the sample can be visualized simultaneously with both modalities in the integrated microscope as the light optical and electron optical axes are aligned with respect to each other. Because the integrated microscope has the possibility of simultaneous operation, we refer to this technique as SCLEM (Simultaneous Correlative Light and Electron Microscopy). It should be noted however that in most CLEM applications the FM and EM images are still acquired sequentially. But several novel applications are enabled by using the two microscopes simultaneously. The pictures from the interior side of the integrated microscope are presented in Figure 2.b and c.

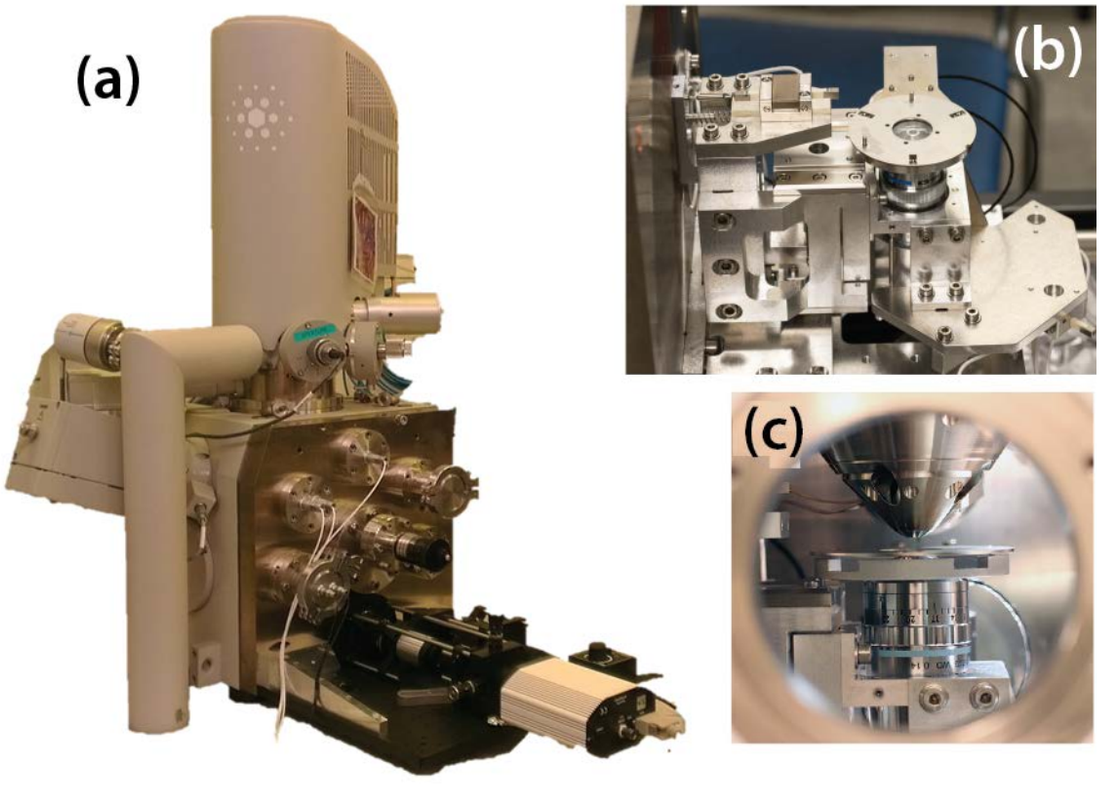

Figure 2. Integration of a high-NA light microscope in a SEM. (a) Picture of the integrated microscope. An inverted epi-fluorescence microscope is constructed on a bread-board attached to the door-plate of the SEM. The components for optical illumination/detection are placed outside the vacuum. **(b)** The sample and the vacuum part of the light microscope, are mounted on the interior side of the door plate. **(c)** Picture taken through a side opening of the SEM. The sample is positioned between the light objective lens (below) and the final electron lens (above).

Scope and Outline of the Thesis

The integrated microscope explained in the previous section was developed to facilitate a fast and easy method for correlative microscopy and accelerate CLEM studies. The work presented in this thesis aims to introduce and explore the potential of the integrated microscope for linking biomolecular and dynamic FM with high-resolution EM.

The first part of the work, Chapter 2 to Chapter 4, demonstrates the novel possibilities, which are introduced by the integrated microscope, for CLEM studies of fixed and dehydrated samples. Chapter 2 introduces the method of Simultaneous Correlative Light and Electron Microscopy (SCLEM), and demonstrates correlation of high-NA fluorescence imaging with cellular ultrastructure. Our protocol for the sample preparation for SCLEM imaging, and with the imaging procedures are presented in Chapter 3. This protocol could help researchers adopt their workflow for integrated microscopy. Chapter 4 presents the addition of multi-color capabilities to SCLEM and show that the overlay method for FM-SEM image registration can also be employed for correcting chromatic distortions in between different FM color channels.

The focus of the second part of this work, Chapter 5 to Chapter 8, is on imaging samples in liquid in the integrated microscope. The achievable resolution in liquid SEM imaging for nanoparticle bio-labels is investigated in detail with simulations and experiments in Chapter 5 and Chapter 6. Chapter 7 sets out the design and fabrication process of a holder for correlative light and scanning electron microscopy of whole cells in liquid. Finally, Chapter 8 presents the novel method of on-demand SEM in which instantaneous SEM snapshots of dynamic biological processes are captured based on in-situ live cell FM observations.

Chapter II

Simultaneous Correlative Scanning Electron and High-NA Fluorescence Microscopy

Correlative light and electron microscopy (CLEM) is a unique method for investigating biological structure-function relations. With CLEM, protein distributions visualized in fluorescence can be mapped onto the cellular ultrastructure measured with electron microscopy. Widespread application of correlative microscopy is hampered by elaborate experimental procedures related foremost to retrieving regions of interest in both modalities and/or compromises in integrated approaches. We present a novel approach to correlative microscopy, in which a high numerical aperture epi-fluorescence microscope and a scanning electron microscope illuminate the same area of a sample at the same time. This removes the need for retrieval of regions of interest leading to a drastic reduction of inspection times and the possibility for quantitative investigations of large areas and datasets with correlative microscopy. We demonstrate Simultaneous CLEM (SCLEM) analyzing cell-cell connections and membrane protrusions in whole uncoated colon adenocarcinoma cell line cells stained for actin and cortactin with AlexaFluor488. SCLEM imaging of coverslip-mounted tissue sections with both electron-dense and fluorescence staining is also shown.

This chapter is published as:

Liv, N., Zonnevylle, A. C., Narvaez, A. C., Effting, A. P., Voorneveld, P. W., Lucas, M. S., Hardwick, J. C., Wepf, R. A., Kruit, P., Hoogenboom, J. P. (2013). Simultaneous correlative scanning electron and high-NA fluorescence microscopy. *PloS one*, *8*(2), e55707.

Introduction

Understanding cellular structure-function relations requires the complementary capabilities of both fluorescence and electron microscopy. Fluorescence microscopy (FM) visualizes individual proteins in color through the use of immuno-fluorescent or endogenous labelling [67]. Optical super-resolution techniques have enabled protein localization with accuracies down to 20 nanometer [68], but intrinsic to fluorescence measurements is the fact that only the labeled components are visible. Electron microscopy (EM) on the other hand maps the cellular ultrastructure at nanometer scale resolution. Correlative microscopy bridges the gap between optical and electron microscopy by rendering an overlay image after application of both techniques on the same area of the specimen. The possibility to map protein locations onto the cellular structure retrieved at nanometer scale accuracy with electron microscopy, has in recent years sparked interest in correlative light and electron microscopy (CLEM) [49,54,58,62,69–76].

Typically, in CLEM research, inspection with FM and EM is performed on the two separate microscopes. In this way, both types of microscopy can be used at their full capabilities, including super-resolution FM [49,76]. However, CLEM procedures are arduous and require expert operation for several reasons. First, it is intrinsically difficult to retrieve a region of interest (ROI) identified with FM in EM, as the mechanisms for contrast generation in both microscopes are widely different. Thus, specialized sample holders or navigation markers are needed to facilitate ROI retrieval [48,49,74,76,77]. Second, the time involved in a CLEM experiment with transfer between both microscopes and retrieval of ROI's typically takes several days. Third, the transfer between both microscopes makes the sample vulnerable to contamination or damage. Fourth, for re-inspection with FM after one CLEM cycle in order to identify additional ROI's, the transfer procedure needs to be performed over again. This limits the amount of data that can be extracted in a CLEM measurement and puts strict requirements on the success rate of sample preparation and staining procedures. Last, the accuracy with which the retrieved ROIs in FM and EM images can be overlaid is limited and typically worse than the resolution of the microscopy techniques themselves. The widespread application of CLEM for examining biological structure-function relations requires simplified and routinely applicable techniques that meet the demands outlined above.

The retrieval of ROI's can be facilitated using external markers on the sample holder that allow definition of a universal coordinate system in both FM and EM [74,77]. The need to mount the holder in the two microscopes typically limits the accuracy in the order of micrometers. Also commercially available algorithms can be used that recognize features that are intrinsically present in both images [77]. Alternatively, fiducial markers that can be observed with both FM and EM can be used [48,49,76]. The definition and identification of reliable markers over large areas is not trivial and requires great care. With fiducial markers, such as fluorescent or gold nanoparticles, a ROI can be identified with high accuracy (50-100 nm) [48], but the search-and-find procedure can still be laborious and a typical research targets a single or a few ROI's. In addition, these procedures do not target the other issues involved in CLEM.

Integrated approaches, where an optical microscope is integrated in an EM vacuum chamber, offer a practical solution to several issues. This approach was pioneered in an SEM in the early work of Wouters *et al.* [78]and recently extended to TEM by Gerritsen and co-workers [62]. In the latter microscope, called iLEM (integrated Light Electron Microscope), the sample is automatically transferred within the vacuum chamber from FM to TEM after identification of a ROI by 90° rotation of the sample stage. The integrated approach reduces CLEM process times from days to hours or less and removes the risk of sample contamination [62]. The optical microscope that can be integrated in a TEM is however necessarily low-NA and long working distance. In addition, the internal transfer from FM to EM still limits the overlay accuracy to the order of micrometers [62].

In the SEM, a high-NA optical microscope can be integrated into the vacuum chamber [78]. We have recently presented a design that gives the possibility to perform high-resolution FM inside an SEM without compromise to SEM operation [66]. Here, we demonstrate that this integrated microscope enables a novel approach to CLEM, which relies on the possibility to apply both high-resolution light and electron microscopy *simultaneously* to the same area of a sample. While in correlative microscopy both modalities are applied sequentially, the fact that both the LM and the EM can illuminate the same area at the same time removes the need for sample transfer, ROI retrieval, and definition of markers. This procedure makes correlation unambiguous, straightforward, and fast, enabling routine application of high-resolution correlative microscopy. In addition, both optical and electron microscopy can be used at their full capabilities, extending the possibilities for quantitative FM-EM investigations of large numbers of ROI's.

Results

Simultaneous CLEM

For Simultaneous Correlative Light-Electron Microscopy (SCLEM), we use an integrated microscope where the objective lens is positioned in the vacuum chamber of a Scanning Electron Microscope (SEM), directly underneath the sample (see Figure 1.a). Contrary to previous integrated solutions [62,63,78], the electron and optical axes are aligned parallel to each other and normal to the substrate from opposite sides. The distance between both axes is typically controlled to within 10 μm. Better axial alignment, down to 1 μm, can in principle be achieved but is not necessary as the electron axis can be shifted over the remaining distance electronically using the beam deflectors in the SEM column. Axial alignment in the micrometer range ensures that this beam shift does not introduce aberrations in the SEM image. All technical details of the integrated microscope, including the axial alignment procedure, are described in detail in [66].

As can be seen in Figure 1.a, the objective lens is mounted inside the SEM vacuum chamber similar to an inverted optical microscope. Illumination and detection occurs in epi-configuration. Using vacuum-compatible immersion oil, objective lenses with numerical aperture up to 1.4 can be used. Light collected by the objective lens is guided by a mirror through an optical window mounted in the door of the vacuum chamber. As is schematically illustrated in Figure 1.b, components for

optical illumination and detection can be arranged at will outside the vacuum chamber. In this research, light from a 470 nm LED source is collimated and sent through a dichroic mirror into the vacuum chamber where it illuminates the sample through a 100x 1.4NA objective lens immersed with a vacuum compatible immersion oil. The collected fluorescence light is directed through the dichroic mirror and focused onto a CCD camera. The SEM is operated in usual fashion with electron excitation and detection from above the sample.

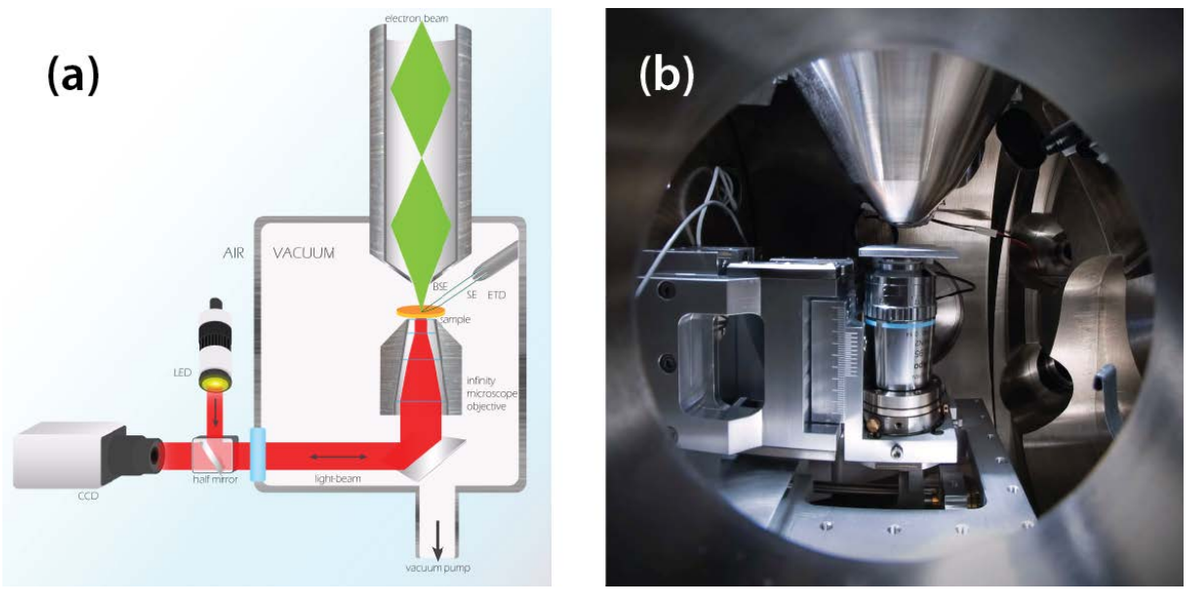

Figure 1: Simultaneous Correlative Light and Electron Microscopy (a) schematic lay-out for SCLEM, BSE: backscattered electrons, SE: secondary electrons, ETD: Everhard-Thornley detector, LED: light emitting diode, CCD: charge coupled device camera. (b) inside view of the integrated microscope for SCLEM showing optical objective lens in epi-configuration underneath sample holder and electron lens.

Image formation in the SEM occurs through detection of either low-energy, secondary electrons (SE) or high-energy back-scattered electrons (BSE). Among other contrast mechanisms, SE imaging gives nanometer scale detail of surface topography, while the BSE signal originates from a larger sample volume contrasting differences in atomic number or density. In our SCLEM setup, samples need to be mounted on a transparent substrate. The use of transparent conductive ITO-coated glass cover slides eliminates the need for a conductive over-coating of biological materials [71]. Cells can be cultured directly on the ITO-slides [79] and details in surface topography can be imaged without additional staining procedures. Alternatively, thin sections can be cut from a larger three-dimensional sample and mounted on the ITO-slides. In this case staining for SEM has to be performed to yield SE and/or BSE contrast. Below, we will demonstrate SCLEM for both sample types: First, uncoated, fluorescent labeled whole cells without EM staining, second thin tissue sections with both EM and FM staining.

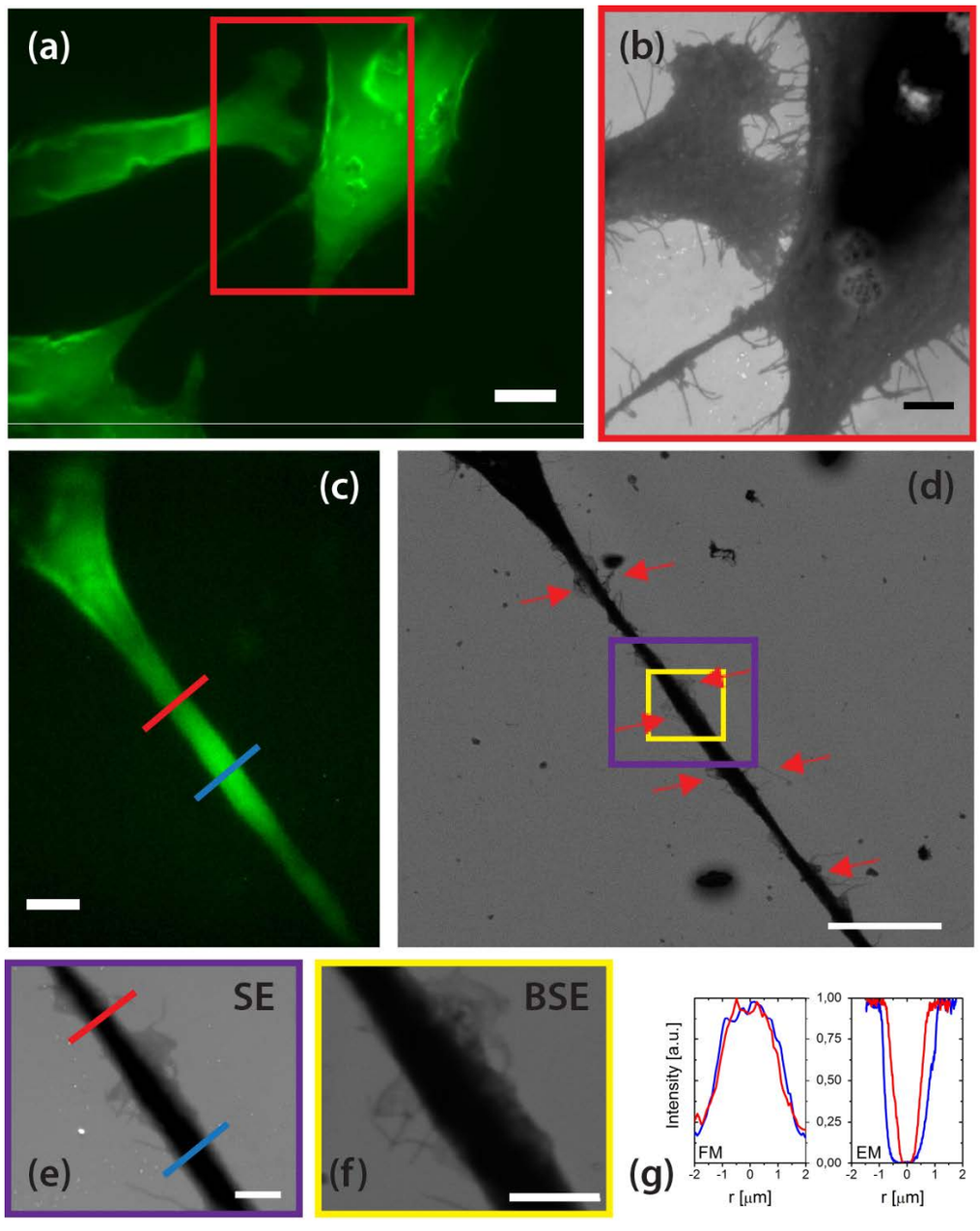

Figure 2: SCLEM of whole uncoated cells (a) FM image of three adenocarcinoma cells actin labeled with Alexa488. The three cells are connected via tentacles and larger extrusions. (b) SEM image of the boxed area in (a), showing detailed information on the connections between the cells. A dense network of tentacles and lamellae stretches between the upper and the right cell. (c) FM image of an extension connecting another two adenocarcinoma cells. Clear variations in actin concentration along the extrusion can be observed. (d) BSE image of the extrusion in (c). Red arrows mark areas with increased concentration of tentacles that occur before and after the thinner parts of the extrusion. (e, f) SE and BSE high-magnification images of the boxed areas in (b) showing a region rich in tentacles and small lamellar extrusions. (g) Fluorescence and SE intensity profiles, normalized on the maximum, taken along the red and blue lines in (c). Scalebar is in (a) 5µm, in (b) 3µm, in (c) and (d) 10µm, in (e) and (f) 2µm.

Cell-cell connections in uncoated, unstained whole cells

The formation and growth of cellular extensions and protrusions, such as filopodia, lammelipodia, and invadopodia, plays a crucial role in cell motility and cell-cell signaling. These processes involve a wide variety of proteins. The role that these proteins play in the development and maturation of cellular topography, is an area of active research. SCLEM on uncoated, whole cells may serve as a powerful technique to investigate the role of protein localization as the SEM can record a detailed map of the network of cellular protrusions.

As a first illustration of the application of SCLEM, we immuno-labeled SW480 colon adenocarcinoma cell line cells for actin with phalloidin-Alexa488. Wide-field fluorescence allows for rapid identification of labeled cells and selection of a region of interest. In Figure 2.a, three nearby cells can be seen with a few actin-containing tentacles stretching out in between the cells. The cellular topography can be imaged (Figure 2.b) and overlaid with the FM directly after identification of the region of interest. Note that in this image the ITO-surface appears bright due to the stronger electron scattering on indium and tin atoms [71] compared to the cellular materials. The high-magnification SEM image in Figure 2.b reveals inclusions on the upper cell membrane. Importantly, the detailed network of tentacles and small lamellae connecting the cells is clearly resolved. The typical lateral size of the thin tentacles stretching between the two cells visible in Figure 2.b is 60 nm. In other cases, cell-cell connections were found to consist of larger extensions stretching several tens to hundreds of micrometers. In Figure 2.c-f fluorescence and electron images of such an extension connecting two neighbouring cells are shown. The fluorescence image displays variations in actin concentration and thickness of the extension. With the SEM, the lateral dimensions can be determined. Figure 2.g and h shows the line profiles at the marked positions from both the fluorescence and electron images. To display and compare both curves, intensities have been normalized to their maximum. The lateral size is found to be 1µm resp. 2µm. In the SEM images, we also observe the outgrowth of tentacles and small lamellae from this larger extension. Interestingly, it can be seen that the outgrowth of tentacles and lamellae occurs at the positions where the filament size changes, as marked with red arrows. Figures 2.e and 2.f show detailed images of such a region.

Cortactin distribution and cellular topography

Next, we labeled the SW480 adenocarcinoma cells for cortactin, again with Alexa488. Cortactin is involved in rearrangement of the actin network and as such important in the formation of filopodia, lammelipodia, and invadopodia. In Figure 3.b and c, we show SEM resp. FM images of an adenocarcinoma cell where cortactin is labeled with Alexa488. In Figure 3.c, different regions with increased fluorescence compared to the surroundings can be observed. First, there are large areas with strong fluorescence in the cell interior, two of which are marked with blue arrows. Second, regions with increased fluorescence, several hundreds of nanometers long, stretch along the outer cell membrane. Examples of such regions are marked with red arrows. Finally, in extruding areas such as in the lower part of the cell, smaller areas with a local increase in fluorescence can be observed (marked with yellow arrows).

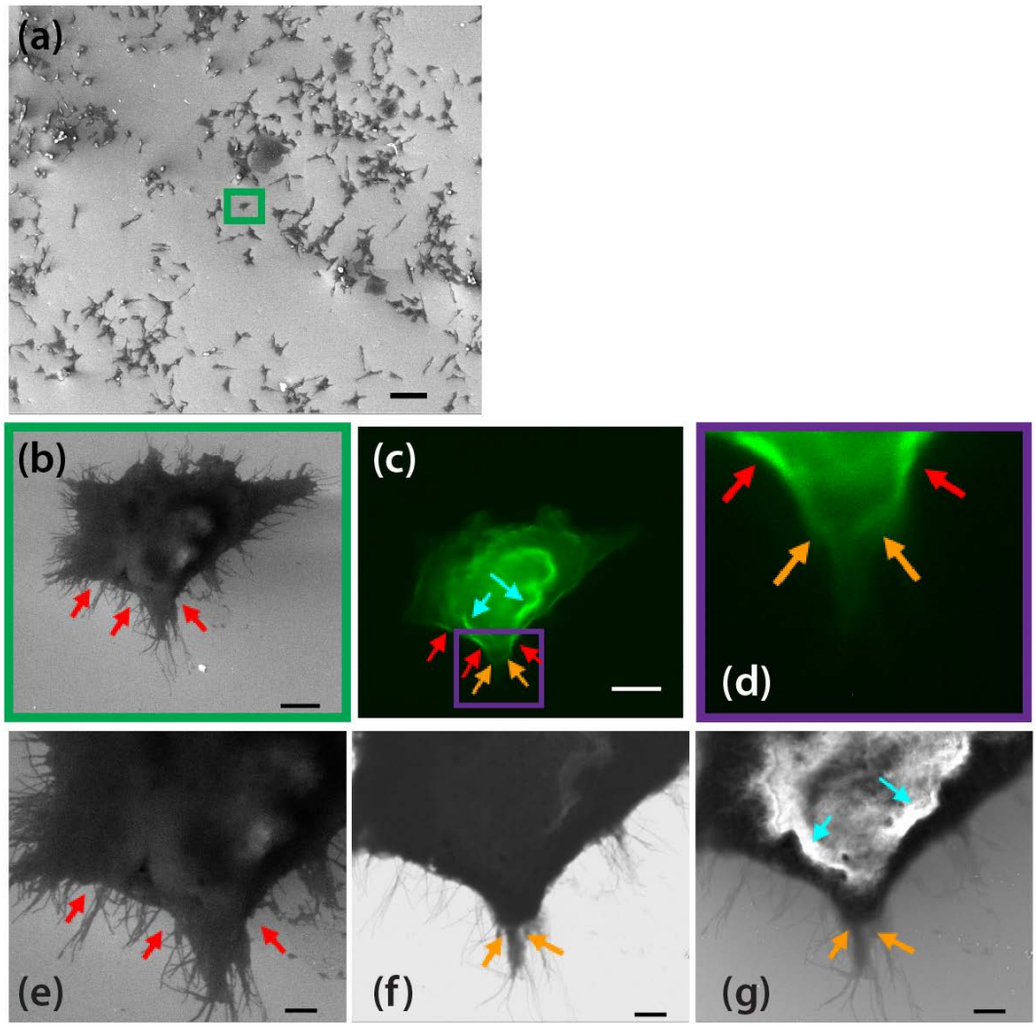

Figure 3: SCLEM inspection procedure with Cortactin labeled adenocancerinoma cells. (a) After mounting the sample and vacuum pumping of the SEM chamber, a low-magnification image in SEM mode is taken to inspect surface coverage and position the sample stage. (b) An isolated cell is identified and the SEM focus is fine-tuned for high-magnification imaging. (c) The fluorescence image is recorded after the marked cell was selected. Based on the spatial variations in cortactin distribution and the structural overview in (b), regions of interest are identified for high-magnification imaging in SEM mode. Blue, red, and yellow arrows indicate different type of regions with a local increase in cortactin density. Corresponding areas are also marked in the SEM images. (d) Zoom in of the purple boxed area in (c). (e) SE image recorded at 20 keV of the region of interest identified in (c). The cortactin-rich areas marked with red arrows are directly neighboring regions with larger extrusions and high density of tentacles (f) BSE image recorded at 5 keV. (g) SE image at 5 keV reveals the details in surface topography. It can be clearly seen that the blue marked cortactin-rich regions located in the cell interior correspond to an increase in cell thickness. The cortactin-rich regions marked with yellow arrows surround a larger thin lamellar outgrowth with numerous extending tentacles. Typical time involved in such a procedure (sample mounting & pump down – a,b – c – d,e,f) amounts to 20-35 minutes (4min – 5 min – 5 min – 5-15 min). Scalebar in (a) 100 µm, in (b) and (c) 5 µm, in (e), (f), and (g) 2 µm.

The same areas are marked in the SEM images in Figures 3.b, and 3.d-f. From the SE image in Figure 3.f, it can be seen that the blue marked areas have a strong SE contrast. This indicates a large increase in cell height, as SE can only escape from a few nanometers deep. Thus the strong increase in cortactin concentration observed in the FM image, can be, at least in part, ascribed to an increase in membrane surface area. Contrarily, the variations in cortactin concentration observed at the outer membrane edge, can be directly linked to tentacles and larger extrusions of the cell membrane. In the Figures 3b and d, it can be seen that the cortactin-rich areas are adjacent to areas with more and larger outgrowth. The apex of the extrusion in the lower part of the image consists of a filopodium-like structure (Figure 3.e). The location at which this structure extrudes from the membrane is again surrounded by cortactin accumulations on the cell membrane (yellow arrows). This illustrates how SCLEM can correlate protein localization to cellular extrusions and, ultimately, cell motility. The use of high-NA objective for FM enables the extraction of high-resolution fluorescence data. Moreover, as there is no specimen transfer, or re-adjustment of a ROI involved, SCLEM allows for routine inspection of a large number of cells. This will enable the extraction of quantitative CLEM data, e.g. in this case correlating position-dependent fluorescence intensity with statistics on the number, length and lateral dimensions of cellular extensions. Such investigations are currently underway.

SCLEM offers reduced inspection times and sampling of multiple ROI's

As mentioned above, one of the important results of SCLEM is that there is no need for specimen transfer and re-adjustment of a ROI to combine high-NA FM data with structural data retrieved with SEM. Correlative imaging is achieved without adding fiducial markers to either the specimen support or the sample itself. This greatly simplifies the experimental workflow for CLEM and allows a user to search for a new ROI directly after inspecting another one. As a demonstration, the total time involved in a typical inspection procedure, as with the cortactin-labeled cancer cells shown in Figure 3, was measured.

Figure 3 shows a sequence of images taken in the experiment. After mounting the sample and SEM vacuum pump down, we first perform a low-magnification inspection of the sample with the SEM in order to evaluate the surface coverage of cells. This way we can determine areas on the coverslip where a substantial amount of single cells can be found (Figure 3.a). After sample translation to such an area, higher magnification FM and SEM images are taken (Figure 3.b-c), where the FM image serves to identify the ROIs for SEM high-resolution structural inspection. We then perform the SEM zoom-in to display the structural detail of selected parts of the cell (Figure 3.d-f). This experiment, from sample mounting and vacuum pump down to full inspection, takes 20-35 minutes. The 15 minutes margin depends on the amount of high-magnification investigations that are performed with the SEM. This includes the investigation of different areas per cell, as well as various detectors (BSE and SE) and electron energies (see, e.g., Figure 3.d-f). As the axial alignment between FM and SEM is fixed and the sample stage is translated, identification of and transfer to a new ROI typically only takes 5 minutes, followed by another 10-25 minutes of detailed investigations. This constitutes a drastic decrease of experiment time when compared to CLEM

experiments with high-NA FM and EM on separate microscopes, where, in addition, typically only one to a few ROI's can be sampled.

Often in the practice of FM, sample inspection is started with a low-magnification, low-NA objective lens to identify a ROI for high-resolution inspection. It is important to note that the field of view of the SEM easily extends millimeters squared and is thus much larger than that of the integrated high-NA FM. Thus, low-magnification SEM is well suited to perform a quick inspection of the sample, e.g. to analyze the surface coverage of cells (see Figure 3.a). It is important to note that in Figure 3.a, low-magnification SEM imaging was done before capturing the FM image in Figure 3.c. Usually, fluorescence investigations are performed prior to EM to prevent accelerated bleaching during electron-beam exposure. However, similar to photo bleaching, electron-beam induced bleaching is a dose-dependent process. We observed that exposure during low magnification SEM imaging, i.e. at the multi-cellular or cellular level (cf. Figure 3.a-b) does not visibly affect the fluorescence in these and other samples. This provides us with the possibility to use the large field of view of the SEM to inspect the sample for areas with a suitable coverage of cells. The sample is then translated such that this area is in the field of view of the high-NA FM. The typical inspection procedure that we use in SCLEM is depicted the sequence of images in Figure 3.

Clearly, prolonged exposure to the electron beam, such as after a high-magnification sub-cellular zoom-in, does lead to bleaching. The rate at which this occurs is dependent on electron energy, but also on the composition and thickness of the substrate and, importantly, the type of fluorophore [80]. We note that the possibility to move back and forth between FM and SEM provides a unique possibility to study electron-fluorophore interactions in detail.

Tissue sections with FM and EM staining

Thin tissue sections can be investigated with SCLEM after combined FM and EM staining. Several approaches have been reported that allow for EM staining while preserving fluorescence [69], even up to the point where optical super-resolution can be performed [49]. We prepared 100 nm sections of human skin stained for EM with osmium tetroxide and uranyl acetate and for FM with DiIC18. The fluorescence serves to navigate and quickly identify the corneocytes, epidermis, dermis, and other parts of the skin tissue.

Figure 4 shows FM and EM images of dermal tissue. In the fluorescence image structural components can be discerned based on differences in fluorescence intensity. In the middle part of the image, three lager structures, two with strong fluorescence, the other with almost no fluorescence can be identified. The corresponding SEM image clearly resolves the underlying ultrastructure in detail. Here, we note that SCLEM offers a fast procedure to identify such regions in FM and inspect the ultrastructural detail with SEM.

In the SEM image in Figure 4.b various cellular constituents can be identified. A nucleus can be seen in the upper right corner. Collagen fibers running parallel to the plane of scission can be seen

in the middle of the image and in the lower left corner. In other areas, such as in Figure 4.c, collagen fibers, approximately 100 nm wide, are seen to run perpendicular to the plane of view. Clearly, the applied EM staining visualizes the structural detail in the tissue, while the fluorescence signal is maintained sufficiently to perform rapid tissue inspection and select regions for SEM inspection.

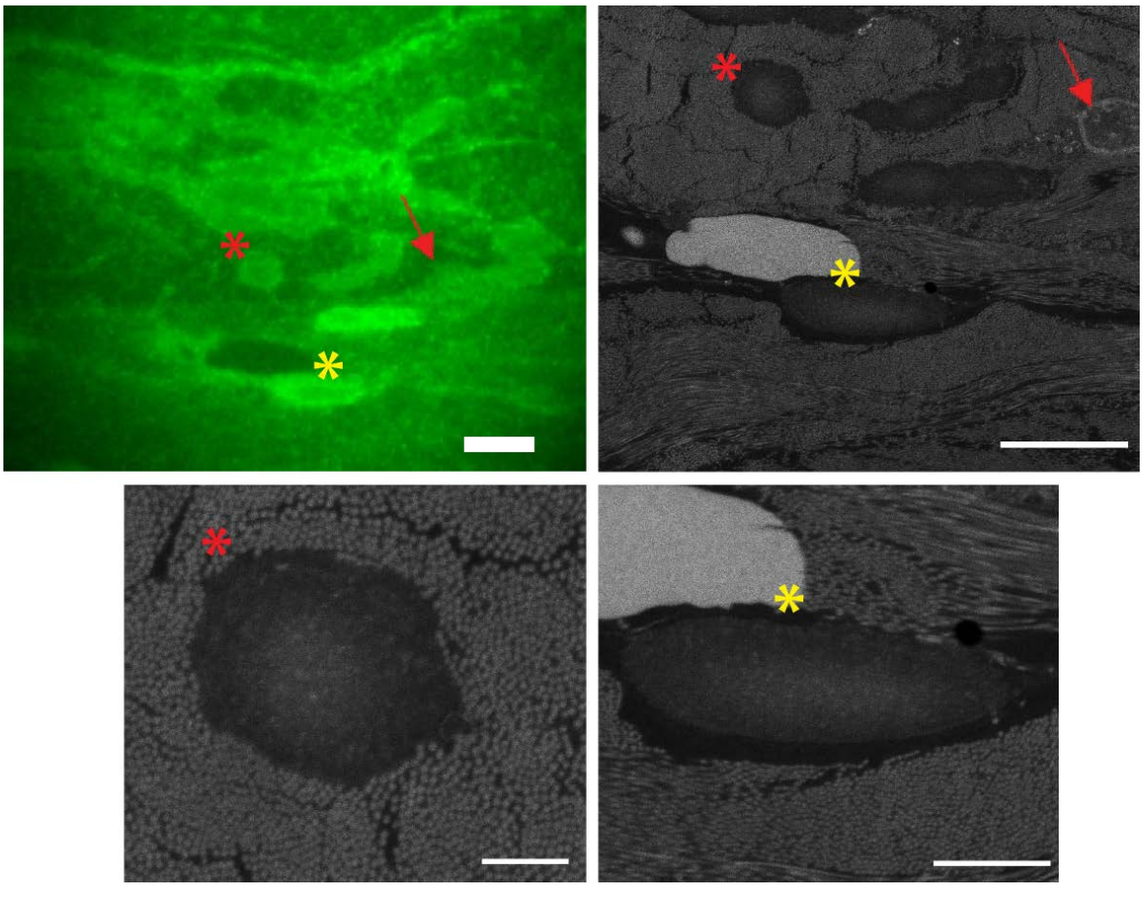

Figure 4: SCLEM on FM and EM stained tissue sections. (a) FM image of human skin tissue stained with DiIC18 fluorescence and uranyl acetate and osmium tetroxide for EM contrast. (b) BSE image of a selected region from (a), showing a cell nucleus not discernible in (a) (marked with a red arrow), and bundles of longitudinally and transversally cut collagen fibers. (c, d) High-magnification images of the areas marked with (c) a red star, and (d) a yellow star. Scalebar in (a) and (b) 5µm, in (c) 1µm, and in (d) 2µm

Discussion

The method of SCLEM removes the need to retrieve a ROI as the alignment between SEM and FM optical axes is fixed while the sample is translated through focus. Thus, the SCLEM time for identification and inspection of a ROI is on the order of few tens of minutes, in which a user can move back and forth arbitrarily between the different SEM and FM detectors. In this way, a sample can be quickly scanned for ROI's in either SEM or FM mode of operation and a large number of ROI's can be investigated in a short time compared to CLEM operation on the two microscopes. In addition, issues involved in sample transfer between the microscopes, such as contamination risk, are removed from the workflow. Obviously, this also means that the sample has to be prepared to render contrast in both FM and SEM mode of operation. As we have illustrated with examples this can be done by either performing double staining, or by inspection of whole, uncoated cells with only fluorescent labeling. Alternatively, labeling with dual-contrast probes, like semiconductor quantum dots [81] or fluorescent labeled gold nanoparticles, would yield visibility in both modalities. However, the strength of EM in CLEM research is the possibility to visualize the ultrastructural detail which would then still require an additional staining step.

The development of probes and preparation protocols for correlative research has emerged in recent years. Watanabe *et al.* have demonstrated a protocol that preserves fluorescence to such an extent that super-resolution fluorescence techniques like PALM and STED can be performed on EM-stained sections [49]. One of the main advantages of inspection of coverslip-mounted sections with the SEM is the possibility to analyze large arrays of sections from a 3D sample in an automated fashion. For example, in array tomography, the array of sections is inspected first in FM and then in SEM to retrieve a correlated 3D view of protein distributions and ultrastructure [29]. For 3D reconstruction, speed of operation and automation are crucial aspects. With SCLEM, the entire process of array tomography could be performed fully automated in a single pass. The development of more robust probes, more possibilities for multi-color labeling in conjunction with EM staining, or a wider palette of genetically engineered probes dedicated for CLEM applications [58], would increase the possibilities for (S)CLEM in this respect.

The surface topography of entire cells can be inspected with SEM without the need for EM staining or even conductive coating of the sample. Cells can be cultured directly on glass substrates that have a transparent, conductive ITO coating, as demonstrated by others [71,79] and by us in this work. In principle, inspection on non-conductive glass substrates would also be possible, although inspection times would need to be short to prevent resolution loss and imaging artifacts due to charging. We used labeling with an Alexa-dye, but a wide range of fluorophores, including fluorescent proteins [71], can be used in conjunction with fixation protocols compatible with inspection under the SEM vacuum.

SEM inspection of whole cells probes cellular surface structures important in cell motility and cellular signaling, such as tentacles, lammelipodia, filopodia and cell-cell connections. As illustrated in this work, SCLEM can quantitatively correlate protein distributions to densities and sizes of such

surface features. As the electron beam penetrates, depending on electron energy, for several micrometers into the sample, investigation of sub-membrane structures could also be possible, albeit at progressively lower resolution. This would then require incorporation of an EM stain that generates BSE or SE contrast, like in our example of tissue sections. Still, due to scattering of the probe beam, high-resolution imaging would be limited to about 100 nm below the surface.

In the presented SCLEM set-up fluorescence microscopy is performed with a wide-field optical microscope. The low axial resolution of the wide-field microscope does not play a role in the investigation of sections or the thinner progressing or retracting parts of a cell. For samples with a thickness of a micrometer or more, the fluorescence signal may need to be optically sectioned in order to establish a correlation with the SEM signal that originates from the upper part of the sample. As most optical components, such as filters, source and detector, are placed outside the SEM vacuum chamber, illumination and detection paths can be easily adjusted or expanded without the need for vacuum-compatible components. Confocal filtering could in principle be achieved through the insertion of a pinhole. With the use of high-NA immersion objectives optical sectioning at sub-micrometer resolution should be possible. We note that also phase shaping to correct for aberrations due to refractive index differences in thick samples could be possible through the insertion of a spatial light modulator or related optics.

We equipped the fluorescence microscope with a high-NA 100x objective lens using vacuum-compatible immersion oil. The possibility to use a high-NA objective lens with coverslip-mounted samples means that total internal reflection microscopy, and super-resolution techniques like PALM, could be used directly in a SCLEM experiment. For super-resolution microscopy, with protein localization at a few tens of nanometer resolution, the precise positioning of proteins with respect to the ultrastructure becomes increasingly important [49,76]. It should be noted that in our embodiment, the ITO-coating on the coverslip could give rise to aberrations that affect the achievable optical resolution. However, alternatively, one could resort to the application of plain glass slides with a conductive coating on top of the sample as in the super-resolution experiments of Watanabe *et al.* [49]. A SCLEM-type set-up could thus bring the thrilling prospect of performing an optical super-resolution experiment in–situ in an SEM such that at any moment the underlying cellular structure can be directly measured.

SCLEM relies on the possibility to perform both electron and optical microscopy simultaneously. We have observed that low-magnification SEM imaging at 20 keV does not lead to a visible degradation of sample fluorescence. This gives us the possibility to perform wide field of view SEM inspection prior to FM investigation. Interestingly, SCLEM brings the possibility to study bleaching induced by electron-beam exposure in a quantitative and dynamic way by recording the fluorescence signal as a function of electron dose. This would not only provide a novel way of analyzing electron-induced reactions in molecules, but would also enable one to study the electron-stability of organic fluorophores and fluorescent proteins. The latter option could be particularly valuable for the development of dedicated novel probes for CLEM in general.

In conclusion, the method of SCLEM offers a fast and easy method for correlative microscopy. The same area of the sample can be illuminated by both light and electron microscope at the same time. This removes complications related to retrieval of regions of interest or the definition of fiducial markers from the correlative workflow. Inspection times are reduced to the order of minutes, there is no risk of sample contamination or damage as a result of transfer between microscopes, and a user can switch between both modalities during inspection of a region of interest. Importantly, large areas can be inspected without re-evaluation of the overlay between both images and without the need for stitching images from different areas.

We have demonstrated SCLEM with a high-NA objective lens, which allows for quantitative fluorescence microscopy in correlation to cellular ultrastructure. Equivalently, SCLEM could be performed with a large field-of-view low-NA objective lens if fluorescence labeling is solely used as a marker to track rare events suitable for EM investigation. The described implementation of SCLEM with a high-NA objective lens could be used with different optical modalities, including super-resolution microscopy. We have shown SCLEM on coverslip-mounted tissue sections, as well as on whole, uncoated cells without any EM-specific staining. In the latter case, protein distributions measured in fluorescence can be correlated to the growth and size of extrusions and protrusions of the cell membrane. Thus, SCLEM could be a valuable method in the investigation of cell motility and cell-cell signaling. The ease of use and versatility of SCLEM may enable the widespread application of quantitative correlative microscopy in biology and biomedicine.

Methods

SCLEM

All imaging experiments were done on in-house developed optical microscope integrated in a commercial SEM (Quanta^{TM} 200 FEG microscope (FEI, Eindhoven, The Netherlands)) as described above. All technical aspects of the integration platform are described in detail elsewhere [66]. SEM images were made at standard high-vacuum settings with varying acceleration voltages and different magnifications as stated in the manuscript. An Everhart-Thornley detector and a solid-state backscatter detector were used for SE and BSE detection, respectively.

Fluorescence imaging was done at room temperature using the custom made epi-fluorescence microscope which has an objective lens mounted just beneath the sample holder in the SEM chamber. The epifluorescence microscope was equipped with a 470 nm LED light source (Thorlabs M470L2-C), a CCD camera (Photometrics CoolSNAP, Tucson, Arizona, USA) and an 100X 1.4 NA objective lens (Nikon CFI Plan Apochromat VC 100x). The light from the LED source passes through a collimator lens (Thorlabs LED collimator for Nikon microscopes), a planoconvex lens to focus the beam in the back-focal plane of the objective, a band-pass filter with a center wavelength of 485 nm and a transmittance range of 475 - 495 nm (Newport Spectra-Physics 10XM20-485), a dichroic mirror with an edge wavelength of 506 nm, which has a reflection band of 446 - 500 nm and a transmission band of 513 - 725 nm (Semrock FF506-Di03), and then

through a 10 mm thick, 50 mm diameter, 425 - 675 nm anti-reflection coated BK7 glass window (CVI Melles Griot) into the SEM vacuum chamber. The detection path further consists of a long-pass filter with an edge wavelength of 500 nm (Semrock BLP01-488R), and a standard Nikon 1X tube lens. Vacuum-compatible immersion oil was supplied by DELMIC BV (Delft, the Netherlands).

Cell culture

Colorectal cancer (CRC) cell line SW480 (ATCC, UK) were maintained in Dulbecco's Modified Eagles Medium (DMEM) from Gibco Invitrogen, supplemented with penicillin (50U/ml) and streptomycin (50µg/ml) and 10% fetal calf serum (FCS). CRC cell line HCT116 SMAD4-/- cell line used for Cortactin labeling (obtained from Dr. B. Vogelstein - John Hopkins, Baltimore) was maintained in the same way.

ITO-coated microscope slides (thickness #1, 22x22 mm with 8–12 Ωsq^{-1} or 22x40 mm with 70–100 Ωsq^{-1}; SPI Supplies, West Chester, PA, U.S.A.) were washed with ethanol and water, placed in 12-well tissue culture dishes with the conductive side upwards and washed with culture medium. The cells were 2x times washed with Phosphate Buffered Saline (PBS), then trypsinized and seeded onto the ITO coated glass slides. Cells were cultured for 16–24 h at 37°C. Cells grown on ITO-coated glass at a confluency of 50%, were then washed twice with PBS containing 0.5 mM $MgCl_2$, fixed for 10 minutes with a mixture of 2.5% paraformaldehyde and 1.25% glutaraldehyde in PBS, pH 7.4. Samples were washed 3 times with PBS after fixation.

Fluorescent labeling

Staining actin with phalloidin (Alexa Fluor 488 phalloidin; Invitrogen, Carlsbad, CA) was performed according to manufacturer's instructions. 5 µL 6.6 µM stock solution was diluted into 200 µL PBS for each coverslip and 1% bovine serum albumin (BSA) was added to the staining solution to reduce nonspecific staining. The staining was carried on for 30 minutes at room temperature and then samples were washed 3 times with PBS.

For immuno-labeling of cortactin, cells were pre-incubated with PBS with 1% BSA and 0.1% Triton for 10 min, then incubated with the primary antibody, Anti-Cortactin (p80/85) (mouse), clone 4F11(Millipore, MA, USA), in PBS/BSA/Triton for 1hr at dilution 1:200 (2µg/ml) at room temperature. Cells were washed 3 times with PBS containing 1%BSA and 0,1%Triton. The cells were then incubated with the secondary antibody, Alexa fluor 488 goat anti-mouse IgG (H+L) (Invitrogen,NY, USA), dissolved 1:200 in PBS/1%BSA/0,1%Triton for 30 minutes at room temperature and then washed again 3 times with PBS containing 1%BSA and 0,1%Triton. After labeling the samples were 3 times washed with dH_2O and left in dH_2O at 4°C overnight to remove any remaining salt residue from the sample. The samples were air dried. Before imaging, conductive carbon tape was used to connect the samples to the sample holder of the SCLEM platform.

Tissue sections

Samples of human skin were high-pressure frozen, freeze-substituted in acetone, and embedded in HM20. During freeze-substitution it was stained with osmium tetroxide, uranyl acetate, and DiIC18. Freeze-substitution was performed as follows: 27 hours at -90°C, temperature rise to -60°C at 10°C/hour, 6 hours at -60°C, temperature rise to -40°C at 10°C/hour, 5 hours at -40°C. Then the stains were washed out and infiltration was started with HM20 (30% and 70% in ethanol, and then 100% overnight). Polymerization was done with UV-light at -40°C for 3 days. 100 nm sections were cut and transferred to ITO-coated thickness #1 glass cover slides. Before imaging, they were connected to the sample holder of the SCLEM platform with conductive carbon tape.

Acknowledgements

We would like to thank Sjoerd Stallinga and Sander den Hoedt for helpful discussions, Ruud van Tol, Frans Berwald, Ger Schotte, and Cor Barends for technical support. A.P.J.E. was supported by a STW Valorization Grant.

Chapter III

Protocol for Simultaneous Correlative Light Electron Microscopy with High Registration Accuracy

Here, the complete protocol for SCLEM with high registration accuracy is presented. We describe our sample preparation protocol for SCLEM imaging of whole cells expressing endogenous fluorophores, of whole cells with immuno-labelling, and of resin embedded cells and tissues. Also the mounting procedure for the prepared samples in the integrated microscope are explained. We also explain and demonstrate the imaging steps required to assure high accuracy registration between the fluorescence and scanning electron microscope images.

Parts of this chapter are included in:

Peddie, C. J., Liv, N., Hoogenboom, J. P., Collinson, L. M. (2014). Integrated Light and Scanning Electron Microscopy of GFP-expressing Cells. *Accepted for publication in the book Correlative Light and Electron Microscopy (Methods in Cell Biology, Volume 124).*

Introduction

Correlative light and electron microscopy (CLEM) is a unique technique that couples the strengths of fluorescence microscopy (FM) and electron microscopy (EM) [56,75,82]. However, extensive CLEM applications are restricted due to cumbersome and complicated experimental routines related to transfer of the sample between the two microscopes. In terms of sample preparation, this procedure may however seems more accessible as FM and EM preparation and inspection protocols can be performed sequentially. Thus, existing protocols can be used without concerns on fluorescence preservation during preparation for EM. However, artefacts such as sample shrinking and distortion during fixation, embedding and sectioning for EM after FM observation seriously limit the achievable image overlay accuracy. In recent years, integrated approaches have been presented, which offer the advantages of faster pin-pointing of the regions of interest identified by FM in the EM images and elimination of the additional handling steps during the transfer of the specimen from FM to EM involves [62,65]. These approaches can lead to faster CLEM procedures and also more accurate data correlation. Recently, we have developed an integrated platform for CLEM that allows for uncompromised, 'simultaneous' application of FM and EM (SCLEM) [83] and enables higher throughput CLEM investigations. In the integrated platform, the FM and SEM share a common axis and their fields of view are aligned within 2µm accuracy [66]. Besides, an automated light-electron image registration with sub-5 nm accuracy is obtained by visualizing the position of electron beam directly in the fluorescence detection channel [84].

Procedures for specimen preparation for integrated imaging in the SCLEM platform can be noticeably more challenging than standard approaches. However a growing number of sample preparation techniques using EM staining while preserving fluorescence in tissue section samples has been reported recently [47–49,51,69]. The observation of GFP fluorescence in a SCLEM microscope after resin-embedding, staining, and sectioning has also been recently demonstrated [52]. It should also be noted that inspection of individual, whole cells can be less demanding as sample preparation protocols can more closely resemble the practices for light microscopy without the need for EM preparation steps that may quench the fluorescence signal. However, the need for inspection in a vacuum environment still poses requirements on the use of dehydration sensitive probes such as GFP and other genetic markers.

In this chapter, we outline the steps for coupling sample preparation techniques with SCLEM inspection procedures in a manner that should be easily reproducible for non-specialists. An overview of all discussed intermediate steps is given in Figure 1. We present the detailed sample preparation protocol we used for inspection of whole cells cultured on conductive ITO slides, both with immuno-labeling as well as with GFP. We also show how CLEM-prepared resin-embedded sections can be mounted and inspected in the SCLEM microscope. The entire protocol for SCLEM imaging is illustrated by mapping GFP labelled paxillin distributions with respect to the cellular morphology of whole MDCK (Madin-Darby canine kidney) cells.

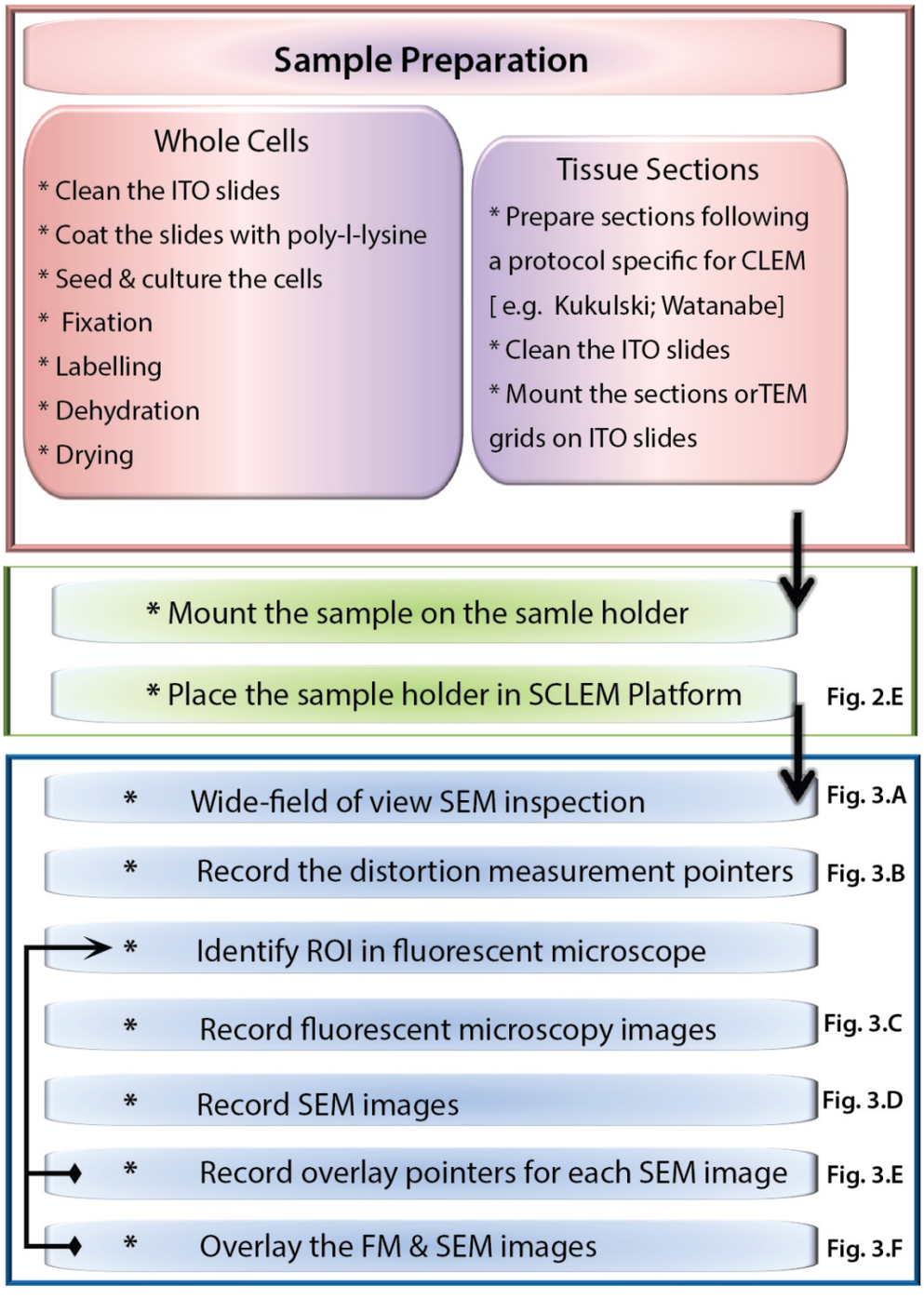

Figure 1. Arrow Diagram of the complete SCLEM Protocol. A distinction can be made between sample preparation for integrated inspection (pink boxed steps), procedure for mounting the sample in the integrated microscope (green boxed steps), and the inspection with both FM and SEM (blue boxed steps)

Methods

A. *Preparation of Whole Cells Expressing GFP*

i. *Principle*

Culturing cells on glass slides is a common procedure for light microscopy applications. However, glass is a strong insulator which would produce unwanted charging artefacts in SEM imaging. The use of glass slides with a thin, conductive and transparent coating of Indium-Tin Oxide (ITO) eliminates the need for a metal coating of the cells themselves, which could quench fluorescent markers and obstruct light microscopy. ITO-coated glass-slides with up to 70- 100 Ω/sq resistivity were shown to provide enough conductivity for SEM imaging, and various types of cells have been shown to adhere and grow on them[71]. The cells can be cultured directly on the ITO-slides, but it is suggested to use an extracellular matrix to promote cell adherence. We used poly-L-lysine and did not observe any adverse effect of the additional layer on SEM imaging. Similar procedures for cell culture and fixation as used for light microscopy can be followed, only care should be taken to not use fixatives that de-gas in the vacuum environment of the SECOM microscope as this would contaminate the microscope.

ii. *Protocol*

1. The ITO slides were cleaned prior to cell seeding by sonication for 2 minutes in ethanol (absolute grade) and subsequent rinsing with ddH_2O. If in following steps problems arise with adhesion to the ITO substrate, the slides can be optionally exposed to an O_2-plasma at 250 Watt power for 15 minutes to increase surface hydrophilicity. In this case, step 2 or 3 should be carried out immediately after removal of the slides from the plasma machine.
2. The cleaned slides were placed in culture dishes with the conductive side facing up. If an adherent matrix was desired, the slides were incubated with 0.01% poly-L-lysine for 30 minutes at 37°C. Care should be taken to keep track which side of the slide has the conductive ITO-coating if the coated surface does not have clear markings. If needed, a quick measurement of the surface conductivity using a multi-meter can be performed at any time to determine the conductive side (see Figure 2.a).
3. Either coated with an extracellular matrix substance or not, ITO slides were washed with culture medium prior to seeding. The GFP expressing cell-line was grown in DMEM+ pen/strep and L-glutamine, with 10% FCS. The cells were washed two times with Phosphate Buffered Saline (PBS), then trypsinized and seeded directly onto the ITO coated glass slides. The cells were grown on the slides for 1-2 days in normal medium and in 1% FCS containing medium for the last 6 hours
4. Before fixing the cells were washed with PBS (pH 8.5) and fixed by adding a mixture of 4% paraformaldehyde in PBS (pH 8.5) to an equal volume of culture medium for 2 hours.
5. The cells were dehydrated in degraded ethanol series (20%, 50%, 70%, 90% and 100%) by dipping the sample at least 2 minutes per concentration.
6. The samples were air-dried.

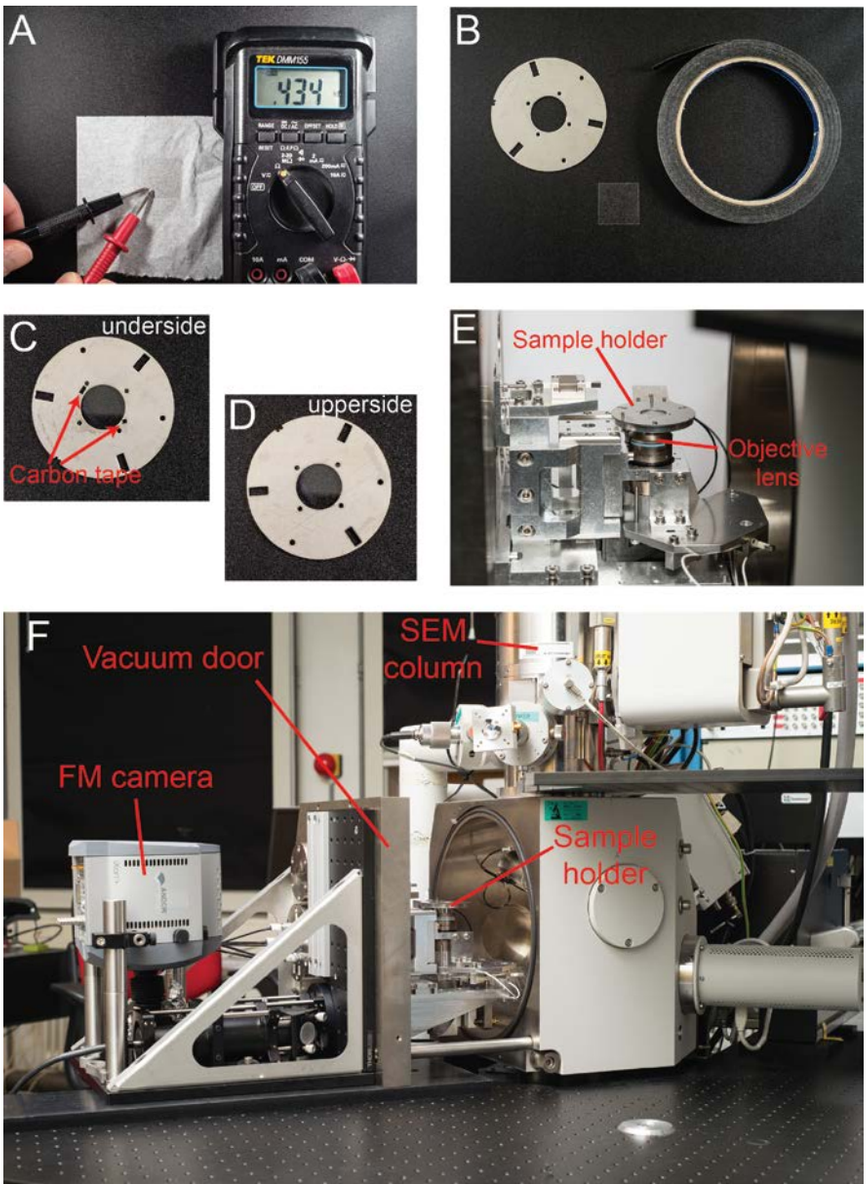

Figure 2. Mounting samples into the integrated microscope. A: At any time during sample preparation and mounting procedures, the conductive ITO-coated side of the glass slide can be determined with a quick resistivity measurement, placing both tips of a multimeter at distant positions on the slide. The ITO-coating has a finite resistance (measured in Ω or kΩ). **B, C, D:** The ITO-coated glass slide is mounted onto the underside of the SECOM sample holder using carbon tape. The ITO-coating should be in contact with the holder. **E:** The SECOM holder is placed onto the sample stage of the integrated microscope with the underside facing the objective lens. **F:** The integrated SECOM microscope where the sample and objective lens go into the SEM vacuum chamber and all other LM components are mounted on the outside of the door of the vacuum chamber.

B. *Preparation of Whole Cells with Immuno-labelling*

i. *Principle*

The sensitivity and ease of application of fluorescence has led to a wide-spread use and label variety for the specific labeling of nucleic acids, proteins and other biomolecules. The precise labelling conditions depend on the antibodies and labels used for immuno-CLEM. Therefore, each labeling step should be optimized independently prior to SCLEM. If labelling/co-labelling is desired with a non-genetic fluorophore, this labelling should be done after the fixation step. However, cell-permanent stains, such as MitoTracker, Tubulin Tracker, or Hoechst can be used prior to fixation.

ii. *Protocol*

The protocol for preparing whole cells with immuno-labelling is similar to the protocol for cells expressing endogenous labels until the fixation step 4.

7. Before fixing the cells were washed with PBS (pH 7.4) and fixed by adding a mixture of 2.5% paraformaldehyde and 0.25% glutaraldehyde in PBS (pH 7.4) at an equal volume of culture medium for 2 hours.

   Formaldehyde based fixatives penetrates tissues rapidly but may be extracted by repeated washing. On the other hand, glutaraldehyde penetrates tissues slower and crosslinks proteins into permanent stasis. Cell membranes are partially permeabilized but cells remain osmotically active. Glutaraldehyde is autofluorescent and therefore not widely used in fluorescence microscopy applications. Addition of a very low (0. 25%) percentage of glutaraldehyde to the fixative solution offers a good compromise as it produces only limited autofluorescence and yields a better ultrastructural preservation. Additionally, the optimal fixation conditions can vary depending on the cell types and on the antibodies used if immuno-labelling will be performed on the sample. Therefore, it is advised to optimize fixation conditions in every cell type and every labeling step a priori in a fluorescence microscope.

   Osmium tetroxide, which reacts with lipids, is widely used in electron microscopy as a secondary fixative. The unsaturated bonds of fatty acids are oxidized by OSO_4 and it is reduced to a black metallic osmium (mw-254.2) which is electron dense and adds contrast to biological tissue as a secondary label. However, presence of OsO_4 may quench the fluorescence and therefore it is not advised to be used for (S)CLEM of whole cells.
8. For additional immuno-labelling, and/or staining actin via phalloidin, cells were washed with PBS, permeabilized 15 minutes at RT with 0.1%Triton in PBS, rinsed with PBS-0.1% Tween, and re-washed with PBS 2x5 minutes. The cells were incubated at least 1 hour at RT with 5% BSA in PBS-T to block nonspecific binding of the antibodies. Then they were incubated 45 minutes at 37°C with primary antibody in PBS-T 1%BSA. They are rinsed with PBS-T and intensely washed 2x5 minutes, 1x15minutes with PBS. Then cells were incubated 45 minutes at 37°C with secondary antibody in PBS-T, rinsed with PBS-T, and 2x5 minutes, 1x20 minutes washed with PBS.
9. A similar procedure can be also used for immuno-gold labelling.
10. The cells were dehydrated in degraded ethanol series (20%, 50%, 70%, 90% and 100%) by dipping the sample at least 2 minutes per concentration.
11. The samples were air-dried.

C. *Preparation of Resin-Embedded Cells or Tissues*

i. *Principle*

SCLEM can be used to image thin tissue or cellular sections after combined FM and EM staining. Several approaches have been reported that allow for EM staining while preserving fluorescence [47–49,51,52,69]. Additionally, small semiconductor nanocrystals, or quantum dots, can be used to label proteins of interest in tissue sections subjected to CLEM [81]. Their distinct fluorescent properties and electron-dense structure makes them good markers for SCLEM applications.

ii. *Protocol*

12. Clean ITO Slides
    The slides are sonicated in EtOH for 2 minutes and rinsed with ddH2O.
13. Prepare Tissue Sections
    The tissue sections are prepared following the selected preparation protocol and mounted either directly on cleaned ITO slides or on TEM grids as usual.
14. Mount the Grids on ITO Slides.
    If sections are mounted on the TEM grids, the grids are attached to the conductive side of the ITO slides with conductive carbon tape or silver adhesive.

D. *Imaging in the Integrated Light and Scanning Electron Microscope*

i. *Principle*

Integrated light and electron microscopes offer the advantages of fast retrieval of regions of interest identified in FM in the EM. Additionally, the risk of sample contamination or damage during transfer between separate microscopes is mitigated. In the SECOM system, an inverted epi-fluorescence microscope has been positioned underneath the sample stage in a scanning electron microscope. A sample mounted in the SECOM microscope can thus be observed in epi-fluorescence from below, through the ITO-coated glass slide, and with the scanning electron microscope from above. High-magnification and high-resolution fluorescence microscopy can be performed using vacuum compatible immersion oil. Both microscopes share the same field of view, such that higher magnification SEM images can be recorded at any position within the fluorescence field of view. A new fluorescence field of view is selected by translating the sample remotely. This allows inspection of a large number of regions of interest.

In the integrated microscope used for SCLEM, an axial alignment of 10 μm between FM and SEM is assured. This can be further improved down to sub 1 μm with the beam deflectors present in the SEM [66]. In SCLEM, a more precise light and electron image registration, up to a notable accuracy of sub-5 nm, can be achieved by monitoring the position of electron beam generated cathodoluminescence (CL) in the fluorescence microscope [84]. This procedure can also be used to correct aberrations between different spectral detection bands in the FM measurements (see Chapter 4). Below, this procedure is briefly outlined although at the time of writing it is already being incorporated and tested as an automated procedure in the commercial SECOM software.

ii. *Protocol*

In situ fluorescence microscopy

15. The cover slide was mounted onto underside of the sample holder for the SECOM platform with the ITO-coated side contacting the holder. We used conductive carbon tape to fix the sample to the holder but silver adhesive can be alternatively used. Mounting samples into the integrated microscope is illustrated with pictures in Figure 2.
16. A drop of (vacuum-compatible) immersion oil (refractive index of 1, 52) was applied to the objective lens. The sample holder was placed on the integrated microscope with the underside facing the objective lens and the upperside with sample facing the SEM column. The objective lens was raised to bring the droplet in contact with the glass slide.
17. The vacuum door was closed and the SEM chamber was pumped down.
18. Making use of the large field of view of the SEM, a low magnification SEM image with a field of view of several millimeters squared was recorded. Based on this image, regions on the substrate were selected for focusing the fluorescence and electron microscopes (see Figure 3). The sample stage was translated to bring the respective regions into the center of the SEM field of view and focusing procedures were carried out.
19. Array of CL pointers are formed and recorded in the FM.
    Multiple arrays are recorded and averaged for a better accuracy. Pre-known array coordinates in SEM are compared with the measured coordinates in the FM images. The necessary local transformation function is calculated and the global distortion map is generated.
    This distortion map is determined once for the FM field of view and stored for later reference.
20. Based on the low-magnification SEM image of the sample (see 18) regions of interest, e.g. containing single or few touching cells, were selected. The sample was translated to bring the first region of interest into the center of the SEM field of view and fluorescence images were recorded. An LED light source with a wavelength of 485 nm and a power of 172mW (Spectra, Lumencor) was used for excitation of GFP and the emission was detected through a 520/10 nm band-pass filter (Thorlabs) with a CCD camera (Clara, Andor). An exposure time of 1 second with LED power of 10 mW was sufficient in most cases.

Electron imaging and whole cell analysis

21. Based on the FM observations, ROIs for SEM high-resolution structural inspection are selected, and SEM image(s) of the selected ROIs are recorded.
    After the acquisition of FM images, the same area was imaged by SEM and higher magnification images were recorded to capture details of filopodia and cellular extensions (Figure 3). Care was taken to record all fluorescence information before image the area by SEM as at this magnification, electron exposure bleaches the fluorescence.

The SEM was operated in both Secondary Electron (SE) and BackScattered Electron (BSE) mode using the Everhart-Thornley Detector (ETD) and solid-state BackScatter Detector (BSED), respectively.

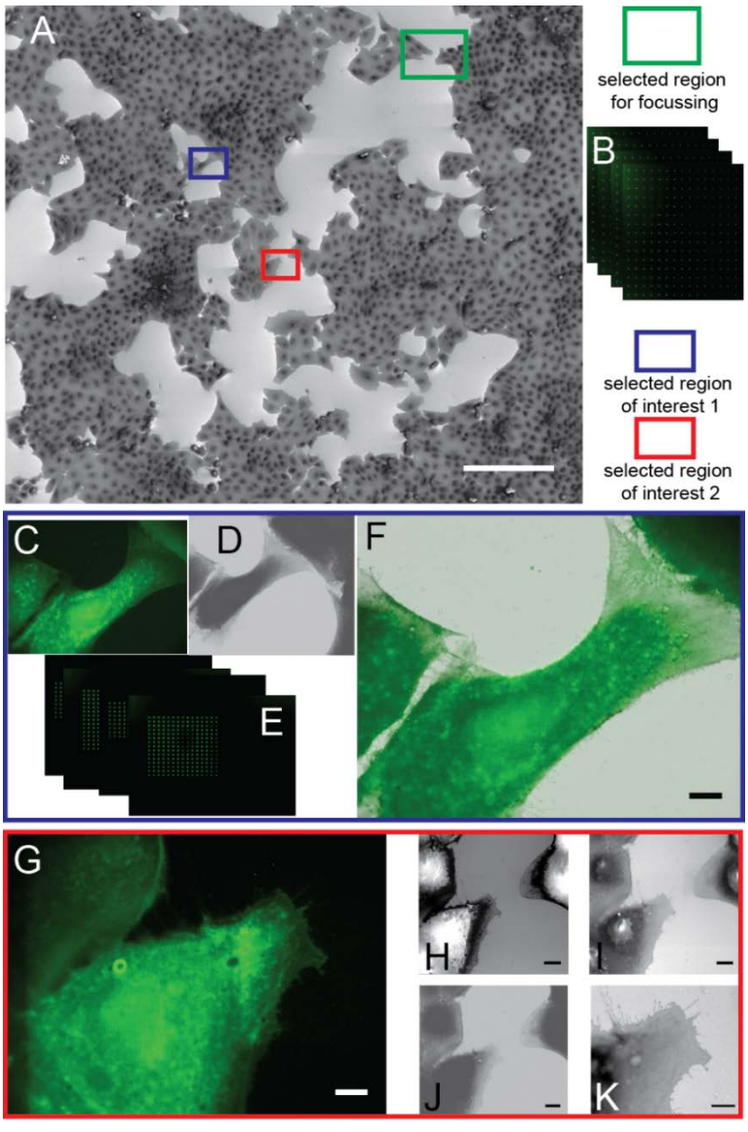

Figure 3. Integrated light and scanning electron microscopy of whole MDCK cells expressing Paxillin-GFP. A: Low-magnification SEM image recorded as a sample reference. Scalebar is 200µm. Sample regions for fine focusing of the microscopes and CLEM investigation have been marked with colored boxes. **C:** Fluorescence image showing GFP signal from the blue-boxed area in A. **D:** SEM BSED image of the same area recorded at 5 keV. **E:** Pointer arrays for distortion map calculations are formed and recorded in the FM. **F:** Recorded FM and SEM images of the blue-boxed region in (A) are overlaid according to the calculated transformation. Scalebar is 5µm. **G:** Fluorescence image showing GFP signal from the red-boxed area in A. Scalebar is 5µm. **H-I:** SEM images recorded with the ETD at electron voltages of 2 keV (H) and 5 keV (I). **J:** SEM BSED image recorded at 5 keV. **K:** Higher magnification ETD image showing detail on the filopodia network at the cell edge. Scalebars are 10 µm in (H), (I), (J) and is 5 µm in (K).

The SE are low energy electrons (<50 eV) generated by inelastic collisions when the incident electron beam hits the sample. SE's only escape the sample from a shallow depth which makes the SE signal particularly sensitive to the sample surface. On the other hand, the higher energy BSE's reveal topographic information as well as internal features of a sample. In addition, the electron acceleration voltage affects the penetration depth of the incident electrons and thus higher voltage electrons can probe a larger sample depth. This is illustrated in Figure 3.H and I, which show SEM images made with the ETD at acceleration voltages of, respectively, 2 keV and 5 keV. For comparison, Figure 3.J shows the image recorded with the BSED at 5 keV landing energy, which clearly reflects less surface detail than both ETD images. Note that as the mean atomic number of the ITO-coated substrate is higher than that of cellular features, the latter are imaged with a negative contrast in the BSED images. The thicker and/or denser parts in the sample, like the nucleus and surrounding area appear dark in the BSED image. We also want to note here that as discussed by Pluk et al. not only the acceleration voltage but also the ITO coating thickness influences the BSED image contrast [71]. The higher magnification SEM image in Figure 3.K was recorded to show the structural detail at the cell edge. Filopodia at the edge not facing neighboring cells (marked with an asterix) are relatively shorter and appear more rounded compared filipodia at the opposite edge that faces a neighbouring cell (marked with an arrow).

The optimized SEM imaging parameters for imaging inter-cellular connections in MCDK cells cultured on ITO coated glass coverslips (Figure 3.D and K), were as follows: accelation voltage was 5 keV, beam current was 0,4 nA, and the image was recorded with 10 µs dwell time (4096 X 3536 pixels), at a working distance of 8 mm, in high vacuum conditions.

22. An array of CL pointers is defined within the SEM field of view, and recorded in FM.
23. Measured pointer positions are corrected according to the corresponding vectors in the pre-recorded distortion map.
24. Translation, rotation and linear scaling are determined.
    In this way, automated overlay per image pair can be achieved, for a typical array size of 10 - 1000 CL pointers, in 0.1 - 10s.
25. Recorded FM and SEM images are overlaid according to the calculated transformation.

In the series of fluorescence (Figure 3.C), BSED (Figure 3.D) and overlay (Figure 3.F) images two regions with a finely detailed network of cell-cell connections can be observed (marked with arrows), showing how SCLEM can enhance the fluorescence image with structural detail. The composite overlay image (Figure 3.F) was made as detailed above (see 19-25).

Remarks

Here, we have presented the complete protocol for SCLEM with high registration accuracy. The procedures for preparation of samples intended for SCLEM imaging, and mounting the prepared samples in the integrated microscope were explained comprehensively. We also explained the imaging steps required to assure high accuracy registration and demonstrate the procedure by imaging spatial distribution of GFP labelled paxillin with respect to the cellular morphology of whole MDCK cells cultured on ITO slides (Figure 2).

We believe that the SCLEM approach will become of importance to biological sciences. It can expand the routine use of correlative microscopy and increase the throughput of CLEM studies. The SCLEM system we have worked with has in the meantime been commercialized as the SECOM system by Delmic. At the time of writing three SECOM systems have been installed at customers. Also other, although in our opinion less powerful, integrated solutions have been brought to the market in the past few years, such as the iCorr by FEI [50,62,85] and the Clairscope by JEOL [42,64,65]. Particularly, SCLEM can enable high-throughput 3D correlative studies on protein distributions and ultrastructure, complimented with approaches such as array tomography [29,86]. Also, the possibility of automated molecular level image registration within the FM and SEM images will open up new opportunities for precise quantitative analysis of protein localizations with respect to ultra-structural information of the SEM images. The availability of sample preparation protocols and inspection procedures for integrated microscopy that can be applied and followed by non-specialists is crucial in opening the technology for the wider biological research community.

Acknowledgements

We would like to thank Martijn de Gruijter, Gert van Cappelle and Prof. Adriaan Houtsmuller for the samples and biological questions resulting in Figure 3. We also thank Robert Moerland for photographs in Figure 2.

Chapter IV

Image Registration and Chromatic Distortion Correction in Multi-Color Correlative Light-Electron Microscopy

The identification of multiple bio-molecules within cellular ultrastructure needs correlation of multi-color fluorescence expression with electron microscopy (EM) data. Integrated light and electron microscopes may make for facile CLEM inspection procedures amenable to the quantitative imaging of large amounts of tissue data. However, flexibility in the use of multi-color fluorescence microscopy has so far been limited and image registration procedures for multi-color CLEM rely on the use of several distinct fiducial markers. Here, we show that multi-color fluorescence excitation and detection can be easily and flexibly incorporated in simultaneous correlative light and electron microscopy (SCLEM). Precise light and electron image registration can be performed by monitoring the position of electron beam generated cathodoluminescence in the fluorescence microscope. We show that by the detection of cathodoluminescence, channel mis-registration in the dual color fluorescence microscope can be characterized and corrected for. The total approach enables investigation of the physical proximity of fluorescently labelled molecules, combined with high resolution, ultra structural information from the SEM images in a way that could be adopted with fully automated inspection procedures.

This chapter is in preparation for publication as:

Liv, N., Haring, M. T Peters, H. G. P., van der Hoeven, B., Legerstee, K., Barcena, M., Cappelle, G., Houtsmuller, A., Koster, A., J., Kruit, P., & Hoogenboom, J. P. (n.d.). Image Registration and Chromatic Distortion Correction in Multi-Color Correlative Light and Electron Microscopy. *In Preparation.*

Introduction

Correlative light and electron microscopy (CLEM) emerges as an important tool facilitating studies into biological structure- function relations at the nanoscale level. As CLEM can provide ultra-structural (EM) and functional (LM) information together about cellular elements within the vast context of the cells and tissues, it has been shown to be an effective tool to study unique and rare events [69, 81, 54, 71, 87, 88, 49, 76, 89]. To investigate biological processes it can be very powerful to image the interplay of multiple proteins. It is one of the strengths of fluorescence microscopy(FM) that 3- 4 or sometimes even more labelled biomolecules can be followed in time [29,90]. As fluorescent markers can provide the functional information in CLEM, availability and applicability of many fluorescent labels enrich CLEM studies and enable identification and co-localization studies of various bio-molecules with ultrastructural cellular components [67].

Correlation of fluorescence with electron microscopy (EM) can be facilitated with integrated approaches, of which several have been presented during the past few years. The first integration was presented by Wouters et al. [61], in a scanning electron microscope(SEM) and integration has also been implemented in a transmission electron microscope (TEM) [62]. More recent integration approaches for SEM were presented by Nakamura and coworkers, who drilled a hole in the center of a light objective lens to allow passage of the electron beam [63], and by Nishiyama and coworkers, who imaged the sample by the SEM through a thin membrane with the light microscope located above the thin film in the ambient atmosphere [42]. From a technological side, integration can be complicated and the mentioned approaches compromise on the stand-alone capabilities of LM and/or EM [66], and may also hamper the use of multi-color FM at its full capabilities. In addition, for high-resolution, quantitative CLEM studies, it is important to achieve the best possible registration between the different color images and the EM image.

We have recently presented a microscope that allows for Simultaneous CLEM (SCLEM) and integrates a FM and a SEM without compromising on the capabilities of the stand-alone systems. Apart from the usability of high-NA oil immersion objectives, additional advantages are: a precise overlay of the fluorescence image and the SEM image, and flexibility in the configuration of the LM instrumentation [66,83]. Here, we will demonstrate that the LM setup can be used for multi-color FM, both through excitation and emission filtering. Various excitation sources and emission channels which can be easily integrated in multi-color SCLEM offer different combinations for usable fluorescent labels. In general, two- or more color FM can be achieved in two ways or by a combination of these two. One is by changing the excitation wavelength, hence exciting different dyes of which the emission is detected sequentially on the same detector. The other is by using single color excitation and separating the emission of dyes with different Stokes shift through filters. In the latter case, either multiple detectors can be used or one detector can be used sequentially by changing the filters.

A general issue in multi-color FM with multiple emission detection channels is the mutual registration of the color channels. Chromatic aberrations and distortions induced by imperfections in or misplacement of inserted elements, such as filters, can lead to misregistration and thus

improper image overlay and co-localization errors. Considering diffraction limited optical setups, a geometrical correction in between color channels is typically applied. With a resolution limit of ~250 nm, a geometrical correction is sufficient and for many wide-field fluorescence applications there will be no need for additional high precision registration methods. Custom-made objective lenses that contain elements for the correction of chromatic aberrations can be purchased, but the correction is typically defined only at specific wavelengths and may vary between 10 to 100 nm. High precision registration, as e.g. needed in super-resolution microscopy [16, 49, 76] needs additional careful calibration using calibration samples or the insertion of fiducial markers in the samples. A variety of methods and evaluations have been previously reported for co-localization of fluorescent emitters [91, 92, 93, 94, 95]. In those studies, the transformation is mostly achieved using fluorescent beads as fiducial markers. Fiducial beads are imaged over the field sequentially with respective fluorescence detection channels and a mapping is calculated by determination of a group of control points [96]. However, it is hard to assure the presence of fiducials at the required density and it can be difficult to introduce such fiducials to certain biological samples [97]. Also registration based on fiducial markers may be hard to combine with imaging large amounts of tissue [33,52,89] where registration should be reproducible from image to image and preferably be determined in an automated fashion. As stated above, also calibration samples can be used and stepped through the field of view with a piezo-stage, but precise image overlay would require calibration before each measurement series as the nanometer scale image alignment may vary over time. Given the nanometer scale detail of the EM, correction of chromatic registration errors down to the nanometer scale is especially important for multi-color CLEM [98]. A desired method for image registration in CLEM should therefore satisfy the following requirements: (i) it should have an appropriate (sub-10 nm) precision for ultrastructural studies, (ii) it should be applicable regardless of the bandwidth of the fluorescent staining of the sample, (iii) it should be comprehensive considering the range of samples it can be applied on, and last but not least, (iv) it should be entirely reproducible and preferably automatable.

Recently, we have presented a methodology for Automated Light-Electron Overlay at High Accuracy (ALOHA) [84]. ALOHA is based on monitoring the position of electron beam (e-beam) generated cathodoluminescence from the sample substrate in the fluorescence microscope to achieve a light and electron image registration with (bio)molecular precision, i.e., 5 nm or lower. Here, we show that the same approach can be used to correct for chromatic distortions in between different FM color channels and to register multi-color fluorescence images and a SEM image in a single coordinate frame.

Results and Discussion

Multi-Color Fluorescence Microscopy in the integrated microscope

We implemented both excitation and emission filtering as indicated in Figure 1.a. For multi-color imaging, the integrated high-NA fluorescence microscope was equipped with a multi-color excitation source. The excitation was obtained with a four color LED light source and the

corresponding emission filters *(Spectra, Lumencor)*. A filter wheel that can house 6 distinct filters was inserted in the detection path to spectrally resolve the emission lines with a single CCD camera.

The inset in Figure 1.a shows a result for a standard commercial fluorescence inspection sample (*FluoCells*R *prepared slide #1, Invitrogen*). It consists of bovine pulmonary artery endothelial cells (BPAEC) labelled with Alexa Fluor 488 Phalloidin for actin filaments, and with MitoTracker Red CMXRos for mitochondria. These fluorophores were excited with 485/20 nm and 560/25 nm sources and detected through 520/10 and 620/10 nm filters, respectively. Actin and mitochondria signals were recorded as sequential monochrome images and then superimposed. A 100X, 1.4 NA, oil- immersion lens (Nikon, CFI Plan Apochromat VC 100x) with vacuum-compatible immersion oil was used. To illustrate the performance of the integrated fluorescence microscope, a line profile was taken over one actin filament (Figure 1.b). The presented intensity profile has a full width at half maximum of 290 nm, indicating diffraction limited operation. As this test sample is embedded between a coverslip and a glass slide, it is unsuitable for correlative microscopy.

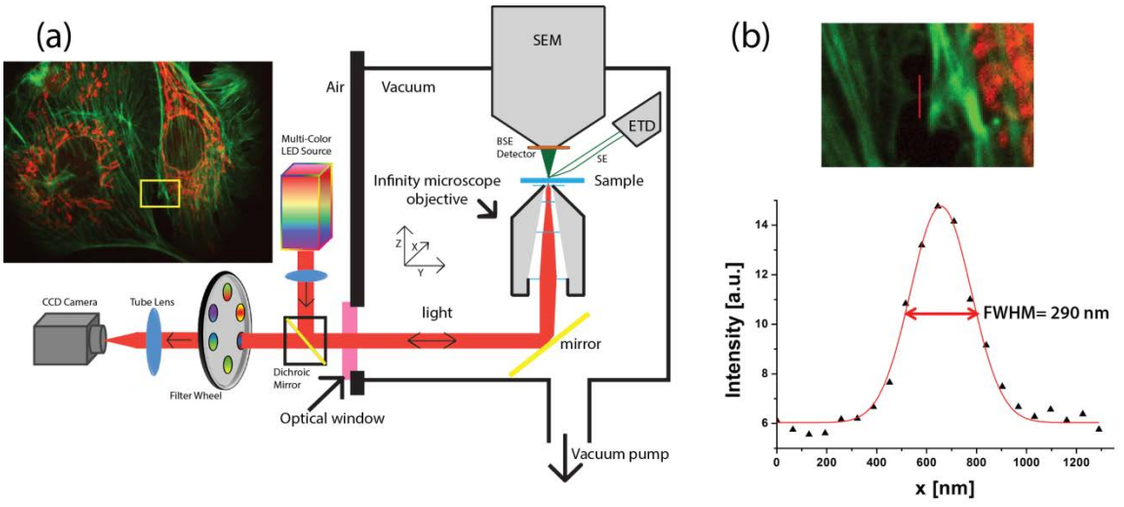

Figure 1. Multi-color SCLEM platform (a) Schematic illustration of the platform. The objective lens and the sample stage is mounted on the door plate, inside the SEM vacuum chamber. Light is guided by a mirror through an optical window mounted in the door of the vacuum chamber. Illumination and detection occurs in epi configuration. For multi-color fluorescent imaging, the platform is equipped with a 4-line LED excitation source and multiple emission filters hosted in a filter-wheel. The SEM is operated as accustomed. The fluorescent image is acquired in the integrated microscope, from a standard fluorescence inspection sample in which the actin filaments are labelled with Alexa Fluor 488 Phalloidin, and mitochondria is labelled with MitoTracker Red CMXRos. The image in **(b)** shows an enlarged image of the yellow boxed area in (a). The intensity profile taken over an actin filament as indicated by the red line is presented below, and has a FWHM of 290 nm.

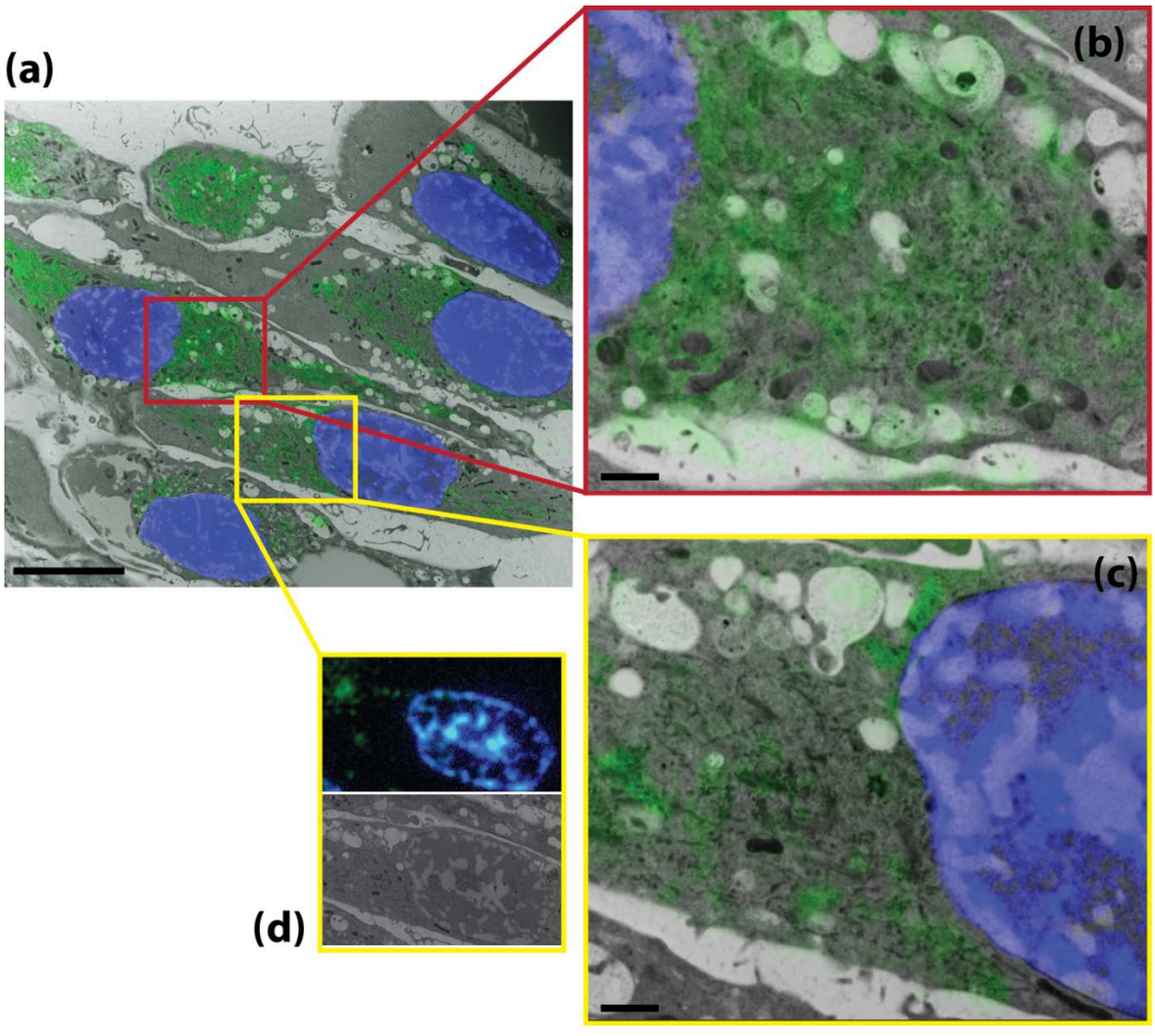

Figure 2. Imaging thin tissue sections with multi-color SCLEM.
EAV infected cells, where EAV expresses GFP from its replicase gene and the cell nuclei are stained with Hoechst 3458 imaged with two-color SCLEM. The fluorescent images were superimposed onto the corresponding SEM images. **(a)** An image with a large field of view is presented. This is useful to navigate and select regions of interest for higher magnification images. **(b)** A higher magnification image from the red boxed area in (a). **(c)** A higher magnification image from the yellow boxed area in (a). **(d)** The fluorescent image and the SEM image are separately provided for the cellular region depicted with a yellow rectangle. The fluorescence provides information about the location of the viruses, and the SEM image shows the underlying structure with higher resolution. Scalebars are 10 µm for (a), and 1 µm for (b) and (c).

Multi-Color Fluorescent Imaging with Excitation Selectivity

First, we illustrate two-color SCLEM using excitation selectivity. Recently, strategies to preserve fluorescence after EM staining have been reported [51]. These allow SCLEM to be applied on thin tissue sections. Here, we perform SCLEM to image Equine Arteritis Virus (EAV) infected cells, where EAV expresses GFP from its replicase gene [99]. The nuclei of the infected cells are labelled with Hoechst 34580. We chose a combined Hoechst and GFP staining as they can be excited with different wavelengths (390 nm and 485 nm, respectively) and detected sequentially onto the same camera without exchanging emission filters. Application of correlative light and electron microscopy to characterize the replication complexes of these positive strand RNA viruses has been also previously reported [100].

The fluorescence imaging of the thin sections was done with an aberration corrected CFI Plan Apo Lambda 40X objective lens (Nikon). The GFP signal, revealing positions of the viruses was detected using a 485/20 nm excitation and a 520/10 nm band-pass filter. Hoechst 34580, which binds to DNA and therefore shows the cell nuclei, was imaged using a 390/18 nm excitation and the same 520/10 nm detection band-pass filter. The narrow detection band allows both dye signals to be directly overlaid without chromatic distortion. SEM imaging was done with a FEI Quanta FEG 200 microscope, using a primary beam energy of 6 keV. The SEM image was recorded using a solid state backscatter detector. After applying a green and a blue LUT for GFP and Hoechst images respectively, they were overlaid onto each other. The two-color image was then overlaid onto the SEM image using the nuclei as registration markers. Figure 2 shows the final overlay image, together with a higher magnification images of selected regions depicted with a red and a blue box.

Chromatic Distortion Correction in the Integrated Microscope

When separate color channels are used for detection, the two monochrome images formed in different channels will not map directly onto each other due to the limited aberration correction range provided by the objective lens and possible deviations introduced by the exchange of emission filters. To achieve a high co-localization accuracy, one would typically need a non-linear transformation with respect to each other before being overlaid[96].

In the multi color SCLEM, we determine this transformation by recording, in the respective fluorescence detection channels, the cathodoluminescence (CL) signal that the electron beam generates in the substrate that supports the sample. We use ITO-coated glass for which the CL signal is broadband and therefore can be used for all fluorescence emission channels[101]. By focusing the electron beam into a single spot and exposing multiple spots within the integration time of the camera, we form an array of 'pointers'. The pixel positions of these pointers within the SEM image frame are known. The same array is exposed twice to record it in both fluorescence detection channels. The positions of the pointers in the FM images are then determined using a localization algorithm[102]. The dwell time per e-beam point is chosen to optimize the signal to noise ratio and thus minimize localization errors (a S/N ratio of 8 and 30 was achieved for 5 keV and 30 keV, respectively). Next, the transformation functions are calculated to map each fluorescence channel

onto the SEM coordinate frame. This FM-EM method, referred to as ALOHA, has been described in detail in[84]. It has been shown to yield a sub-5 nm FM-EM image overlay. We now use the SEM coordinate frame as a unique reference to determine the ultra-precise registration between the FM image channels.

To illustrate multi-color ALOHA, Figure 3 represents a grid of 169 pointers recorded in both 520/10 ('green') and 620/10 ('red') detection bands sequentially. Figure 3.a shows the two-color image as obtained by direct overlay of the two images. ALOHA was applied to the image sets from each detection channel as described above, overlaying them onto the SEM coordinates. For each grid this yields a set of coordinate pairs corresponding to the green and red pointer positions in the SEM coordinate frame. A frame offset between the red and green detection channels is clearly visible (see zoom in Figure 3.a, right) which is most probably introduced by different wedge angles in the emission filters (see also Supplemental). As this offset dominates over all other distortions, it was firstly removed to illustrate the remaining EM- FM transformation for each detection channel (Figure 3.b). For both channels, general tendency follows a hyperbolic like profile, but with clear local variations between both channels. In Figure 3.c, we plot the difference between each channel pair of transformed coordinates. Figure 3.d shows the same superimposed grids but after the transformation presented in Figure 3.b & c is applied. Comparing the zoom in images of single pointers in Figure 3.a and 3.d, the reduction of displacement in between channels is clearly visible after applying the transfer function on the misaligned grid pair. The pixel size in the represented images is 214 nm and circles are drawn around the fitted point centers of a single pointer in the zoom in images. The average displacement of fitted point centers between the red and green channels is 493 nm before the transformation, whereas it is improved to sub-15 nm after the calculated transformation is applied.

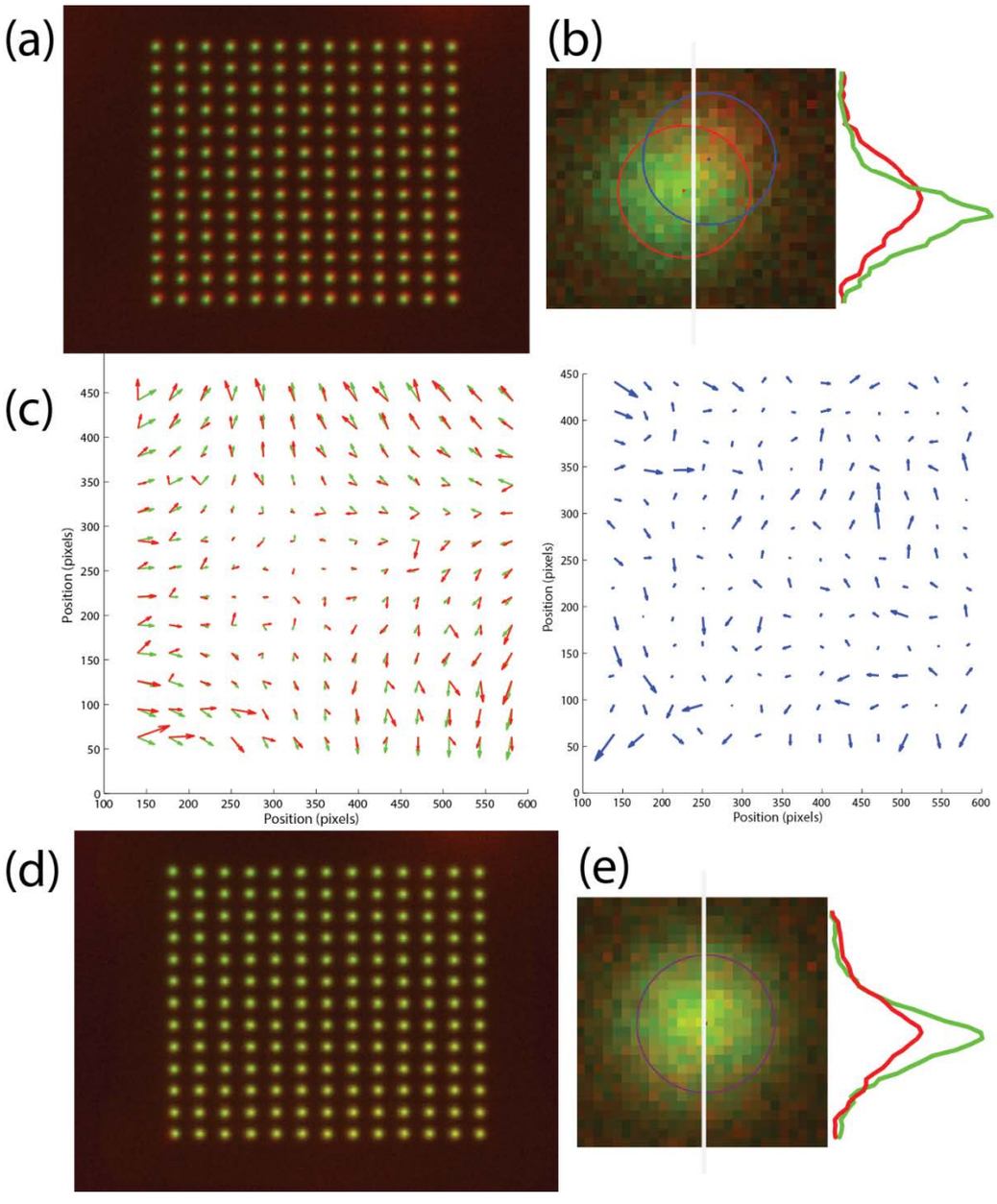

Figure 3. Correction of chromatic distortions in SCLEM. A grid of 169 CL points was created with the e-beam and recorded in both fluorescent channels. **(a)** Superimposed grids recorded in the green channel and in the red channel. **(b)** Circles where drawn around the fitted point centers in the zoom in image of a single pointer. Line profiles taken from the depicted white line in the image are shown next to the image for red and green colors. **(c)** A quiver plot representation of the calculated local transformation for both channels (left) and the difference between the transformations for each channel (right). **(d)** The superimposed grids after the calculated transformation is applied. **(e)** Zoom in images of single pointers and the line profiles clearly visualise the improvement of the alignment in between channels. Before correction, the average displacement of points between both channels is 493 nm (b) whereas it is sub-13 nm after the transformation (e).

Image Registration in Multi-Color SCLEM

The method presented above assures an accurate registration between the multi-color fluorescence images and the corresponding SEM images. To illustrate image registration in multi-color SCLEM, we imaged MDCK cells stably expressing GFP-paxillin and also immuno-labelled with TRITC for phospho-paxillin. As the fluorescent signals from GFP and TRITC labelling should overlap, this sample can nicely visualize the image registration.

Figure 4 shows the application of the method for image registration in multi-color SCLEM. The cells were plated on ITO coated glass coverslips, fixed, permeabilized and immuno-labelled with a primary antibody of rabbit anti-paxillin"phosphoY31" (*AbCam*) and a secondary antibody of goat anti-rabbit conjugated with TRITC. For fluorescence imaging of GFP a 485/20 nm excitation filter and a 520/10 nm emission filter were used. For TRITC the same exciation range was used but detection was done through a 620/10 nm filter. The SEM images were recorded with a solid state backscatter detector, using a primary beam energy of 5 keV. After recording a pair of fluorescence images and the corresponding SEM image, ALOHA was carried out using an array of 256 CL pointers that were detected with both of the fluorescent detection channels sequentially.

Two fluorescence images and the SEM image of the same area are presented in Figure 4.a. As expected both green and red fluorescence channel show the same features. The overlay of the fluorescence images before and after registration with ALOHA is shown in Figure 4.b. The marked, numbered areas in Figure 4.b, are shown enlarged in Figure 4.c, before and after registration. We note the improvement in the co-localization of red and green fluorescence signals after the transformation is applied. Line intensity profiles of the selected adhesion complexes are also presented next to the enlarged images (Figure 4.c (right)). The profiles from GFP-paxillin (green) and phospho-paxillin (red) predominantly overlaps with a slight variation in size as also reported previously by others [103].

Upon comparison of the fluorescence images and the SEM image, there is a striking similarity between the features occurring in each image. Figure 4.d shows the final overlay of the two fluorescence and the SEM images. Figure 4.e shows the higher magnification images of the red and blue boxed regions in Figure 4.d. The correspondence between the red fluorescence and the dark regions in the SEM image suggests a direct visibility of phosphorylated bio-structures in SEM. This we are currently investigating in more detail. We note here that this nicely illustrates how the possibility to routinely visualize various fluorescently labelled bio-molecules in registry with EM images can serve to investigate the bio-molecular composition of cellular structures. With the precision that can be reached with ALOHA, this can even be extended to the single-molecule level allowing the study of rare proteins, or the integration of fluorescence super-resolution techniques. The technique would be especially suited for correlative array tomography, in which a 3D sample is reconstructed through the inspection of thin serial sections[86]. As the thickness of the sections can be in the 30-50 nm range, this allows for high-resolution imaging in all three dimensions This 3D volume imaging with SEM, and also the imaging of large 2D tissue samples[89], ultimately requires

automated image recording and processing [33,104]. As our SCLEM methodology can be run in fully automated fashion, it may be an important step to integrate CLEM with large scale or 3D imaging.

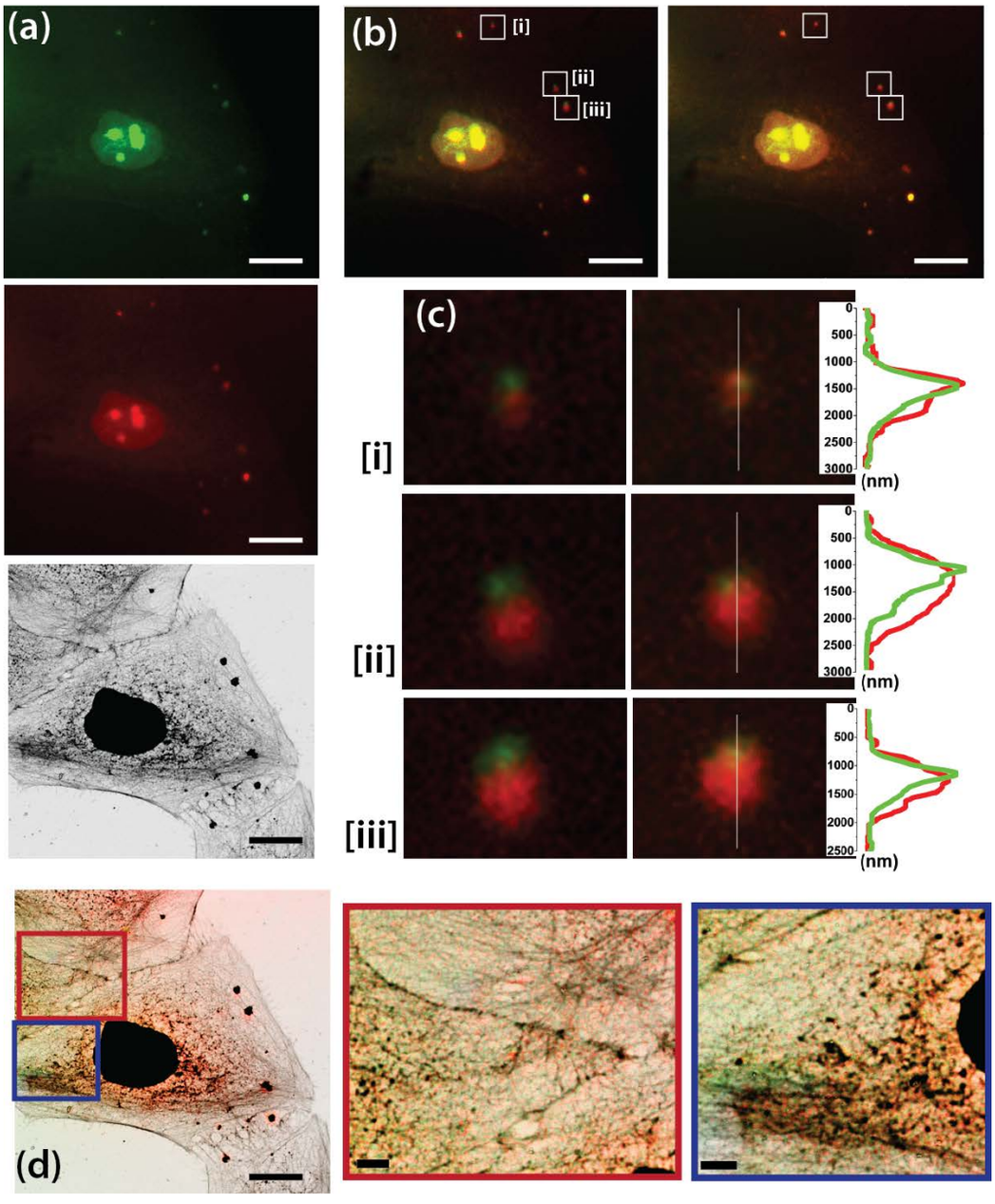

Figure 4. Image registration in multi-color SCLEM (a) Fluorescent images of GFP-Paxillin (green) and TRITC-Paxillin-"PhosphoY31" (red) and SEM image of the same area recorded with a solid state BSE detector **(b)** The overlay of the fluorescent images before (left) and after (right) the calculated transformation is applied. **(c)** Enlarged images of the depicted areas in (b) before (left) and after (right) correction. Horizontal full width of the images are 3,98 µm for [i], 2,9 µm for [ii], and 4,93 µm for [iii]. **(d)** Final superimposed image of the fluorescent image pair (green & red) and the SEM image. **(e)** Enlarged images of the red and blue boxed regions in(c). The images possess co-localization information together with the underlying structural SEM image. The scalebars are 10µm for (a), (b), and (d). The scalebars in (e) are both 2µm.

Conclusions

In conclusion, we presented the integration of multi-color fluorescence microscopy in SCLEM via both excitation and emission selectivity. Multi-color SCLEM can provide a fast and reproducible way for co-localization studies of multiple fluorescently labeled with ultra-structural information. This was illustrated with both EAV infected cell tissue and paxillin-labelled MDCK cells. We have shown that chromatic distortions between different fluorescence detection channels can be corrected for using the cathodoluminescence generated by the electron-beam in the sample substrate. This method also performs the image registration between the fluorescence and the corresponding SEM images. The presented method can be fully automated, does not require incorporation of fiducial markers in the sample or the sample substrate and is indiscriminative of the type of fluorescence labelling. It performs a local non-linear image registration over the entire fluorescence field of view and assures a high precision overlay between the fluorescence images and the structural SEM data. Automated recording of tissue data by SEM is crucial in emergent applications like large scale and 3D imaging. Thus, the multi-color SCLEM methodology presented here may be an important asset to integrate fluorescence detection of multiple bio-molecules in large scale imaging.

Material and methods

SCLEM Set-Up

The experiments were performed on a home-built integrated high NA light-electron microscope where an inverted epi-fluorescence microscope is integrated into a commercial SEM (FEI Quanta FEG 200). The integrated microscope is explained in detail elsewhere [66]. The set-up is also schematically indicated in Figure 1.a. The objective lenses used in the experiments were 1.4 NA Nikon CFI Plan Apo VC 100X oil immersion and 0.95 NA Nikon Plan Apo Lambda 40X. For the multi-color SCLEM, the system was equipped with a Spectra *(Lumencor)* light engine containing four illumination sources of 390/18 nm, 485/20 nm, 560/25 nm and 650/13 nm. A dichroic mirror with an edge wavelength of 506 nm was used to separate excitation form emission. The emission path was equipped with a filter wheel which houses 5 separate filters: 500 nm long-pass *(Semrock)*, 520/10 nm band-pass *(Thorlabs)*, 600 nm long-pass *(Semrock)*, 620/10 nm band-pass *(Thorlabs)* and 655/40 nm band-pass *(Semrock)*. The detection was done with an *Andor Clara E interline* CCD using Micro-manager[105] software.

Preparation of Tissue Sections

BHK cells infected with EAV expressing a GFP-tagged viral protein were high pressure frozen in medium and stored in liquid nitrogen. A long freeze substitution protocol using 0.1% UA as fixative was applied as reported before [48]. They were embedded in HM20 lowicryl, and polymerized with UV. 200 nm sections were cut and transferred onto TEM grids. The sections were stained for 20 min with Hoechst 34580. Prior to SEM imaging the TEM grids were attached on ITO coated glass slides.

Cell Culture, Fixation and Immuno-labeling of MDCK cells

The MDCK (Madin-Darby Canine Kidney Cells) epithelial cell-line, was grown in DMEM+ pen/strep and L-glutamine, with 10% FCS. The stable MDCK cell-line expressing Paxillin-GFP (obtained from A.B. Houtsmuller, EMC, Rotterdam) was maintained in the same way. Prior to seeding, ITO-coated microscope slides (thickness #1, 22x40mm with 70– 100 Ωsq−1; SPI Supplies.) were washed with ethanol and water, placed in 12-well tissue culture dishes with the conductive side upwards and washed with culture medium. The cells were 2x times washed with Phosphate Buffered Saline (PBS), then trypsinized and seeded onto the ITO coated glass slides. The cells are grown on the ITO coated coverslips for 18-24 hours aiming for ~60% confluency on the day of staining. Before the fixation the cells were washed several times with PBS and there after fixed in 2% paraformaldehyde in PBB for 10minutes. After the fixation cells were washed with PBS, permeabilized 15 minutes at RT with 0.1% TritonX100 in PBS, rinsed with PBS-0.1% Tween, and re-washed with PBS 2x5 minutes. The cells were incubated at least 1 hour at RT with 5% BSA in PBS-Tween to block nonspecific binding of the antibodies. Then they were incubated 45 minutes at 37°C with primary antibody (rabbit anti-paxillin "phosphoY31") in PBS-Tween 1%BSA. They were rinsed with PBS-Tween and intensely washed 2x5 minutes, 1x15 minutes with PBS. Then the slides were incubated 45 minutes at 37°C with secondary antibody (goat anti-rabbit conjugated with TRITC) in PBS-T, rinsed with PBS-T, and 2x5 minutes, 1x20 minutes washed with PBS. After the labeling the cells dehydrated in degraded ethanol series (20%, 50%, 70%, 90% and 100%), and air dried.

Acknowledgements

We would like to thank Barbara van der Hoeven, Montserrat Barcena and Bram Koster for sections of BHK cells infected with EAV & Karin Legerstee, Martijn de Gruijter, Gert van Cappelle and Prof. Adriaan Houtsmuller for the MDCK cells stably expressing Paxillin-GFP and biological questions resulting in Figure 2 and 4, respectively.

Appendix IV.A

Origin of the Chromatic Offset in Dual-Color SCLEM

In the dual-color fluorescence experiments using different fluorescence detection bands (Figures 3 and 4), we observed a significant offset between both color channels (see Figure 3.a). In this appendix, we investigate the origin of this offset and show that it can be attributed to the wedge angles of both band-pass filters.

In Figure 3.b in the previous chapter, we showed the remaining local FM-EM transformation for each color channel after correction for the offset. Figure 1.a and b, shows the original transformation plots without this offset correction. These experiments have been performed with narrow band emission filters (520/10 nm and 620/10 nm respectively). The narrow band filters were used to minimize chromatic distortion in the recorded pointer spot profiles. The result was obtained by recording 24 individual grids of 13x13 pointers and averaging over the 24 grids.

The filter wheel in the fluorescence detection path was now equipped with two additional filters that are specified to have zero wedge angle, a 500 nm and a 610 nm long-pass filters (both of *Semrock*). Figure 2.a and b displays the FM-EM transformation plots obtained with each of these filters. We note that now there is hardly a visible difference between both transformation, which is to be expected given the broad and, for >610 nm, overlapping spectral profile of detection channels. In fact, when an empty position in the filter wheel was used, we retrieved a similar transformation plot as well

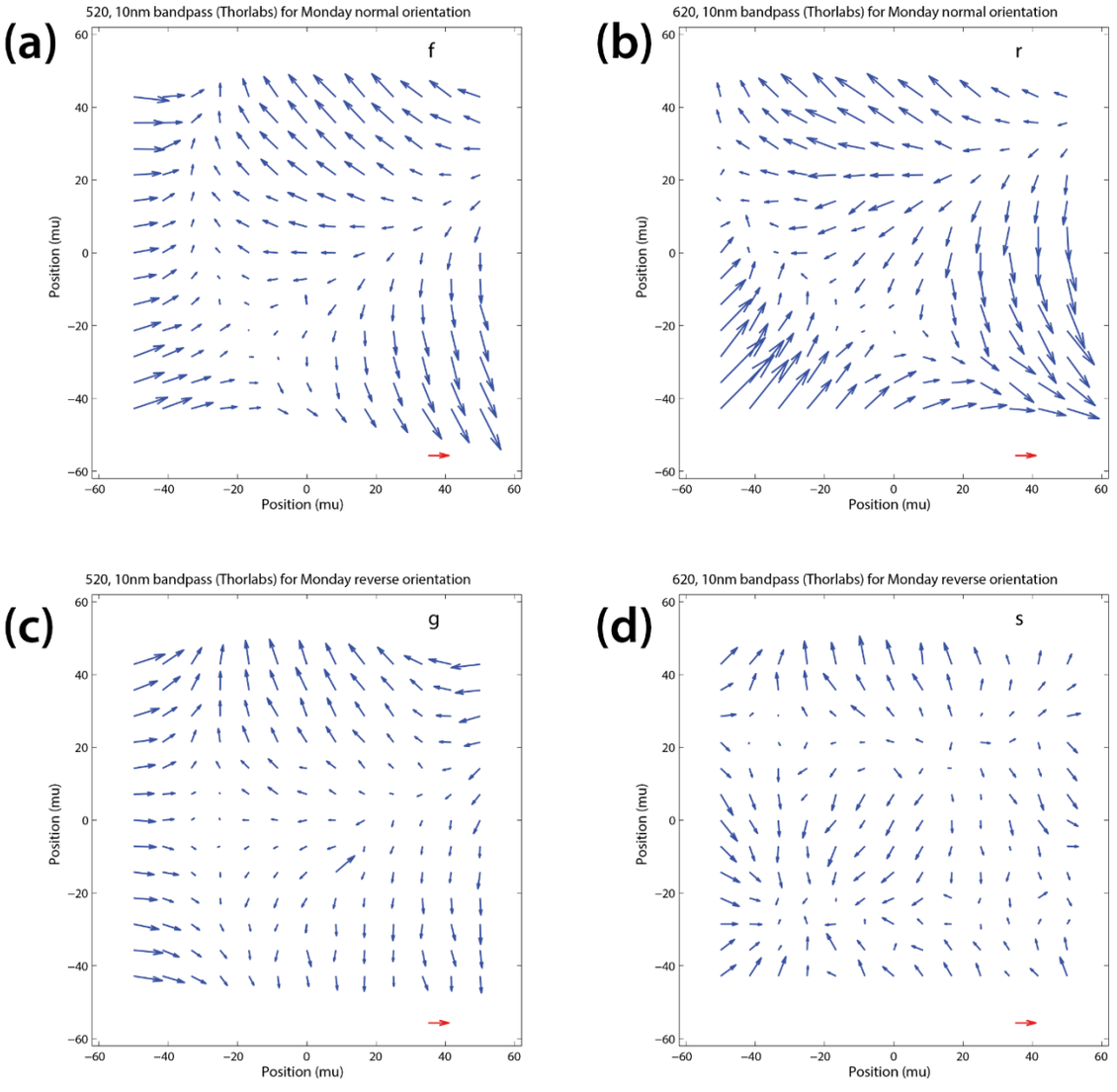

Figure 1. Transformation plots for narrow band-pass filters without offset correction. (a) 520/10 nm band-pass filter with normal orientation. **(b)** 620/10 nm band-pass filter with normal orientation. **(c)** 520/10 nm band-pass filter with reverse orientation. **(d)** 520/10 nm band-pass filter with reverse orientation.

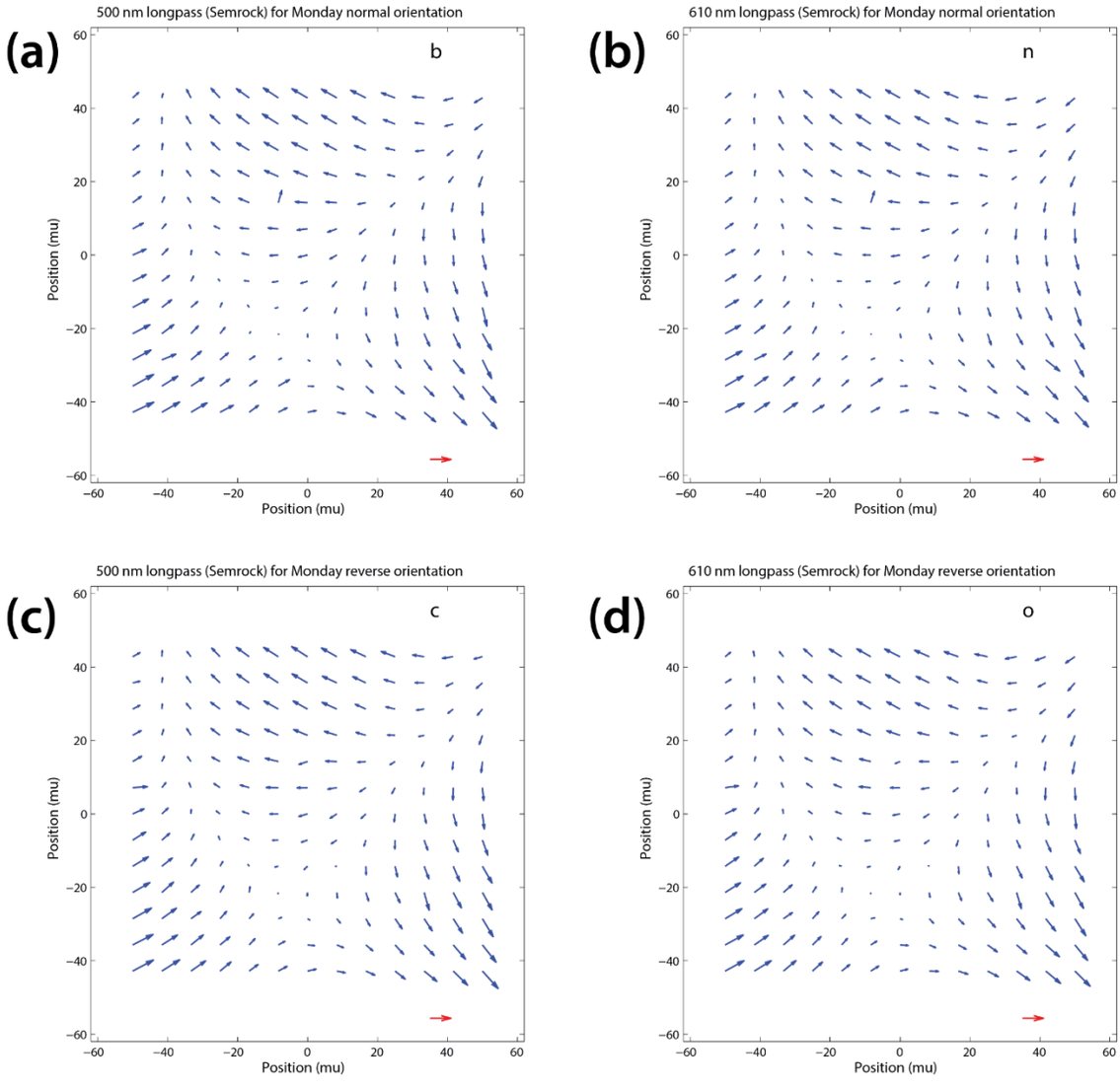

Figure 2. Transformation plots for long-pass filters without offset correction. (a) 500 nm long-pass filter with normal orientation. **(b)** 610 nm long-pass filter with normal orientation. **(c)** 500 nm long-pass filter with reverse orientation. **(d)** 610 nm long-pass filter with reverse orientation.

Next, we flipped the filter wheel and repeated the transformation measurement. Figure 1.c, d give the resulting plots for the original band-pass filters, and Figure 2.c, d for the zero wedge long-pass filters. It is immediately obvious that the plots for the zero wedge filters remained unchanged, while the flipped band-pass filters show a clear difference with the original configuration. In Table.1 we list the center position for each pointer grid averaged over the 24 measurements. These center positions were taken relative to the center position recorded without emission filter. It can be clearly seen that the change in x-position after flipping is negligible for the zero-wedge filters compared to the original filters. The change is y-position (direction of the flipping axis) is given as

a reference. An additional measurement exposing new pointer grids on a fresh sample gave results that were similar to within 7 nm (data not shown). Thus, we conclude that the observed offset in Figure 3.a in previous chapter is attributed to wedge angles in the used filters, which, together with remaining distortions between the detection channels, are corrected for by our registration procedure.

	x-position	**x-position flipped**	**x-position difference**	**y-position**	**y-position flipped**	**y-position difference**
520/10 nm band-pass	132	-154	286	1197	1209	12
620/10 nm band-pass	766	-765	1531	404	431	27
500 nm long-pass zero-wedge	-27	-33	6	-1	5	6
610 nm long-pass zero-wedge	-81	-63	18	-12	-10	2

Table 1: Center positions (*x,y*) of pointer grids for the different filters. Centers were taken relative to a grid recorded without a filter present. All positions are in nm. Filters were flipped along the *y*-axis.

Chapter V

Scanning Electron Microscopy of Individual Nanoparticle Bio-markers in Liquid

We investigated SEM imaging of nanoparticle biomarkers suspended below a thin membrane, with the ultimate goal of integrating functional fluorescence and structural SEM measurements of samples kept at ambient or hydrated conditions. In particular, we investigated how resolving power in liquid SEM is affected by the interaction of the electron beam with the membrane. Simulations with the Geant4-based Monte Carlo scheme developed by Kieft and Bosch (2008)[106] are compared to experimental results with suspended nanoparticles. For 20 nm and 50 nm thin membranes, we found a beam broadening of 1.5 nm and 3 nm, respectively, with an excellent agreement between simulations and experiments. 15 nm Au nanoparticles and bio-functionalized core-shell quantum dots can be individually resolved in denser clusters. We demonstrated the imaging of single EGF-conjugated quantum dots docked at filopodia during cellular uptake with both fluorescence microscopy and SEM *simultaneously*. These results open novel opportunities for correlating live fluorescence microscopy with structural electron microscopy.

This chapter is published as:

Liv, N., Lazić, I., Kruit, P., & Hoogenboom, J. P. (2013). Scanning electron microscopy of individual nanoparticle bio-markers in liquid. *Ultramicroscopy, 143, 93–99*.

Introduction

Electron microscopy (EM) is the preferred method for visualization of structural detail with nanometer scale resolution. In recent years, progress in thin film processing has enabled electron microscopy of samples under atmospheric conditions or even in liquid [41,107–113]. In these experiments, a liquid enclosure is used that contains one (for Scanning Electron Microscopy (SEM)[40,41,113]) or two (for Transmission Electron Microscopy (TEM / STEM)[110,111]) windows consisting of thin, electron transparent membranes**.** Considerable effort has been devoted recently to atmospheric TEM and STEM [107], showing, e.g., in-situ analysis of nanoparticle growth kinetics [109,114] and diffusion dynamics [109,115], and the investigation of fully hybridized biological cells [38]. Less attention has been paid to SEM [113]**,** while, as also demonstrated in the initial work, an SEM offers the distinct advantage of using a variety of additional detectors [41], including integrated light microscopy [42,63,66,78] . Notably, the space available beneath the sample makes the insertion of an inverted high-NA fluorescence microscope possible [66], which permits Simultaneous Correlative Light and Electron Microscopy (SCLEM) [83]: The straightforward projection of optical or fluorescence measurements onto the structural detail measured in EM. SEM through a membrane would then be particularly useful for live optical monitoring of cellular dynamics in-situ in an SEM. An important open question is the amount of structural detail that can be measured with SEM through a membrane.

Inherent to all applications of atmospheric- and liquid-EM is a loss of resolution due to the scattering of the probe beam in the membrane [41]. Work so far has indicated high resolution can still be attained [42], most notably for STEM [116]. The further development of liquid-SEM will benefit from a quantitative understanding of the broadening of the probe beam and the resolving power of liquid-(S)EM as a function of membrane thickness. Obviously, the thinner membrane will give more resolving power, but on the other hand, as the membrane needs to withstand an atmospheric pressure difference, limits the usable window area and increases the chance for membrane rupture. A reliable, a priori evaluation of the maximum membrane thickness that can still be allowed in an experiment is thus an indispensable tool for future work in liquid-(S)EM and liquid-SCLEM.

Thiberge and co-workers addressed beam broadening and imaging conditions for SEM in liquid [41]. They observed that beam energies in between 10-20 keV maximize the total signal originating from gold features as compared to water. However, in their research they used a comparatively thick (145 nm) polymer membrane, which substantially increases the beam broadening. The beam broadening in ~100 nm thick polymer samples has also been discussed in order to assess STEM imaging conditions for organic specimens [117]. Silicon nitride (SiN) membranes with thickness down to 20 nm can alternatively be used. For Si_3N_4 membranes of 50 nm thickness near atomic resolution was demonstrated in STEM, but here, beam energy typically amounts to 200 keV [116]. In the early work of Green and Kino [118], the use of SiN membranes was examined for SEM with thickness of 30-100 nm but only for beam energies from 20-50 keV. In addition, issues related to window curvature and additional sample-membrane spacing resulted in poor image definition resolving sub-micrometer scale features [113]

The high resolution in liquid-STEM was used by Dukes *et al.* [119] to show the imaging of single colloidal Quantum Dots (Qdots) bound to Epidermal Growth Factor (EGF) receptors of whole cells in saline water. QDots are promising probes for correlative light and electron microscopy applications as they exhibit visibility in both microscopes. By transferring the sample from a light microscope to the STEM, correlation between fluorescence and EM of the same cellular region could be achieved. However, liquid SEM imaging of single bio-conjugated QDots has not been demonstrated yet, while this would pave the way towards live-cell correlative microscopy.

Here, we quantitatively investigate how image resolution and contrast in liquid-SEM is affected by electron scattering in the membrane as a function of membrane thickness. We directly compare experimental results obtained with a model sample of Au nanoparticles with the results of the Geant4-based Monte Carlo simulations with low energy interaction model (<50 keV) which was implemented recently by Kieft and Bosch [106]. While we focus our attention to SEM imaging, the observed excellent agreement between simulations and experiments indicates the feasibility of this simulation approach for assessing other experimental conditions. We show that single nanoparticle biomarkers can be readily observed through a membrane. The potential of these results for integrated correlative light and electron microscopy is illustrated by pinpointing with both fluorescence and electron microscopy single bio-conjugated quantum dots during cellular uptake.SEM and (S)CLEM on Samples in Liquid

Figure 1.a illustrates the experimental realization of a sample contained under atmospheric or hydrated conditions in a SCLEM microscope [66,83], as used in our experiments. SEM occurs from above the sample, detecting electrons exiting the upper membrane. Light microscopy can occur from below the sample, through a transparent glass window or a thin membrane equivalent to the upper window. In Figure 1.b, we schematically depict the experimental situation for the electron imaging: the focused beam of primary electrons (PE) traverses a membrane of finite thickness *d*, and hits a sample attached to the membrane. Scattering of PE in the membrane occurs in both backward and forward direction. In the backward direction, Back-Scattered Electrons (BSE_M) and Secondary Electrons (SE_M) give rise to background signals on both the BSE detector (BSED) and the SE, or Everhardt-Thornley, detector (ETD). In the forward direction, PE scattering leads to a broadening of the primary beam in the membrane. Unscattered PE and high-energy forward scattered electrons exiting the membrane interact with the sample giving rise to BSE_S and SE_S signals. While the mean free path of the SE_S is insufficient to leave the membrane, a detectable SE signal from the sample may still occur as a result of secondary electrons generated in the membrane by electrons backscattered from the sample (SE_{BM}) [41]. Thus, on the BSED we detect a signal that originates from both membrane and sample, (BSE_M+BSE_S). The ETD signal is generated in the membrane by both primary beam and the electrons scattered from the sample, (SE_M+SE_{BM}). In both cases, the first term is a background term and the second originates from the sample. A thicker membrane will then not only lead to a loss of image resolution as a result of forward scattering of the electrons, but also to a loss of image contrast because the back scattering in the membrane decreases the signal and increases the background.Experimental Details

Liquid SEM of Nanoparticles

For liquid SEM imaging, a microfluidic enclosure with a Si_3N_4 membrane on top was used. First, the microchip bearing the Si_3N_4 membrane was placed in the enclosure. The Au nanoparticles or the Quantum Dots(QDots) was deposited on the membranes and dried. After drying, 70 µl of water was added in the enclosure, it was sealed with the lid and placed in the SEM chamber. The SEM (FEI, Quanta 200 FEG) was operated under High Vacuum with 20 keV primary beam energy and a working distance of 10 mm to 8 mm. The images were taken with 1024x1024 pixels with a pixel dwell time of 30 µs. Contrast and brightness were adjusted for maximum visibility and the whole line profile analysis was done with ImageJ on the original data, without applying any filters.

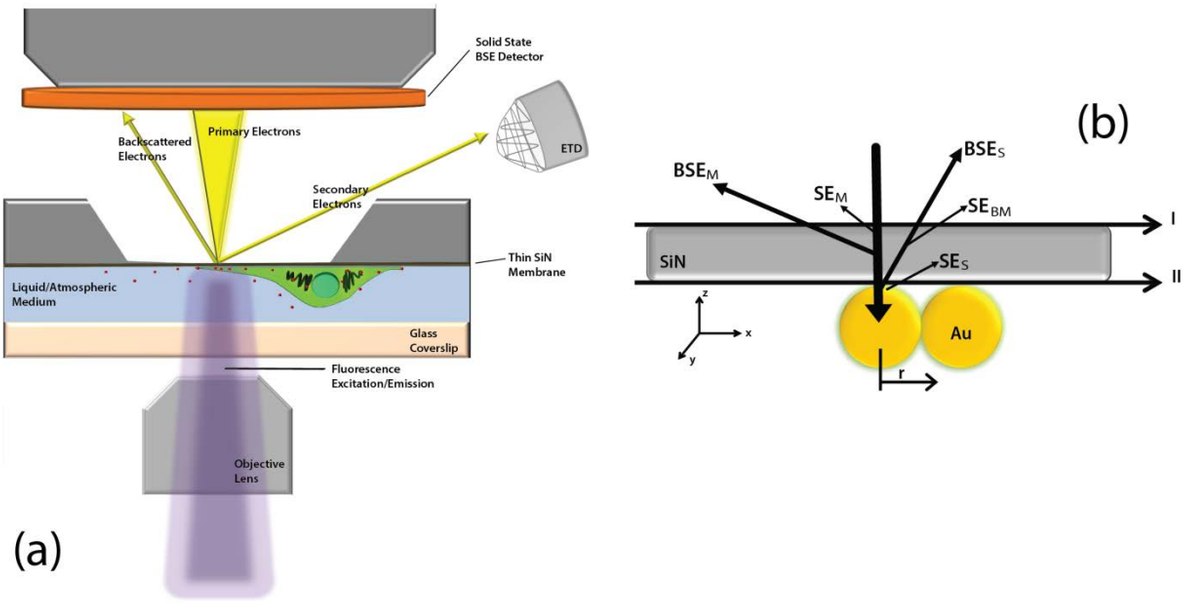

Figure 1: (a) Schematic illustration of the simultaneous observation with fluorescence and scanning electron microscopy of a sample shielded from the vacuum by a thin, electron-transparent membrane. (b) Scattering of primary electrons by a membrane (of thickness *d*) and a (Au) sample. High-energy backscattered electrons are generated in the membrane (BSE_M) and the sample (BSE_S). Low-energy secondary electrons are generated in membrane (SE_M, SE_{BM}) and sample (SE_S). SE_{BM} constitute an additional source of SE resulting from the interaction of BSE_S with the membrane. Similar scattering in the forward direction (not depicted) leads to a spreading of the primary beam in the membrane in the radial (*r*) direction. I and II indicate the planes where, in our simulations, backward, resp. forward travelling electrons are collected.

Geant4 Simulations

Geant4-based Monte Carlo scheme developed by Kieft and Bosch [106] is used for simulations on the evaluation of beam spreading and the evaluation of signal to background ratio in liquid SEM imaging. To record the energy, position and direction of each electron that is scattered or generated, any volume of real or artificial material can be defined as a sample, detector or simultaneous sample-detector within the Monte Carlo model based on Geant4 platform. Figure 1.b shows the schematic of the applied geometry for our simulations. In simulation runs, volumes on or above the surface of the membranes are defined as detectors of material with artificial properties, detecting the electron as soon as it enters the detector but not interacting with it (ideal detectors). For the evaluation of beam spreading, an ideal detector was defined below the Si_3N_4 membrane of thickness t_{memb} and the simulations were run for 10^6 electrons with a primary energy of 20 keV for each value of t_{memb}. Primary energy decision was based on the previously reported results, which show an intermediate energy range where the backscatter and secondary yields are highest for liquid SEM imaging [41]. Then, all electrons exiting the membrane (i.e., arriving at plane II indicated in Figure 1.b) are collected with their position relative to the primary beam and their energy. To evaluate the signal to background ratio, different sizes of Au Nanoparticles are placed below the membranes in the applied simulation geometry. The detector is defined above the SiN membrane and the primary beam is stepped along the x-axis with a step-size of 2 nm, for 10^6 electrons at each position and all electrons exiting the membrane with upward velocity (i.e. at plane I in Figure 1.b) are collected.

Culture and Labelling of CV1 cells

Monkey Kidney Fibroblast (CV1) cell line (Cell Lines Service, Germany), were maintained in DMEM supplemented with 10% Fetal Bovine Serum, Penicillin/Streptomycin and 2 mM Glutamine at 37°C under 5% CO_2. The cells were washed with Phosphate Buffered Saline (PBS) (pH 7.4), trypsinized with 1X TrypLE™ Express (Invitrogen) and then seeded onto sterile, poly-L -lysine coated, 50 nm thick Si_3N_4 membranes and they were grown overnight. Prior to Quantum Dot (QDot) labeling, the cells were incubated in serum free medium for 4 hours at 37° under 5% CO_2. For Qdot-EGF labeling, EGF-QDot conjugates were formed by incubating EGF-biotin (Invitrogen, USA) with streptavidin-QDot655 (Invitrogen, USA) for 2 h at room temperature in 50 mM borate buffer, pH 8.3. A microcentrifuge purification column (Ultracel-100YM, Millipore) was used to remove unbound EGF-biotin. Then the cells were incubated with 5 nM EGF-QDot655 in Tyrode's buffer (Sigma), supplemented with 0.1% BSA (Sigma) and 50 mM D-glucose (Sigma-Aldrich) for 15 min at room temperature [119]. After the staining, the cells were washed three times in PBS (Gibco) and fixed for 30 min with 2.5% glutaraldehyde in PBS. After fixation, the cells were washed three times with PBS, placed in the liquid enclosure which was sealed with an ITO coated cover-glass at the bottom. 70 µl of previously stated Tyrode's Buffer was added in the enclosure, and the sample was imaged in liquid in the integrated microscope.

SCLEM of CV1 cells

All SCLEM experiments were performed on a home-built integrated high NA light-electron microscope where an inverted epi-fluorescence microscope is integrated into a SEM (FEI Quanta FEG 200). The detailed description of the integrated microscope can be found elsewhere [66]. For SEM imaging of the CV1 cells with QDots, the SEM was operated under High Vacuum with 14 keV primary beam energy and a working distance of 8 mm. The images were taken with 1024x1024 pixels with a pixel dwell time of 100 μs.

For the fluorescence imaging of Qdot uptake in CV1 cell, the integrated microscope was equipped with a Nikon CFI PLAN APO, 40X, NA 0.95 dry objective lens and a Nikon 1.5x tube lens. A 470 nm Thorlabs LED source was used for illumination. A dichroic mirror (Semrock FF506-Di03), which has an edge wavelength of 506 nm, separates excitation and emission light. The detection path consisted of a 655 nm band-pass filter (Semrock 655/40 nm BriqhtLine®) and a CCD camera (Andor Clara). Images were recorded using μ- Manager1.2 with an exposure time of 2 seconds and no binning.

Results and Discussion

Resolution in scanning electron microscopy of liquid-immersed nanoparticles

We experimentally investigated the influence of membrane thickness on image quality in the SEM, by attaching a model sample consisting of 35 nm diameter Au nanoparticles (NP) to Si_3N_4 membranes of varying thickness. The Au NP-coated membranes were used to seal a water-containing enclosure that was placed in a FEI Quanta 200 FEG SEM. As a reference, the same Au NPs were imaged on a bare Si wafer in vacuum. Samples were imaged at an acceleration voltage of 20 keV in both BSE and SE detection mode. Brightness and contrast settings were adjusted through the video scope until the waveform nearly saturates the full dynamic range. No background subtraction, contrast stretching or gamma correction was applied to the SEM images to provide unbiased comparisons with the simulation results.

In Figure 2.a, we show SEM images of the hydrated Au NPs under membranes of 20 nm, 50 nm, and 100 nm thickness, together with the non-hydrated reference sample. Indeed, as membrane thickness increases, the image becomes blurred and contrast degrades. While for the 20 nm membrane the typical Au NP asphericity can still be clearly observed, edge information gets progressively lost for the 50 nm and 100 nm membranes and the particles appear more rounded.

We quantify the beam spreading by application of the Geant4-based Monte Carlo platform with low energy interaction model (<50 keV) implemented by Kieft and Bosch [106]. These simulations provide realistic results, not only for low energy (50 keV) regime, but also for SE detection, by taking into account all scattering cross-sections in the electron-material interactions with ray tracing through the material. The details about the simulation runs are mentioned in the corresponding section above. Electrons arriving at plane II indicated in Figure 1.b are collected with the

information about their position and their energy A significant amount of these are low-energy (<100 eV) secondary electrons, while only higher-energy unscattered or forward scattered PEs contribute to the BSE_S signal. The radial distribution function for the high-energy (>260 eV) electrons exiting the membrane is then calculated and integrated to obtain the cumulative number of electrons as a function of the radial distance *r* from the primary beam. We then calculated the Full Width 20 (FW20), FW50, and FW80, which are the distances containing the first 20%, 50%, and 80% of the electrons respectively. These provide an adequate measure of the size of the probe beam irrespective of its mathematical shape.

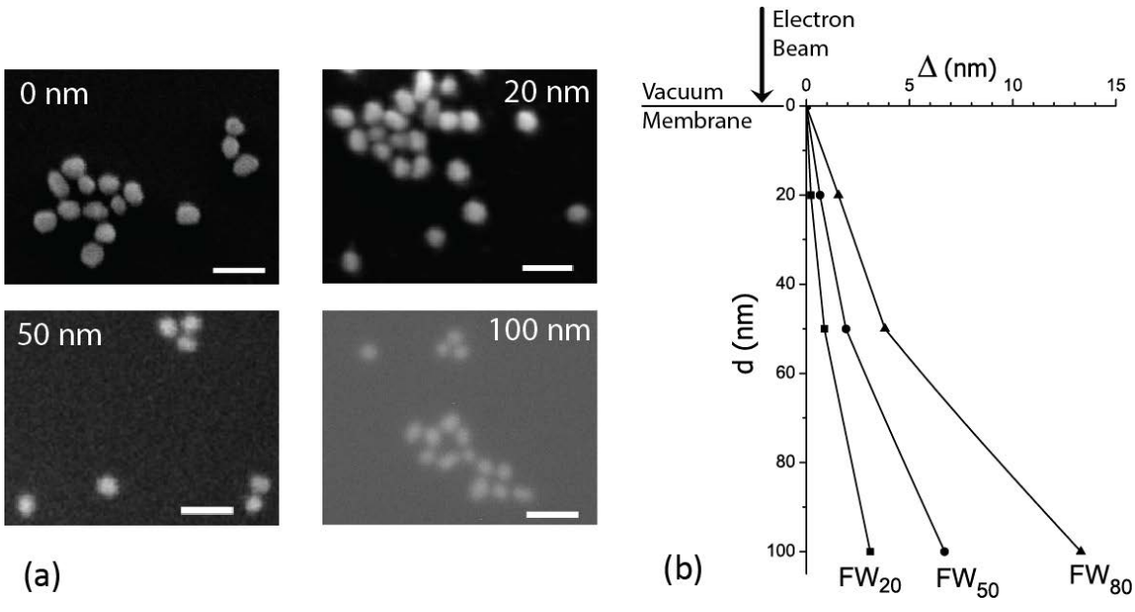

Figure 2. (a) Loss of resolution and degradation of signal to background contrast as a function of membrane thickness: SEM images of 35 nm diameter Au particles on top of a Si wafer in vacuum without membrane (top left, 0 nm) and in H_2O below membranes of varying thickness *d* (*d* = 20, 50, 100 nm). Scalebars are all 100 nm. (b) Simulation results for the spreading of the primary beam, for the values of the membrane thickness *d* that were used in (a). Black symbols denote full width at 20% (FW_{20}), 50% (FW_{50}), and 80% (FW_{80}) of the total number of electrons. Lines are drawn to guide the eye.

In Figure 2.b, we plot, the calculated results for FW20, FW50, and FW80. For the FW80, we find values of FW80 = 1.6 nm, 3.8 nm, and 13.3 nm for *d*=20 nm, 50 nm, and 100 nm respectively. A clear progressive increase of the beam spreading is observed for membranes *d* > 50 nm. The beam spreading due to elastic scattering though a thin foil can also be expressed with an analytical equation [19]. However, as has been reported previously, MC simulations including inelastic scattering events provide a more adequate approximation of the experimental findings [116].

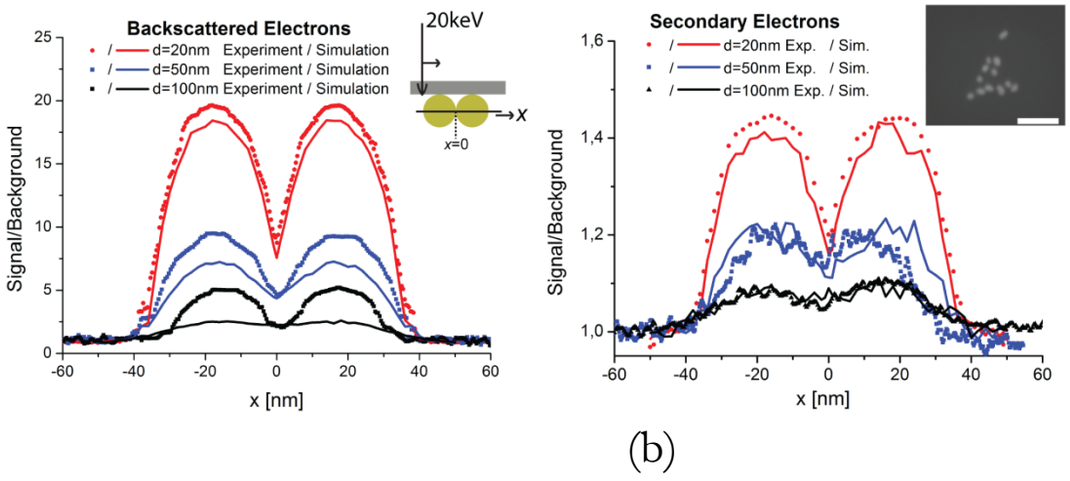

Figure 3: Signal to background ratio in the imaging of two touching 35 nm diameter Au nanoparticles with 20 keV primary energy under Si_3N_4 membranes of varying thickness *d*. (a) For backscatter electron detection, and (b) for secondary electron detection. The inset in (a) shows a sketch of the setup. Inset in (b) is a SE image of the Au nanoparticles in H_2O under a 20 nm membrane, scalebar is 200 nm.

To further investigate the influence of membrane thickness, we evaluated signal to background ratio in simulations and experiments for two 35 nm Au NPs attached below a membrane (see inset in Figure 3.a). All electrons exiting the membrane with upward velocity are collected in the simulations. The resulting curves for signal-to-background for BSE and SE detection are displayed in Figure 3. A similar procedure was followed in the experiments. The signal to background ratio was evaluated by taking line profiles over 50 pairs of touching Au NPs for each membrane. Evaluation of NP pairs allows us to directly assess the ability to resolve individual particles within a cluster. We take x as the direction of the axis through both NPs, with x=0 at the center between the two NPs (also see the inset in Figure 3.a). The intensity profiles were divided by the background intensity in the image, giving us $(BSE_S(x) + BSE_M)/BSE_M$. Then, these curves were averaged over all 50 pairs. The resulting signal to background curves, are shown in Figure 3.a for d=20 nm, 50 nm, and 100 nm with red, blue and black symbols respectively. For the images taken with the ETD the same procedure was followed giving the signal-to-background curves for SE in Figure 3.b. We observe a particularly high signal-to-background ratio of almost 20 for the BSED for the 20 nm membrane, whilst the other membrane individual NPs can also be clearly observed. As expected, the signal-to-background on the ETD is much lower, and individual NPs can only be readily discerned with the 20 nm membrane. For the SE, we observe quite good agreement between simulation and experimental results. For the BSE, agreement is also very good, while especially for 100 nm, the simulations underestimate the actual signal-to-background. In fact, while in the experiment two touching NPs can be clearly resolved under the 100 nm membrane, simulations predict observation of a flattened 200 nm sized feature. We attribute this to the finite collection

angle of the BSED, which was not taken into account in the simulations. As the low atomic number Si_3N_4 membrane scatters a comparatively higher fraction of electrons outside the BSED collection cone than the heavier Au particle, this overestimates the background compared to the signal. We exclude a discrepancy between actual and simulation BSE cross section, based on the agreement between simulated and experimental SE signal-to-background and the fact that in this case the SE signal consists of the SE_{BM}: SEs resulting from the interaction of BSE_S with the membrane. Finally, we note that the finite collection angle of the BSED could in principle be taken into account by ray-tracing all electrons through the SEM column field as originally performed by Kieft and Bosch [106].

Given the good correspondence between experiment and simulations, the ability to resolve individual particles can be investigated for particles of smaller size. In Figure 4.a, the simulation result for the BSE signal-to-background ratio for an Au NP doublet under a $d = 50$ nm membrane is shown for decreasing particle size. It can be seen that for the 50 nm membrane, particles down to 10 nm in diameter can be individually resolved. For smaller particle size, or lower material contrast, a 20 nm membrane would be necessary. Indeed, in Figure 4.b, we show BSED images of 15 nm diameter Au NPs in H_2O under a 20 nm membrane. Au NPs or colloidal quantum dots in the 10 nm to 20 nm size range are commonly used as bio-conjugated probes in, e.g., fluorescence microscopy and correlative light and electron microscopy [81]. In the SEM these particles can be readily resolved under hydrated conditions, even in dense clusters (see Figure 4.c). The ability to visualize individual fluorescent nanoprobes through an electron-transparent window opens novel prospects for correlative light and electron microscopy. The locations of labeled components can be easily tracked with fluorescence microscopy, while the subsequent SEM measurement would directly reveal the number of probes, and their individual positions with respect to the cellular structure.

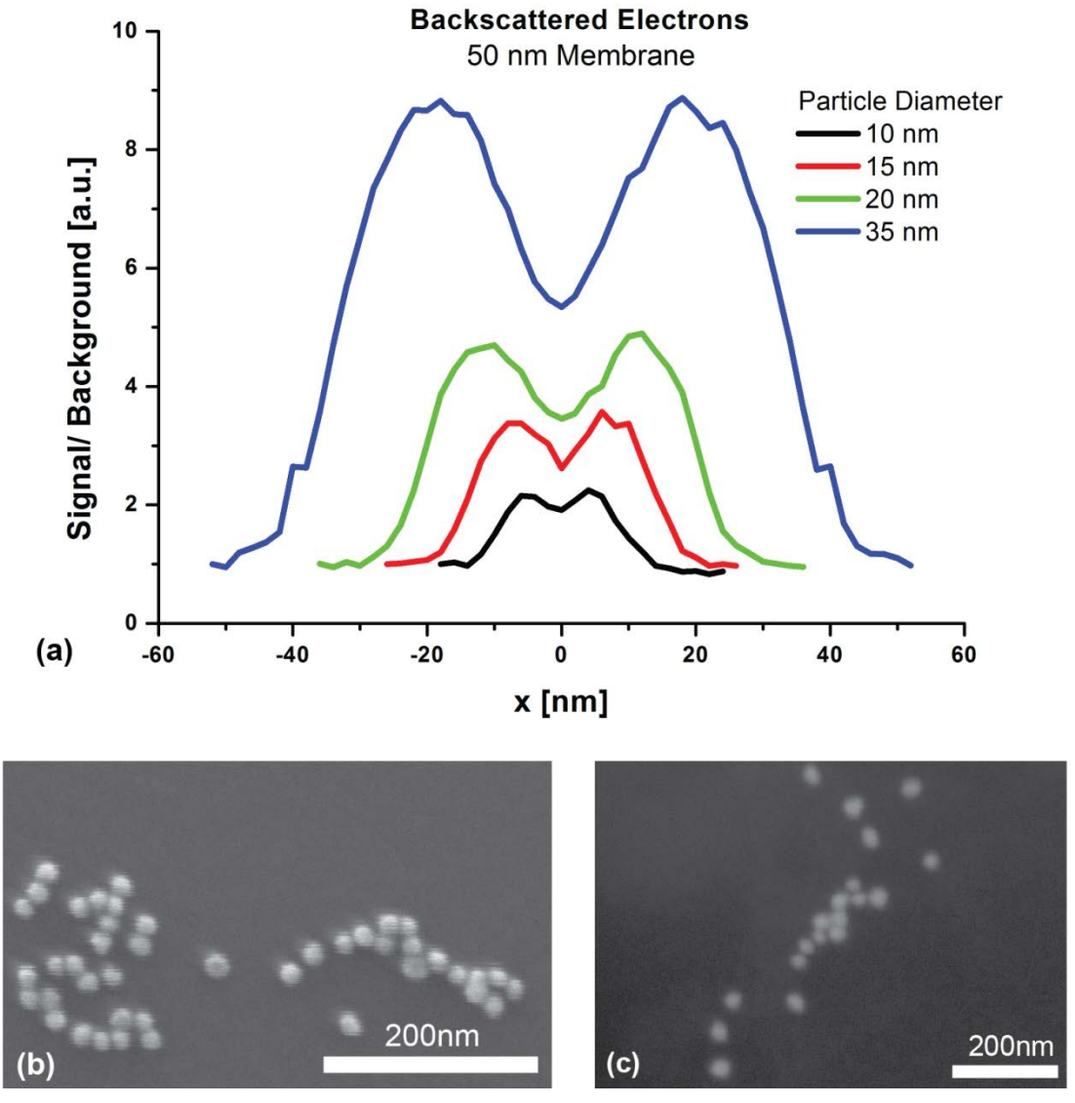

Figure 4. (a) Simulation results showing BSE signal-to-background ratio for Au nanoparticle doublets under a 50 nm Si_3N_4 membrane with Au diameter of 35 nm (blue), 20 nm (green), 15 nm (red), 10 nm (black). (b-c) Experimental BSE images of nanoparticles in H_2O under a 20 nm membrane: (b) 15 nm diameter Au nanoparticles, (c) 15 - 20 nm diameter bio-functionalized CdSe core ZnS shell quantum dots.

Visualization of Individual Bio-markers

In the experiments shown above, particles were imaged that were attached right underneath the membrane. Imaging of particles located deeper in the sample will of course suffer from beam broadening (see also Figure 2, although for electrons traversing through water, air or soft, carbon-containing sample of the same thickness with SiN, beam broadening will be less compared to SiN. See, e.g., the work by Joy and Joy for a discussion on the effects of a water medium on SEM imaging [120]). In many cases, however, a sample of interest can be mounted on the upper, electron-transparent window in which case the area of interest can come within reach of the electron microscope. For biological cells, processes related to cellular motility, signaling or uptake of materials take place in the thinner (100-1000 nm) parts of the cell, in contact with the substrate. We note that cell attachment is a complex process, affected by numerous aspects, like material surface properties, environmental factors and cell type, which should be considered when carrying out study of a biological specimen. SiN substrates, with a cell adhesion layer, have however been used in previous biological experiments [38]. To illustrate imaging of nanoparticle markers in biological material with SEM, we examined CV1 cells which were cultured on a 40 nm-thick SiN membrane and analyzed the uptake of EGF-conjugated quantum dots (EGF-QDots) (Invitrogen,USA) with Simultaneous Correlative Light and Electron Microscopy (SCLEM) [83]. The sample was fixed for 30 minutes after 15 minutes of EGF-QDots incubation and enclosed in a designated holder of which the bottom surface is an indium tin-oxide (ITO)-coated glass coverslide. This holder was then placed in a home-built SCLEM microscope, in between the SEM final lens and a NA=0.95 objective lens (see also Figure 1.a). The SCLEM microscope and its performance is discussed in more detail elsewhere [66]. Inspection of the sample with wide-field epi-fluorescence clearly shows the presence of two cells on the Si_3N_4 membrane (Figure 5.a). The EGF-QDots can be seen in various phases of uptake, from attachment to the outer cell edge to fully internalized up to the cell nucleus. The same area can be imaged with the SEM, in which case the cells are visible in back-scattered electron contrast (Figure 5.b-e). Note that in this and the following images, contrast has been reversed as compared to all previous SEM images. This aids in the visualization and interpretation of cellular structure and is common in biological SEM as contrast is then similar as for TEM. Dense clusters of quantum dot appear dark and they appear to follow the cytoskeleton up to the nucleus. In addition the outer cell edge can be clearly discerned. We now use the fluorescence image as a navigation to identify areas at the cell periphery with docked and internalized EGF-QDots for a high-magnification zoom with the SEM. Figures 5.b to e display various degrees of magnification of the boxed area in each preceding panel. These show not only the cell edge, including structures like filopodia and lamellapodia, but also the individual EGF-QDots can be clearly resolved. Note that the QDots with a producer mentioned core size of 10-12 nm will appear as ~20 nm in correspondence with our previous results. Figure 5.e uniquely demonstrates that several EGF-QDots located within a few hundreds of nanometers from each other (marked with arrows) can be discerned in the SEM and that their position relative to the cell edge can be determined. Also a bigger EGF-QDots cluster can be seen docked close to the tip of the filopodium.

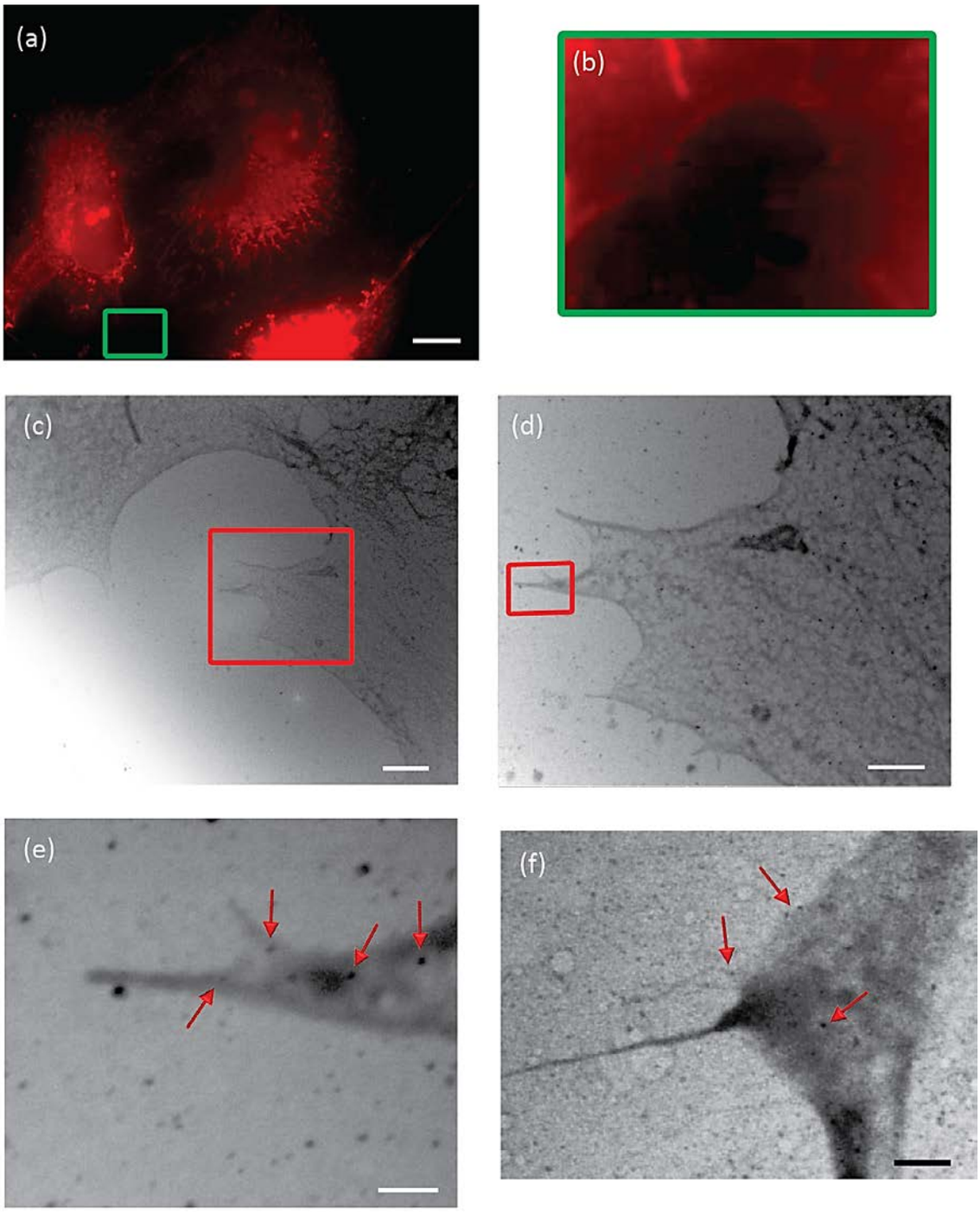

Figure 5. (a) Fluorescence image of three CV1 cells on a Si_3N_4 membrane, fixed during uptake of with EGF-conjugated quantum dots. (b) The enlarged image for the boxed area in (a). (c) SEM image of the same area. Contrast in this image has been reversed with respect to previous images so that the quantum dots appear dark on a bright background. (d, e) Higher magnification SEM images of the boxed area in (c). The cellular structure can be clearly identified, together with single quantum dots (marked with red arrows). (f) Similar high-magnification SEM image of part of a CV1 cell on a Si_3N_4 membrane, taken in liquid. Arrows point to docked and internalized EGF-conjugated quantum dots. Scalebars are 10 μm, 2 μm, 1 μm, 200 nm and 400 nm, respectively.

We note that electron microscopy of soft materials such as cells can be affected by electron beam damage. Here, we focused on the ability to resolve individual nanoparticles in biological material and we did not assess the possible effects of radiation-induced changes to the biological material itself. Nonetheless, even for Figure 5.e, which has the smallest pixel size (1,47 nm^2) and longest dwell time (50 µs), the electron dose was calculated to be ~5 x 10^4 e^-/nm^2. This value is in line with the previously reported value of 7x 10^4 e^-/nm^2, which has been applied for liquid-STEM imaging of fixed cells [38].

The illustration of the nanometer scale localization of a fluorescent quantum dot label with respect to the cellular structure highlights the power of correlative fluorescence and scanning electron microscopy with the use of electron-transparent membranes. Inspection of the sample for regions of interest can be performed in color at hundreds of micrometer length scale, after which four orders of magnitude in scale can be bridged to analyze ultrastructure and single marker locations in the selected regions. Here, we analyzed whole cells without any additional staining for electron microscopy, with a sample fixation protocol as commonly used for optical fluorescence microscopy. The use of the electron-transparent window that seals the sample environment from the SEM vacuum has several clear benefits. First, in case of an atmospheric sample environment, the window prevents contamination of the SEM vacuum chamber from degassing of the sample. Thus, fixation and sample preparation protocols for fluorescence microscopy can be used in the SEM without any vacuum-specific alterations or precautions. This may be an important step to integrate SEM structural detail into fluorescence microscopy measurements. Note also that the degree of nanoparticle marker localization shown here is comparable to the best of optical super-resolution techniques with the added benefit of the structural detail.

A second benefit of an atmospheric sample container is, the protection of the sample against structural changes upon exposure to the vacuum. Third, the sample can be kept in liquid and thus in a near-native state. In addition, the water may assist in preventing charging of the sample and/or the Si_3N_4-membrane. We note that the presence of water does not significantly affect the visualization of structural cellular components attached to the membrane, as illustrated in Figure 5.f. For measurements targeting features located deeper below the membrane, scattering of electrons in water will obviously affect the results compared to that in air. This however is outside the scope of the present investigations. In fact, a fourth benefit of imaging through a membrane lies in the fact that the sample-substrate contact area can be analyzed with the SEM, which for thicker parts of a sample is usually out of reach.

Finally, imaging of biological, or other soft materials in liquid in an integrated fluorescence electron microscope, may ultimately assist in capturing dynamic events with the electron microscope. Electron imaging is highly destructive to biological materials and a major challenge for liquid EM is to capture high-resolution detail at the right moment during dynamic events. In-situ fluorescence microscopy can assist in monitoring live-cell dynamics of nanoparticle markers, defining the exact moment for on-demand application of the electron microscope that can then reveal the nanoscale positions of the markers with respect to the cellular structure.

Conclusion

We have investigated the imaging of nanoparticle bio-markers in liquid in the SEM for integrated fluorescence and electron microscopy. We have observed a good agreement between Geant4-based Monte Carlo simulations and experimental results for the electron imaging of suspended nanoparticles. Beam spreading as a result of electron scattering in the membrane is limited to only 1.5 nm and 3.0 nm for 20 nm and 50 nm thick Si_3N_4 membranes respectively. We have demonstrated that for BSE imaging, Au nanoparticles and colloidal quantum dots down to 10 nm can be individually resolved using a membrane with thickness ranging in between 20 to 50 nm. EGF-conjugated quantum dots identified with an integrated fluorescence microscope can be individually discerned in the SEM together with the outer cellular structure. Ultimately, the combination of fluorescence and scanning electron microscopy of labeled samples in liquid may provide a way to combine the live-cell capabilities of optical microscopy with the structural detail of the electron microscope.

Acknowledgements

We would like to thank Eric Bosch and FEI Company for allowing us to use their version of the Geant4-based Monte Carlo simulation platform that includes the model for low energy interactions. We would also like to thank Carel Heerkens, Vladimir Kutchoukov, and Christiaan Zonnevylle for assistance with fabrication of SiN membranes and the liquid container, and Daan van Oosten Slingeland for assistance with preparation of the CV1 samples. We are grateful to DELMIC BV for providing a prototype of their liquid-sample holder.

Appendix V.A

Resolution and Contrast in Scanning Electron Microscopy of Liquid Samples

Here, the total electron simulation data, including low energy electrons from the Geant4 simulations is presented. The applied geometry in the simulations is illustrated in Figure 1.a. Figure 1.b. shows the radial distribution of all collected electrons as a function of the radial distance from the primary beam. 60% of all electrons exiting the membrane are within 10 nm from the primary beam for a 50 nm thick Si_3N_4 membrane.

However, a considerable amount of transmitted electrons are low-energy (secondary) electrons (Figure 1.c). High-energy electrons can generate a signal from a sample below the membrane. Energy distribution of primary and forward scattered electrons are presented in Figure 1.d. Figure 1.e shows the radial distribution curves of energy filtered electrons from different regions in the energy spectrum.

Also, to evaluate the background signal generated by the film, we simulate the collection of the electrons generated in the Si_3N_4 membranes in interaction with the primary beam with a detector defined above the of Si_3N_4 substrate. (Figure 1.f, inset). Characterization of that background signal is of high importance, as it will have no contribution in the signal generated by the sample. Energy distribution of the background electrons is presented in Figure 1.f. Si_3N_4 membranes of different thicknesses provide a uniform background signal mostly consisting of low energy secondary electrons (<100eV). This background can be easily eliminated if imaging is done with collection of BSE, which will be generated substantially by the sample.

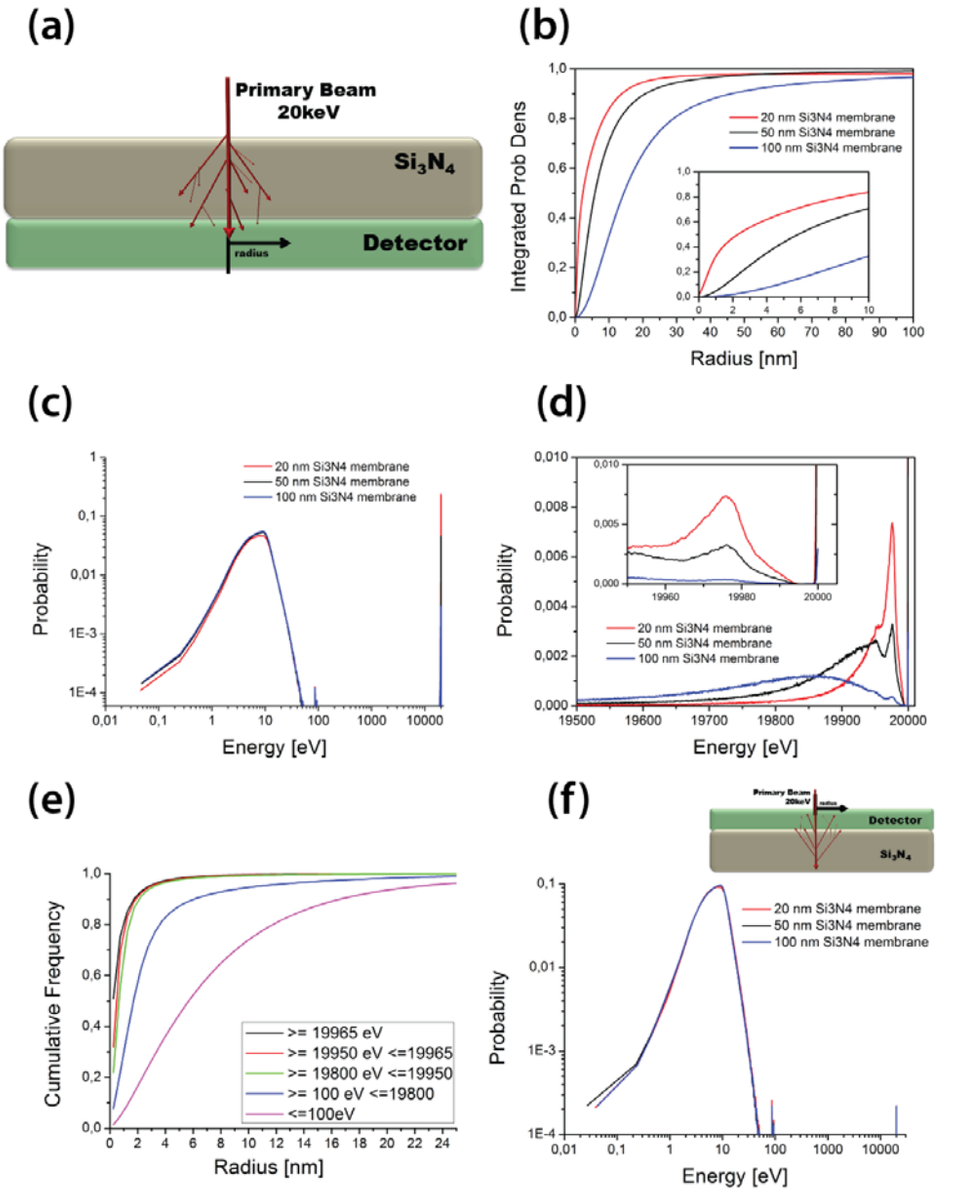

Figure 1. Geant4 Simulations.

Analytical Calculations on Beam Broadening

To calculate the spatial broadening of the probe beam, either Monte Carlo calculations, the Boltzmann transport equation or the multiple scattering integral for the differential cross-section can be used. However, none of these methods would provide an analytical function. On the other hand, the differential cross-section can be approximated by a two dimensional Gaussian function form. And so that also the convolutions can be evaluated as Gaussians. The integration of the convolution function over x and σ (scattering angle) results in projected lateral distribution of the

probe beam, which is the spreading of the focused electron beam due to the elastic scattering events through a material with thickness T [19,20].

$$dx = 1.05 \times 10^{5} \left(\frac{\rho}{W} \right)^{1f\ 2} \frac{Z\left[1 + E\ f\ \ E_0\right]}{E\left[1 + E\ f\ \ 2E_0\right]} T^{3f\ 2}$$

$$E_0 = m_o c^2; \quad E = Ue$$

Where, U is the accelerating voltage, e is electron charge, c is the speed of light and Z is the atomic number [116].

For Si_3N_4;
ρ= 3.2 g/cm^3,
Z= √(3 x 142/7 + 4 x 72/7) =10.6
W= (3 x 28 + 4 x 14)/7 = 20.0 g/mol

According to these data, dx was calculated as 1.63, 6.43 and 18.2 nm for 20, 50 and 100 nm Si_3N_4 membranes respectively. Whereas the results of Monte Carlo simulations where beam spreading was evaluated as a function of membrane thickness were 1.56, 3.81 and 13.3 nm for 20, 50 and 100 nm Si_3N_4 membranes respectively. Figure 2 shows the beam spreading results from the calculations and the simulations together. The calculation results are in line with the simulations of beam spreading for a 20 nm membrane, however the curve shows a divergence as the membrane gets thicker. This divergence is a result of the beam spreading equation considering only the elastic scattering events and the increase in inelastic scattering events with increasing membrane thickness.

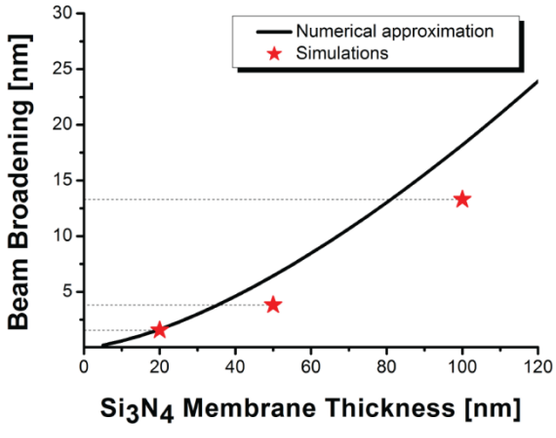

Figure 2. Beam spreading results from the calculations and the simulations.

Chapter VI

Resolution and Contrast in Liquid-SEM imaging of Nanoparticles located at Different Depths

In the previous chapter, we analysed imaging of nanoparticles in SEM through thin electron – transparent windows. Our results have demonstrated that imaging of ≥ 10 nm diameter particles, which can be used as biomarkers, is possible below windows of ≤ 50 nm thickness. In practice, however, a biopolymer adhesion layer, such as poly-l-lysine or collagen, may be needed to promote cellular adhesion. Also, the biomarkers may be located not on the surface but deeper within the biological tissue. Here, we will present some initial simulations and experiments to show that imaging single nanoparticle biomarkers is still feasible even under these conditions. These results may serve as a first step towards more detailed investigations on imaging conditions for the 2D - 3D visualization of liquid immersed biological samples with SEM.

Introduction

Electron microscopy (EM) has made it possible to image samples on a scale below the achievable resolution with light. Traditionally EM needs the samples to be placed in a vacuum environment. However, with the production of thin siliconnitride (Si_3N_4) membranes that are transparent to electrons and are strong enough to withstand atmospheric pressure difference, EM of samples in liquid has become feasible [37,38,40–42,113]. Whole cells can be directly cultured, labelled, and fixed on the SiN membranes for liquid EM observations. Analogous to fluorescence microscopy applications, where fluorescent labels are used to label proteins in cells, nanoparticles (NPs) can be used to study protein distributions in EM of whole cells in liquid. The achievable resolution in liquid EM of labelled whole cells is determined by the broadening of the primary electron beam until reaching the depth, at which the nanoparticle is located. Therefore, highest resolution is achieved when the object of interest is placed just beneath the SiN membrane as the broadening of the primary beam then will be least.

In our the previous chapter, we have characterized the interaction of the electron beam with SiN to investigate the amount of structural detail that can be measured with SEM through a membrane[121]. We have shown that the beam spreading as a result of electron scattering in the membrane is limited to only 1.5 nm and 3.0 nm for 20 nm and 50 nm thick SiN membranes respectively. We have also demonstrated that Au nanoparticles down to 10 nm can be individually resolved using membranes of 20 to 50 nm thicknesses. However, for biological applications, the nanoparticles are not always located directly beneath the SiN membranes. A biopolymer extracellular matrix layer like collagen, gelatine and poly-(l)(d)- lysine may be present on the SiN membranes to promote cellular adhesion. Additionally, the labels may be located not directly on the cell membrane, but deeper in the intracellular structures (see Figure 1). The attainable resolution in imaging these labels located at different depths will be affected by the additional spreading of the electron beam that results from crossing the sample until it reaches a nanoparticle label. Therefore, it is of importance to evaluate the expected resolution in liquid SEM, in relation to the vertical position of the nanoparticles in cellular samples.

Here, we extend our previous results on the resolution achievable in liquid SEM imaging. We use Poly(methylmethacrylate) (PMMA) to model a carbon-rich organic material and compare results from Monte-Carlo simulations with model experiments to discuss the feasibility of liquid SEM imaging of Au nanoparticles located at varying depths in biological samples.

Monte Carlo Simulations

We use the Geant4 platform as described in the previous chapter to simulate beam broadening and signal/background ratio in liquid-SEM imaging of bio-samples labelled with nanoparticles.

Biological samples mostly constitute of carbon based compounds, if we disregard water. An analysis of wet cell composition has shown that it predominantly consists of C (9,4%) H (62,8%) and O (25,4%) atoms whereas the dry composition is C (28,6%) H (50,57%) and O (14%) atoms [122].

For instance the fatty acids, which are the components of cell membranes, are formed of long hydrocarbon chains and they are rich in C, H and O content just like most of the other cellular entities. As beam broadening in a sample is related with its atomic number and density, a compound which is also rich in these elements and have a similar average density with cellular composition should be selected for mimicking the cellular structures in our simulations. We decided to work with Poly(methyl methacrylate) (PMMA) which is a polymeric material with the formula of $(C_5O_2H_8)_n$. PMMA is commonly used as a high resolution positive resist for direct write e-beam lithography and therefore its characteristics upon electron beam exposure is well studied and understood.

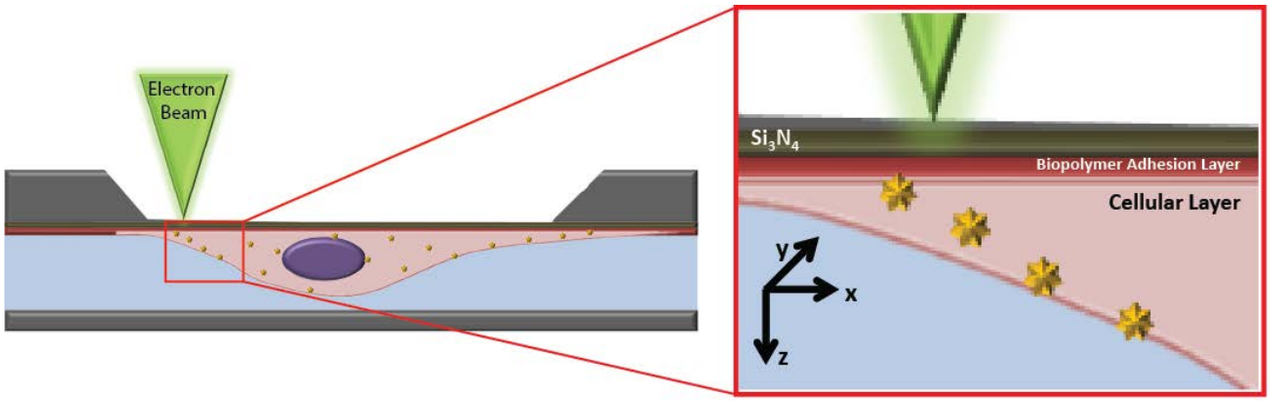

Figure 1. Schematic illustration of liquid-SEM imaging of nanoparticles located at different depths.

Figure 2.a schematically shows the applied geometry for our simulations. A sample geometry which is composed of 3 layers was formed. The uppermost layer was composed of Si_3N_4 membranes, either 20 nm or 50 nm in thickness. PMMA layers of varying thickness were defined below the Si_3N_4 membranes, to imitate the soft biological samples. Finally, an ideal detector was defined below the PMMA. Simulations were run for a primary energy of 20 keV and Si_3N_4 membranes of 20 nm and a 50 nm thickness. For each membrane thickness, a range of PMMA thickness values was simulated running 10^6 electrons for every geometry. All electrons exiting the PMMA downwards and hitting the detector were collected with their position relative to the primary beam. The obtained radial distribution was integrated and plotted for each PMMA layer thickness.

The applied simulation geometry for simulations on the signal to background ratio at different depths is illustrated in Figure 3.a. Like in the simulations of beam broadening, PMMA layers of different thickness were placed beneath 20 nm and 50 nm Si_3N_4 membranes. Two touching Au NPs with a diameter of 15 nm were located below the PMMA layers and the detector was defined above the Si_3N_4 membranes to detect electrons with upward velocity. Line scans were simulated

by moving the primary electron beam along the x-axis with a step-size of 2 nm. The electron beam was simulated with $5x10^4$ electrons at each position and all generated electrons hitting the detector with upward velocity were collected for each *x*-position. From the whole set of collected electrons, those with an energy over 260eV were defined as backscattered electrons, and the rest was analysed as secondary electrons.

Liquid SEM of Nanoparticles

To experimentally reproduce the simulation conditions, we spin-coated PMMA layers on 50 nm Si_3N_4 membranes. Au nanoparticles with a diameter of 35 nm were deposited and dried underneath 25 nm and 50 nm PMMA layers, for characterization of achievable resolution and contrast below the PMMA layers. After drying, the samples were placed in the SEM chamber, as the Si_3N_4 membranes facing up. The imaging was done with 20 keV primary beam, at high vacuum conditions in a SEM (FEI, Quanta 200 FEG). An Everhart Thornley detector and a solid state backscatter detector were used for the detection of SE and BSE, respectively. The images were recorded with a pixel size of 0.7 nm and a pixel dwell time of 30 μs, with 1024x1024 pixels. Brightness and contrast settings were adjusted through the video scope until the waveform nearly saturated the full dynamic range. Line profile analysis was done with the Fiji software directly on the original data, without background subtraction, contrast stretching or gamma correction.

Beam Broadening in PMMA Layers of different Thicknesses

Figure 2.b shows the cumulative number of electrons as a function of the radial distance from the primary beam for 20 nm, 50 nm, 70 nm, 90 nm, 100 nm, 130 nm and 150 nm PMMA layer thicknesses under a 20 nm Si_3N_4 membrane (left) and a 50nm Si_3N_4 membrane (right). Then we calculated the Full Width 50 (FW50), which is the distance containing the first 50% of the electrons, to provide an estimate for the beam size irrespective of its shape. Figure 2.c shows the evolution of the 50% beam broadening diameter, as determined from simulations using an incident beam of zero diameter and normal incidence. We extended our simulations to cover PMMA layer thickness from 20 nm to 7000 nm, until there were no electrons reaching the detector anymore. This means our simulations cover the whole interaction volume in the PMMA layers for 20 keV (Figure 2.c, right panel).

At 20 keV, the limit of resolution just below a 20 nm thick membrane and 150 nm thick PMMA layer is estimated from Figure 2.c at 18 nm. As explained in the previous chapter, a significant amount of collected electrons are low-energy secondary electrons. If BSE imaging is intended, only higher-energy unscattered or forward scattered PEs will contribute to the BSE signal from the sample. In that case, high-energy (>260 eV) electrons can be selected, and the radial distribution function for these can be calculated and integrated like in the previous chapter. The extrapolated beam broadening for these high-energy electrons would be lower, as the BSE signal is generated from a sub-circle of the total broadened beam (see also Chapter.5 and Appendix.5.A).

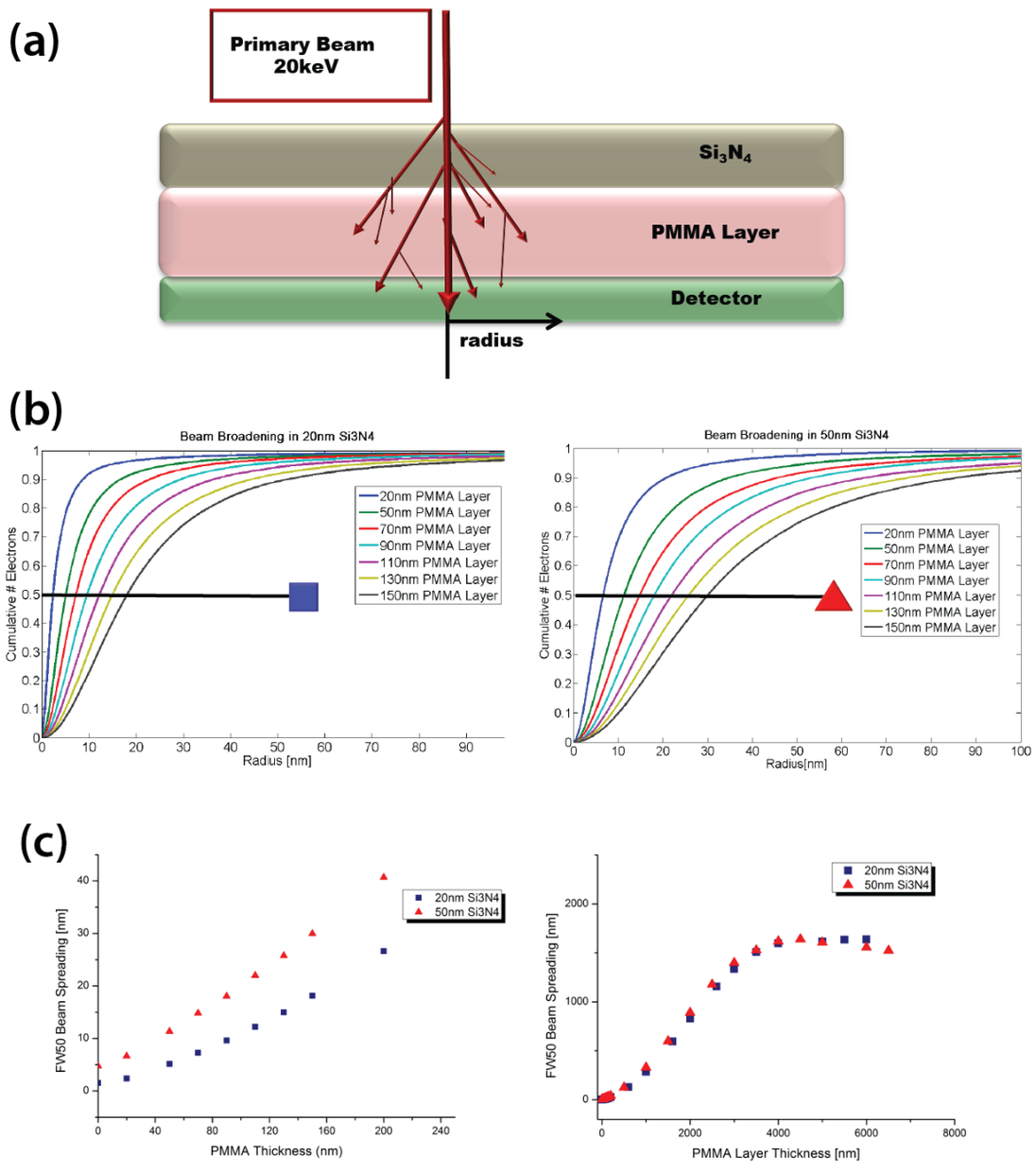

Figure 2. Broadening of the primary beam at different depths. **(a)** The applied simulation geometry for simulations on the evaluation of beam broadening in liquid SEM imaging of NP labels at different depths **(b)** The cumulative number of electrons as a function of the radial distance from the primary beam for varying PMMA thicknesses under a 20 nm Si_3N_4 membrane (left) and a 50 nm Si_3N_4 membrane (right). **(c)** The beam broadening diameter, in which the 50% of the total number of electrons are present with respect to increasing PMMA layer thickness below a 20 nm (blue) and 50 nm (red) Si_3N_4 membrane. A zoom to the first 200 nm of the PMMA layer is presented in the left.

Contrast in PMMA Layers of different Thicknesses

We simulated the signal to background ratio in liquid SEM imaging of NP labels at different depths beneath Si_3N_4 membranes as explained in the methods section. The simulated line scans showing the expected signal-to-background for SE detection and for BSE detection are displayed in Figure 3.b and Figure 3.c, respectively. The curves shows the normalized signal-to-background ratios for 2 touching 15 nm Au NPs beneath 20 nm and 50 nm Si_3N_4 membranes plus 20 nm and 50 nm PMMA layers. The simulated signal to background ratio for SEs (S/BG ~1,1), which are generated in the membrane by electrons backscattered from the sample, and signal to noise ratio (S/N ~3) are quite low for the electron dose simulated here. As expected, increasing number of scattering events in thicker layers increases the background and therefore decreases the achievable SE contrast. However, 15 nm Au NPs can still be discerned below a 20 nm membrane and 20 nm PMMA layer, with SE imaging. On the other hand, BSE imaging provides relatively high signal to background ratios and 2 touching NPs can be discerned even below 50 nm PMMA layers. We note that, beam broadening will be less for carbon-containing samples than Si_3N_4 membranes of the same thicknesses. The BSE contrast of NPs below 20 nm Si_3N_4 and 50 nm PMMA is almost double of the contrast obtainable for NPs below 50 nm Si_3N_4 and 20 nm PMMA (Figure 3.c). Therefore, it is beneficial to minimize the thickness of Si_3N_4 membranes, if NPs labelling intra-cellular structures are objects of liquid SEM imaging.

As presented, liquid SEM imaging of NP labels at 50 nm depth in cellular structures can be attained with reasonable contrast. We want to note that all of our simulations are for a 20keV primary electron beam. The range of the interaction volume and thus the contrast would be different for other acceleration voltages, and this is raising the interesting opportunity of depth imaging with an accelerating voltage series. Several interesting processes in cells, like cell signalling, adherence and cellular movement, actually occur in thinner and adherent parts of cells. It has been previously reported that cells like fibroblasts can grow extremely flat in outgrowing regions of the cells and become as thin as 50 nm at the cell cortex [123]. Microtubules were reported to be present in parts of cells which are thinner than 100 nm and actin rich cellular protrusions were observed to be present as 10-20 nm in size. Liquid SEM imaging offers good contrast and resolution for imaging at these reported depths of cellular structures. Besides, using NP labels of larger sizes would dramatically increase the achievable contrast, as the probability to generate BSEs gets higher. This is presented by experiments of imaging 35 nm Au NPs in the next section.

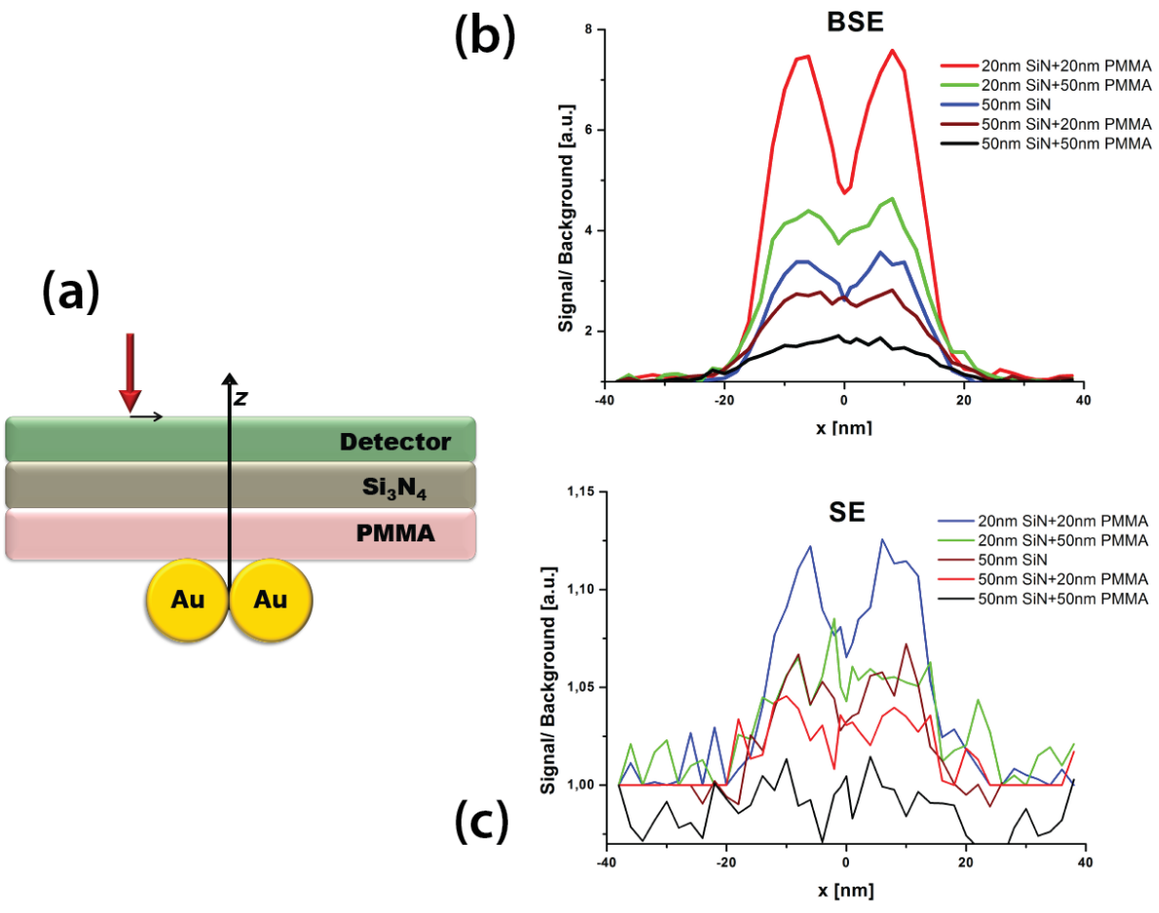

Figure 3. Signal to background ratio in the imaging of two adjacent 35 nm diameter Au particles at different depths. (a) The applied simulation geometry for simulations on the signal to background ratio in liquid SEM imaging of NP labels at different depths. (b) Simulation results showing BSE signal-to-background ratio for 15 nm Au nanoparticle doublets beneath 20 or 50 nm Si_3N_4 membrane plus a 20 or 50 nm PMMA layer. (c) Simulation results showing SE signal-to-background ratio for 15 nm Au nanoparticle doublets beneath 20 or 50 nm Si_3N_4 membrane plus a 20 or 50 nm PMMA layer.

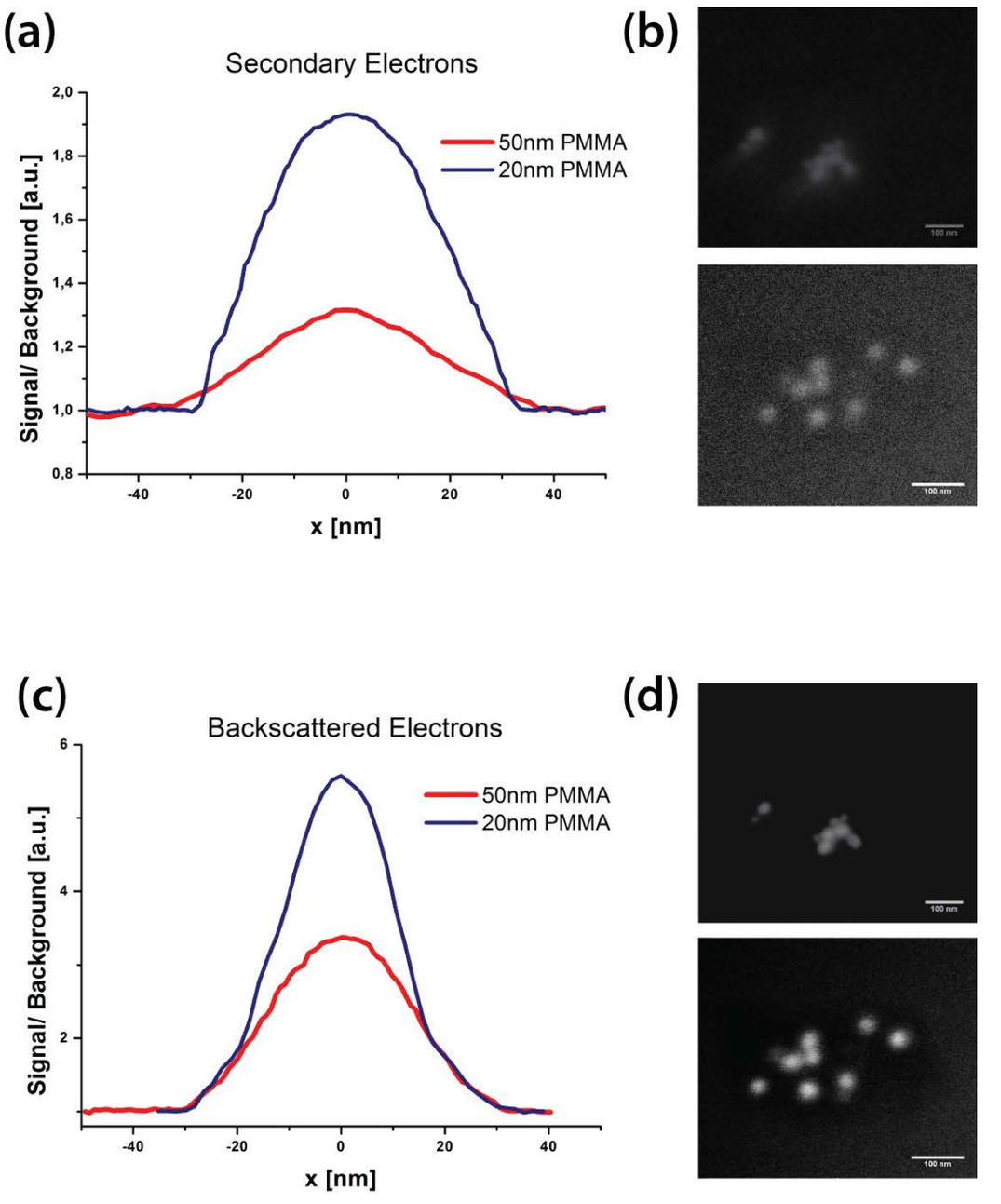

Figure 4. Experimental imaging results of 35 nm diameter Au particles at different depths. **(a)** Average line profile over 30 NPs, for **SE imaging** of the NPs below PMMA layers of 20 nm (blue) and 50 nm (red), beneath a 50 nm Si_3N_4 membrane**. (b)** SEM images, recorded with the Everhart Thornley detector, of the Au NPs below PMMA layers of 20 nm (up) and 50 nm (bottom), beneath a 50 nm Si_3N_4membrane. **(c)** Average line profile over 30 NPs, for **BSE imaging** of the NPs below PMMA layers of 20 nm (blue) and 50nm (red), beneath a 50 nm Si_3N_4 membrane. **(d)** SEM images of the same particles presented in (a), but recorded with the solid state BSE detector, below PMMA layers of 20 nm (up) and 50 nm (bottom), beneath a 50 nm Si_3N_4 membrane.

Experiments

The edge resolution (25%-75%) has been calculated by averaging the line profiles of 30 particles in each experiment and using both sides of the peaks. The resulting averaged curves are presented in Figure 4.a and Figure 4.c for the SE and BSE images, respectively. The calculated edge resolutions show the progressive beam spreading in thicker Si_3N_4 and PMMA layers. For the 25 nm and the 50 nm PMMA layers the edge resolution was quantified as 8.5 ±0.3 nm and 10.1 ±0.6 nm for BSE, and 12.31 ± 0.2 nm and 17±1 nm for SE detection.

Figure 4.b shows the representative SEM images, recorded with the Everhart Thornley detector, of the Au NPs under PMMA layers of 20 nm (up) and 50 nm (bottom), beneath a 50 nm Si_3N_4 membrane. Figure 4.d presents images of the exact same regions, but recorded with the solid state BSE detector. As expected, it is easy to observe that the images become blurred and contrast degrades as the PMMA thickness increases. A particularly high signal to background ratio (S/BG= 2-7) is observable for BSE imaging whereas it is lower but still discernible for the SE imaging for both thicknesses.

Our experimental findings are in-line with the previously presented simulation results. The simulations give an edge resolution of 8.9 nm and 11.1 nm for the 20 nm and the 50 nm thick layers of PMMA in BSE mode, whereas the calculated edge resolution of the experiment was 8.5 ±0.3 nm and 10.13 ±0.55 nm. These results suggest liquid SEM imaging of nanoparticle labelled cells can be achieved with high resolution even if the NP labels are not located on the cellular surface, directly beneath the Si_3N_4 membranes. Imaging with a resolution of 10 nm is possible at a depth of 50 nm, where actually cytoskeletal elements are reported to be present for fibroblasts. Imaging of particles located at even deeper in cells will of course suffer from further beam broadening. However, even at a depth of 200 nm, the expected resolution is higher than 20 nm, which is in line with the usual achievable resolution with super-resolution light microscopy techniques and without the expense of long exposure times, and no need for heavy image processing.

Conclusions and Outlook

We have presented the preliminary results on characterization of the attainable resolution and contrast in liquid SEM imaging of NP labels located at different depths inside the sample. Electron beam broadening, as the main resolution defining factor, was characterized to be 18 nm beneath a 20 nm Si_3N_4 membrane and 150 nm thick PMMA layer. Attainable contrast below carbon-rich-layers was investigated with MC simulations for Au NPs of 15 nm in size. High levels of signal to background ratios were shown to be achievable with BSE imaging for these particles. Experiments with 35 nm Au NPs provided edge resolution values of 8.5 nm and 10.13 nm for 20 nm and 50 nm PMMA layers beneath a 50 nm Si_3N_4 membrane. Monte Carlo simulations agreed with the experimental edge resolution results within the error margin. Considering that intra-cellular structures such as cytoskeletal elements are reported to be present at 50 nm depth in cells, liquid-SEM imaging appears as a promising technique for imaging these structures and study related specific protein distributions with NP labelling.

For more detailed investigation, the direction of BSE's should also be considered in the MC simulations by ray tracing to generate more realistic simulation results. By tracing the generated BSE electrons, efficiency of different detectors can be evaluated for liquid SEM imaging. Additionally, experiments in which energy filtering[124] in electron detection is employed, are planned to be conducted to increase the correspondence between simulations and experiments. Also, the energy dependency of interaction volume is intended be further characterized with a final goal of targeting a specific depth by a specific primary beam energy and 3-D imaging with an accelerating voltage series. The level of blurring can also be used to infer the depth information once the close correspondence between simulations and experiments is assured. Using an accelerating voltage series and recording a series of 2D images at different focus points, 3D imaging of biological specimen could be achieved via deconvolution.

Acknowledgements

We would like to thank Miranda Vaandrager for her work on the experiments and analysis of experiments with spin-coated PMMA layers on 50 nm Si_3N_4 membranes. We would like to thank Eric Bosch and FEI Company for allowing us to use their version of the Geant4-based Monte Carlo simulation platform and Dr. Ivan Lazic with his assistance and help about the Geant4 simulations.

Chapter VII

Preparation and Encapsulation of Whole Cells for *in-situ* Light and Scanning Electron Microscopy

We present the design and fabrication processes of a holder for correlative light and electron microscopy of liquid samples. The holder comprises an electron transparent window on one side and a light transparent window on the other side. The electron transparent window consists of a thin membrane separating the hydrated sample from the vacuum of the electron microscope chamber. With the light transparent substrate, fluorescence microscopy is carried out from below, while the high-resolution electron microscopy can be done from above through the electron transparent window. We provide the detailed sample preparation process for correlative imaging of whole cells cultured on the electron transparent membranes and also show that the holder can be easily advanced to a microfluidic reactor. The presented holder brings novel possibilities for correlative microscopy studies of cells in their near native environment.

This chapter is submitted for publication as:

Liv, N., van Oosten Slingeland, D. S. B., Zonnyvelle, A. C., Effting, A. P. C., Heerkens, C. T. H., Kruit, P., & Hoogenboom, J. P. (n.d.). Preparation and Encapsulation of Whole Cells for in-situ Light and Scanning Electron Microscopy. *Submitted.*

Introduction

Due to its non-invasive character, light microscopy (LM) has become the standard technique for imaging dynamic processes in live cells. Especially with the power of selective fluorescent stains and genetic labels, fluorescent microscopy (FM) has been the key method for investigating protein dynamics at the sub-cellular level. Unfortunately, the resolution in LM techniques is limited by diffraction. Electron microscopy (EM), on the other hand, offers sub-nm spatial resolution, but it typically only provides grey scale images of dehydrated and/or frozen samples. However, comprehensive investigation of biophysical activities of cells at the molecular level requires high resolution imaging of organisms in their natural hydrated, and preferably live, dynamic states.

Electron microscopy (EM) of hydrated samples has been shown possible by isolation of the liquid sample from the EM vacuum chamber with a membraned container. Successful attempts not only for wet- Transmission EM (TEM) and Scanning TEM (STEM), but also for Scanning EM (SEM) have been previously reported [38–40]. Thiberge et al. demonstrated wet-SEM imaging of untreated samples, heavy metal stained HeLa cells, 20 nm gold labeled gastrin receptor in *H.pylori,* and treated & untreated tissue sections[41]. Especially for studies involving lipid membranes, Wet-EM techniques are advantageous as these structures are vulnerable to damage during dehydration. More recently, with the successful use of thin low-stress silicon nitride (SiN) membranes, achievable resolution has improved and Wet-EM approaches have further evolved in the direct visualization of liquid bio- samples. For instance, using a capsule with two SiN membranes and STEM imaging, de Jonge and co-workers visualized 10 nm gold labeled COS7 cells [125].

Recently, efforts have also been made to couple Wet- EM techniques with light microscopy approaches, i.e. for correlative microscopy applications[65,119]. Those methods are very valuable as they propose a strategy to link functional information on cellular dynamics obtained with light microscopy to high resolution structural information in the native environment from Wet- EM. In addition, considering the availability of fluorescent semiconductor materials[81] and dual labeling probes like FluoroNanogold™ [53] merging correlative microscopy with liquid electron microscopy holds great interest and importance. However, the current methods linking LM and EM of liquid samples hold compromises regarding the quality of both imaging techniques. The liquid sample holder used for correlative FM and Wet-STEM imaging consists of two thin SiN membranes in between which the liquid sample is sandwiched. Firstly, the presence of two thin membranes makes the holder quite vulnerable to damage and rupture during sample preparation and imaging processes[111]. Secondly, the use of a cover glass may make it easier to do high NA microscopy and therefore increase the opportunity for coupling with super-resolution LM techniques.

Therefore, there is a need for a liquid enclosure design, which can house the liquid samples in the vacuum chamber of integrated microscope and in the meantime provide uncompromised LM and EM images. The desired holder for liquid CLEM applications should satisfy the following requirements: (i) it should comprise light and electron-transparent windows, (ii) it should be rigid and easy to handle, *i.e.* to culture cells on the electron transparent membranes and process them

for imaging, and last but not least, (iii) it should be ultimately complimented with a flow capability. Addressing this demand and requirements, we designed a liquid enclosure for correlative microscopy compromising an electron transparent window on one side and an optically transparent window on the other side. The optically transparent window is composed of a glass slide to provide unlimited utilization of high NA objective lenses. The enclosure is designed especially to fit an integrated correlative microscopy platform previously reported by Zonnevylle, et al.(2013) to show the possibility to perform simultaneous correlated visualization of samples in liquid[66]. Implementation of liquid electron microscopy in an integrated correlative microscopy platform promises simultaneous and accurate light and electron microscopic visualization of nanoscale structures in a native environment[83].

We also show that the enclosure can be easily advanced to a microfluidic reactor with inlet/ outlet ports to enable loading, de-loading, mixing and manipulating the liquid samples. Correlative microscopy with a μ-fluidic enclosure can provide insight in fundamental reactions and processes of living cells or tissues. First of all, a liquid flow would be beneficial in removing the generated heat, radicals and free electrons by the electron beam exposure in long-run bio-imaging applications. Additionally, it would enable in-situ and sequential labelling for the samples in liquid. With the light transparent substrate, transport of bio-materials and nanoparticles through the channels, into the compartment and underneath the window can be monitored by optical means, while the instantaneous high-resolution electron images can be taken through the window.

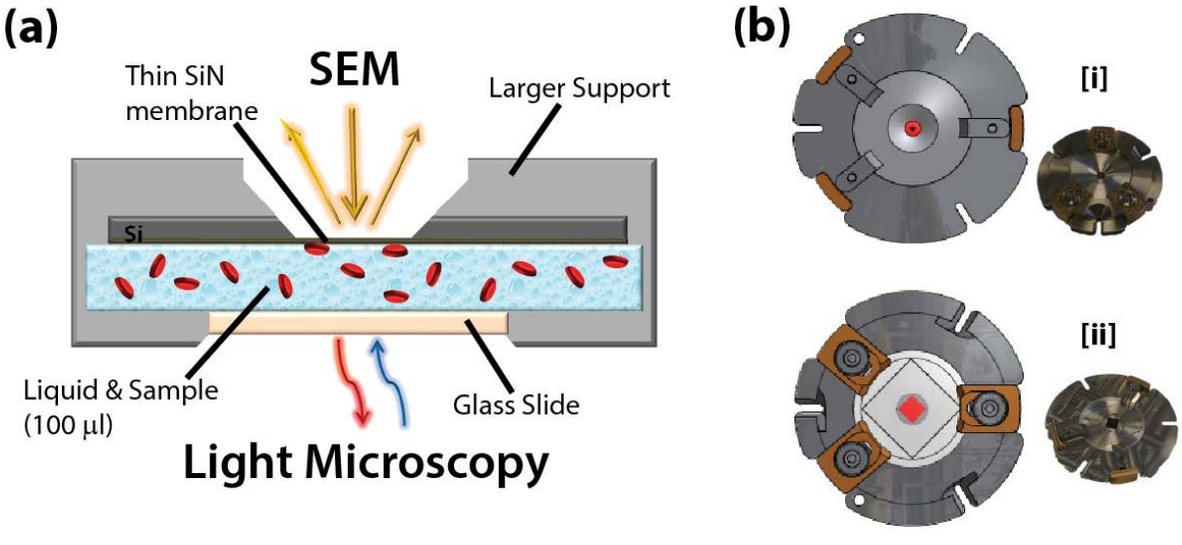

Figure 1. Liquid Sample Holder for Correlative Microscopy. (a) Schematic representation of a holder for liquid samples to be used in simultaneous correlative light electron microscopy. **(b)** Design of the actual holder showing **[i]** the top view, and **[ii]** ,the bottom view of the enclosure. Brown parts are the springs which clamp both sides of the holder, red is the silicon μchip containing the SiN windows(s) (indicated in black), white-greyish part is the plate with the glass microscopy slide glued onto it.

Holder for Correlative Microscopy of Liquid Samples

Design

A holder was designed in order to contain samples immersed in liquid, leak-free in the SEM vacuum chamber. The basic scheme for a holder for liquid samples in simultaneous CLEM is given in Figure 1.a. To facilitate simultaneous correlative light and electron microscopy, the holder has both an electron transparent and a light transparent window. The electron transparent window, a 40 nm thick SiN membrane, is placed at the top. The light transparent window is placed at the bottom side and consists of glass to enable high-NA microscopy using immersion oils.

For ease of use and to allow cell culturing, we chose to have the two windows on two separate metal plates that are clamped together in a leak-free holder. The top and bottom view of the designed holder is presented in Figure 1.b. the glass slide and the microchips (μ-chip) bearing the SiN membranes are each bonded to a distinct metal plate. The size and number of SiN membranes present on the μchips can be decided and optimized based on imaging application. The strength and rigidity of SiN membranes is of great importance as they seal the liquid sample in the high vacuum SEM chamber. Membranes with a smaller surface area are less prone to rupture during handling and the cell culturing processes. On the other hand, for imaging adherent eukaryotic cells with relatively bigger size, it would be beneficial to increase the size of the membranes to maximize the chance of having cells adherent to the membrane areas. As rectangular membranes have been shown less susceptible to bulging[111] , we tested rectangular membranes with different sizes to find the best compromise between strength and imaging area of the membranes. For our application, we chose to work with μchips bearing two 100 x 300 μm^2 membranes per chip. We did not observe any bulging and/or rupturing of SiN membranes with this size or smaller sizes with the same aspect ratio.

The thickness of the SiN membrane was decided such that it could withstand the atmospheric pressure difference between the liquid sample and the SEM chamber for the above mentioned membrane area and in the meantime cause minimal loss in EM imaging resolution[121] . The expected FW50 size increase of the primary beam after passing through a 40 nm membrane is less than 2 nm. This resolution would be satisfactory for most biological imaging applications. Nevertheless, if better resolution is demanded, thinner SiN membranes like 15 nm or 20 nm can be used.

The two metal plates, housing the μ-chip and the glass slide respectively, and the clamping holder are all constructed from stainless steel (1.4401/316) to assure biocompatibility of the holder. A detailed cross section view of the whole enclosure is presented in Figure 2.a. The bottom plate comprises a notch for a 170 μm (no: 1.5 light microscopy standard) glass slide to be bonded in. It also has a hole with a diameter of 10 mm in the center to bring the light objective lens in close proximity for high NA low working- distance imaging. The top plate has 2 designated grooves of which one hosts the fabricated μchip and the glue to bond the μchip. The other groove is for an O-ring, which is used for leak-free sealing (Figure 2.c). A total volume of 10^{-7} m^3 (100 μl) is left free

in between the μchips and the glass slides, when mounted together in the clamping holder (as indicated in Figure 1.a). The holder can be easily mounted on the piezo-stage of the integrated microscope[66]. The detailed fabrication process for the SiN membranes and bonding procedures is explained in the next sections.

Fabrication of microchips

The μchips are fabricated from silicon wafers following the steps listed below and with the same numbering indicated schematically in Figure 2.b. The wafers used in this process are 100 mm, double side polished (DSP), P-type, 0- 10Ω/cm resistivity, 375μm thick wafers with [100] orientation of the crystal lattice**[i]**. The wafers are cleaned with RCA1 (which cleans organic residues and films from the silicon wafer) and RCA2 (which removes all metal ions from the silicon wafer). Both are standard procedures in μ-fabrication processing. Then a 40 nm layer of low stress silicon nitride is deposited on both sides of the wafers using a Low-Pressure Chemical Vapor Deposition (LPCVD)process **[ii]**. One side of the wafers is spin coated with hexamethyldisilazane (HMDS) and baked on a hot plate to promote adhesion of the photoresist layer. The wafers are then spin coated with photoresist(AZ5214) **[iii]**, and again baked. The pattern defining the electron transparent windows, is transferred from a custom designed mask to the wafers by photolithography **[iv]**. Photoresist development reveals the SiN layer in the window areas **[v].** The silicon nitride is selectively etched away with Reactive Ion Etching (RIE) and the remaining photoresist was stripped off the wafers after etching **[vi]**. The exposed silicon is anisotropically etched in a KOH bath which at the end defines the 40 nm SiN membranes in the window areas on the opposite side of the wafer **[vii]**.

After anisotropic etching, the wafers are rinsed with HCl and double- distilled water. The wafers are encapsulated in diluted photoresist (S1805) to protect the silicon nitride membranes during dicing. The wafers are diced in 5x5 mm^2 chips (see Figure 2.c.**[i]**). In this way, each wafer yields 164 individual chips. The chips were released from the wafers by immersion in 50ºC Acetone for ~5 minutes. The chips were rinsed with EtOH, cleaned again with RCA1, rinsed with double-distilled water and dried with nitrogen.

Bonding

One of the critical manufacturing steps of the presented sample holder is the bonding of the microchips and glass slides to the designated metal plates. The decision on the type of glue was made considering and screening numerous glues for vacuum compatibility and biocompatibility. In addition, the selected glue should be transparent and non-fluorescent to prevent any obstruction for fluorescent imaging. Based on these parameters, Araldite 2020, a two component epoxy adhesive, was selected as the best fit for our application. Araldite is specifically designed for glass and ceramic bonding, and has an index of refraction similar to that of glass (n=1,52). It was screened for vacuum compatibility with a mass spectrometer attached to a vacuum chamber. After degassing and curing, the outgassing level of the adhesive was found low enough to be used in high vacuum conditions of the SEM. Biocompatibility of Araldite was checked by culturing adherent CV1 cells on Araldite coated glass slides.

The detailed bonding process is as flows: the metal plates were cleaned by 20 minutes sonication in Acetone and rinsing with IPA. They were dried with nitrogen and stored in a sealed container until being further processed for bonding. The araldite glue was prepared by mixing the two components and the mixture was degassed in a vacuum chamber prior to use. The prepared glue mixture was immediately used. The fabricated μ-chip was placed at the designated position on the top holder plate. 1 μl of the prepared Araldite glue was put on the 4 edges of the microchip to fully fill the blank-left space in the groove. Similarly, 18x18 mm cover-glasses with a thickness 170 μm were placed at the designated position on the bottom plate and 1 μl of Araldite was applied to the 4 edges. Both the top and the bottom plates were placed in the oven at 60°C for 4 hours to cure the glue. After curing, the plates were stored in a sealed container to avoid possible contamination.

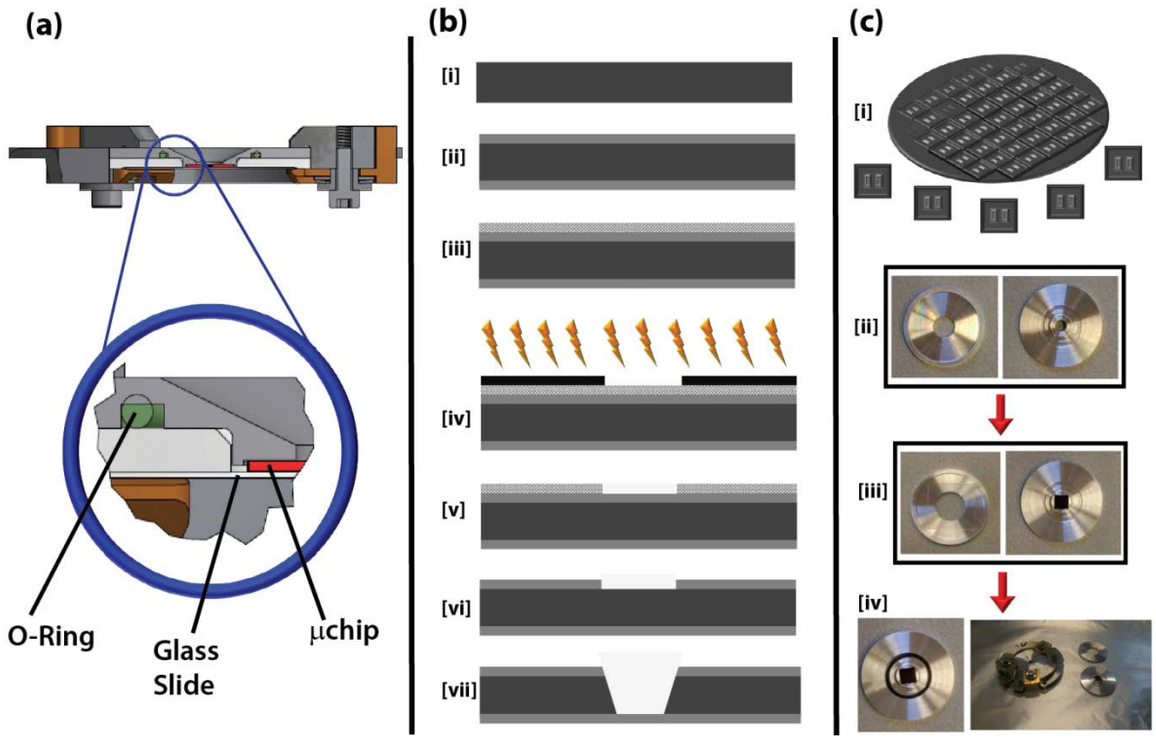

Figure 2. Fabrication of Liquid Sample Holder for Correlative Microscopy. (a) A cross section view of the holder for correlative light electron microscopy of liquid samples. The enlarged circle demonstrates the positioning of the O-ring, the µchip and the glass slide within the holder. **(b)** The µchips bearing the membranes are fabricated from 300µm thick Si wafers with the represented procedure using standard clean-room techniques as described in the main text. **(c)** Preparation of the liquid enclosure for imaging. **[i]** The individual chips are diced from the wafer and cleaned. **[ii]** The top and the bottom metal plates are cleaned. **[iii]** Fabricated µchips and glass slides are placed in the designated grooves in the top and the bottom metal plates, respectively and bonded with Araldite. **[iv]** An O-ring that is placed in its designated groove on the top metal plate provides leak free sealing. Both of the metal plates are inserted together with the liquid sample in the clamping holder to be placed in the vacuum chamber of the microscope.

Preparation of Biological Samples

The sample preparation steps for whole cells in liquid to be imaged in simultaneous correlative light electron microscopy are explained below and shown schematically in Figure 3.a.

Cell Seeding

Cells are seeded directly on μ-chips that were already bonded to the top metal plate of the enclosure. As stated earlier, this makes handling the microchips easier and also prevents possible damage to the membranes. The plates housing the membranes are always handled with sterile Teflon tweezers and special attention is paid not to touch the surface of the membranes. Prior to seeding, the SiN membranes are plasma oxidized to make them more hydrophilic. They are then transferred to petri dishes with the flat SiN membrane surface facing up and coated with poly-L-lysine (0.01% poly-L-lysine for 30 minutes at 37°C) to promote the adherence of the cells to the SiN surface. After this incubation, the chips were rinsed with Phosphate Buffered Saline (PBS) (pH 7.4) and immersed in 2-4 ml of cell culture medium (DMEM in our application).

Confluent cells in culture flasks were washed 2 times with PBS, trypsinized and suspended again in a lower volume of cell medium. 100 μl of this cell suspension was added directly to the membranes in the dish filled with the cell medium. The microchips were inspected after ~2-3 minutes with an inverted light microscope to verify the presence of cells starting to adhere on the membranes. If no cell adherence on the membranes was observed, another 100 μl of cell suspension was added on to the microchips. The preferred number of cells would be 2-3 cells per 100 x 100 μm^2 membrane area. Presence of more cells would prevent their adherence on the surface of the SiN membranes. If there were more adherent cells, the microchips were immediately rinsed with PBS, to detach loosely adhered cells from the surface, and suspended again in cell medium. When the anticipated number of cells per membrane was reached, the plate housing the membranes was transferred to another petri dish filled with cell medium supplemented with 10% Fetal Bovine Serum, Penicillin/Streptomycin and 2 mM Glutamine and cultured overnight at 37°C under 5% CO_2. For some specific labeling applications that require the cells to uptake conjugated labels, it can be beneficial to incubate cells in serum free medium for 3-4 hours prior to labeling.

Cell labeling

The cells adherent on SiN membranes can be labeled following numerous protocols for correlative microscopy applications. Fluorescent labels can be used to image specific organelles, cellular structures and proteins in the light microscope. Similarly, nanoparticles, metal-affine proteins, or stains of materials with high atomic numbers yield contrast in EM and can therefore be used to tag specific cellular components in electron microscopy. Depending on the characteristics of the selected label or staining reagent, labeling should be done before or after the fixation step. If a cell-permanent stain will be used, such as MitoTracker®, Tubulin Tracker™, Hoechst etc., staining can be performed prior to fixation. Live cell labeling protocols can also be applied to label the cells with protein-conjugated tags. These tags can be either fluorescent molecules, nanoparticles or Quantum Dots (QDots). The latter are promising probes for correlative microscopy applications

as they exhibit visibility in both light and electron microscopes [81]. Also recently developed metal tagging probes [24] and genetically encoded tags for CLEM, such as ReAsH and miniSOG can be used for labelling [58]. These methods are based on photooxidation of diaminobenzidine (DAB) which precipitates into an electron-dense product after photooxidation, which can be visualized in EM. Further labeling can be achieved for both light and electron microscopy by applying well achieved immuno-labelling procedures.

As an example, the cells presented in Figure 4. are labelled with epidermal growth factor conjugated QDots by adapting the procedure reported recently by Dukes et al. (2010). EGF-QDot conjugates are formed by incubating EGF-biotin (Invitrogen, USA) with streptavidin-QDot655 (Invitrogen, USA) for 1 h at 37°C in PBS, pH 7.4. A microcentrifuge purification column (Ultracel-100YM, Millipore) is used to remove unbound EGF-biotin. The cells cultured on the SiN membranes are incubated with 5 nM EGF-QDot655 in Tyrode's buffer (Sigma), supplemented with 0.1% BSA (Sigma) and 50 mM D-glucose (Sigma-Aldrich) for 15 min at room temperature. After the labelling, the cells are washed three times in PBS and proceeded for fixation as described in the next section.

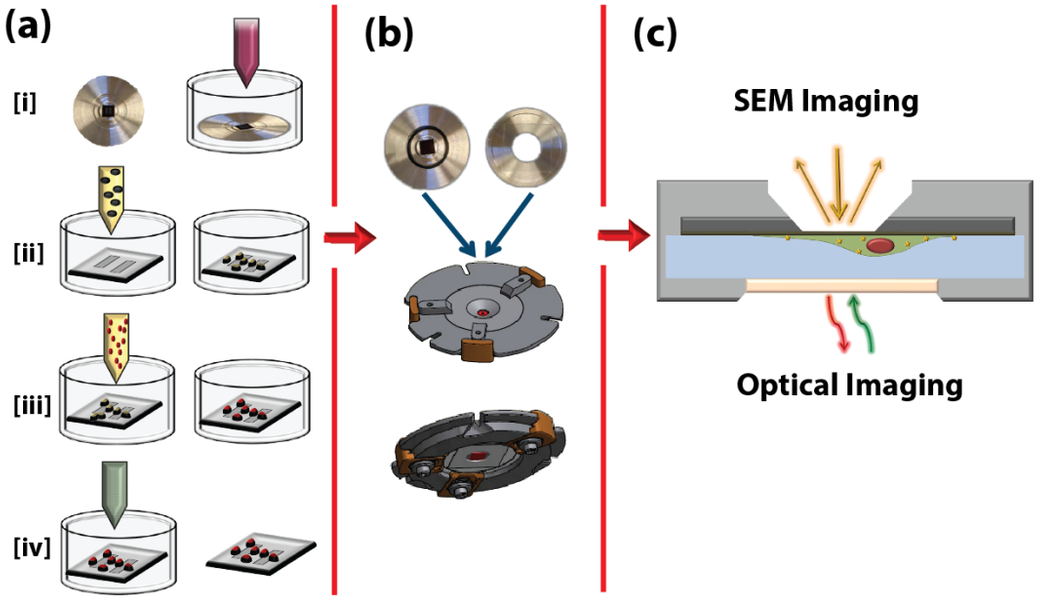

Figure 3. Sample Preparation and Mounting procedure for the Liquid Sample Holder. (a) Sample Preparation procedure for correlative microscopy of adherent cells in the liquid enclosure. **[i]** SiN membranes were plasma oxidized and then they were transferred to petri dishes as flat surface of SiN membranes facing up immersed in 2-4 ml of cell culture medium. **[ii]** Confluent cells which are trypsinized and suspended again in cell medium were directly seeded on the membranes and cultures overnight. **[iii]** The cells adherent on SiN membranes are labeled following a protocol for correlative microscopy imaging. **[iv]** The cells are fixed by adding the fixative solution at an equal volume of culture medium for 15-30 minutes, and then rinsed with PBS. **(b)** The top metal plate with the cells is placed in the clamping holder and 70- 90 µl of imaging buffer is added. The bottom plate housing the glass slide is placed, and the enclosure is clamped. **(c)** The enclosure is mounted in the integrated microscope for correlative microscopy.

Cell fixation and staining

If live-cell imaging is not intended, biological samples can be fixed to preserve their structure and prevent them from decay before and/or during imaging. Fixation of cells on SiN membranes is not any different from fixation of cells on glass for fluorescent microscopy. A wide range of fixatives is available, and the correct choice will depend on the antibodies that would be used for immuno-labelling. Note that in the holder also vacuum-incompatible (i.e. degassing) fixatives can be used (even if no liquid would be required). Perfect fixation would retain the cellular architecture and permit access of antibodies used for labelling to the intracellular compartments. Glutaraldehyde, which crosslinks proteins into permanent stasis, is the most commonly used EM fixative as it provides strong fixation and good ultrastructural preservation. However, glutaraldehyde is autofluorescent and therefore not widely used in fluorescent microscopy applications. On the other hand, formaldehyde based fixatives like paraformaldehyde are commonly used for fluorescent microscopy applications but they don't provide a fixation as strong as glutaraldehyde. A good compromise is generated by addition of a very low (0. 25%) percentage of glutaraldehyde to the formaldehyde based fixative solution. We have found that this mixed fixative solution produces only limited autofluorescence and yields a better ultrastructural preservation. Additionally, osmium tetroxide (OsO_4) is widely used in electron microscopy as a secondary fixative. OsO_4 oxidizes the unsaturated bonds of fatty acids and reduces to a black metallic osmium (mw-254.2) which is electron dense and adds contrast to biological tissue as a secondary label. However, presence of OsO_4 quenches the fluorescence and therefore it is mostly not advised to be used for CLEM applications[51] .

For our application, the cells were fixed by adding a mixture of 2.5% paraformaldehyde and 0.25% glutaraldehyde in PBS (pH 7.4) at an equal volume of culture medium. They were fixed for 15 minutes, rinsed 3 times with PBS and then proceeded for imaging.

Imaging

Correlative imaging experiments were conducted on an integrated correlative microscopy platform mounted on a Quanta 200 FEG SEM microscope (FEI). The details about this platform [66] and the SCLEM method [83] are presented elsewhere. Previous work by others and us have shown that nanoparticles of 10 nm can be discerned a resolution below 10 nm can be achieved for imaging liquid immersed particles below SiN membranes [121,126]. SEM images were made at standard high-vacuum settings with varying acceleration voltages and different magnifications. A solid-state backscatter detector was used for BSE imaging. The FM was operated with a 40x CFI Plan Apochromat objective lens with a numerical aperture of 0.95 and a working distance of 0.25–0.16 mm (Nikon). A LED with a wavelength of 470 nm (Thorlabs) was used for illumination. A dichroic mirror with an edge wavelength of 506 nm, a (Semrock FF506-Di03), was used to separate excitation and emission. The detection was done with a CCD camera (Clara, Andor) placed after a filter wheel housing the emission filters. The cells, which are cultured, labelled and fixed on the µchips, were placed in the holder and 70 µl Tyrode's Buffer was added. The bottom metal plate hosting the glass slide was then placed, the holder was clamped and mounted in the integrated microscope for correlative imaging.

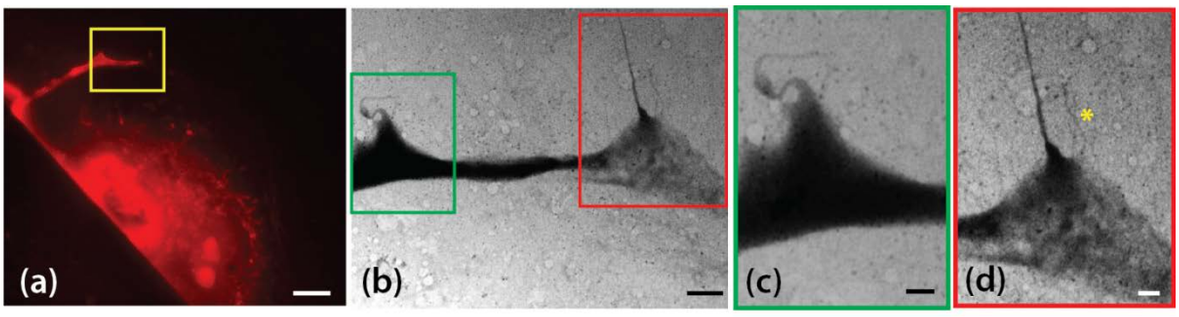

Figure 4. Imaging with Liquid Sample Holder. (a) Epi-fluorescent image of a CV1 cell cultured on the SiN membranes, labelled with EGF-QDots, fixed and imaged in liquid in the integrated microscope. **(b)** SEM image of the area in (a) depicted with a yellow rectangle. **(c)(d)** Higher magnification images of the filopodial structures in (b) shown with a green and a red rectangle, respectively. The yellow asterix denotes a fine filopodial structure that can be visualized in the SEM image. The scalebars are 10 μm in (a), 2 μm in (b), and 500 nm in (c) and (d).

Figure 4. presents correlative imaging of CV1 cells cultured on the SiN membranes, incubated with EGF-conjugated QDots, fixed and imaged in liquid. Epi-fluorescence image shows a cell present on one of the edges of the SiN membrane (Figure 4.a). Internalization of EGF- Qdot conjugates are visualized at different stages like binding to the cellular cortex and transportation in the cytoplasm. The fluorescent image can now be used as a navigation tool to pinpoint regions of interest for higher resolution SEM images. As the fluorescence microscope is coaxially positioned with the SEM in the integrated microscope, the selected regions are just brought to the center of fluorescence field of view and SEM images are recorded at the desired magnifications. The corresponding SEM image of the area depicted with a rectangle in Figure 4.a is presented in Figure 4.b. The image is recorded with the solid state backscatter detector (BSED) at an acceleration voltage of 14 keV and an approximate electron dose of ~1 x 10^4 e^-/nm^2. The outer cell edge and the filopodial structures can be clearly identified in the SEM image. Locations with a dense presence of QDot conjugates provide a higher contrast in the images and appear dark. Higher magnification images of the rectangle areas in Figure 4.b are presented in Figure 4.c and d.

Individual EGF-QDot conjugates being transported along the filopodia, are visible as dark spots in the images. Furthermore, fine cellular structures like the one denoted with an asterix can be visualized with high resolution in liquid.

Integration of micro-fluidics

As discussed earlier, a holder for correlative microscopy with integrated micro-fluidics would bring distinct advantages for bio-imaging studies. Addressing this demand, we also present a first conceptual design and proof-of-principle operation of a liquid flow cell for correlative microscopy of samples in liquid. A series of sequential lithography steps allows us to create the window and several larger flow channels on a single Si wafer. The fabrication of the μ-fluidic chip is similar to the process for fabricating SiN membranes with additional steps to create flow channels. The μ-fabrication steps are schematically illustrated in Figure 5.a and can be listed as follows: **[i]** 4" diameter, 500 μm thick, high resistivity (> 10.000 Ω/cm2), p-type B, double side polished wafers are cleaned with RCA1, RCA2 **[ii]** and coated with photoresist on the "bottom-side". **[iii]** The custom designed mask#1 which defines the area for the SiN membrane as well as some alignment markers is patterned, developed and etched using RIE. **[iv]** The wafers are cleaned and completely covered with a 40 nm layer of low stress silicon nitride using a LPCVD process. **[v]** A layer of photo-resist is applied to the "bottom-side" of the wafer and the custom designed mask#2 is patterned on the wafer that defines the channels and the inlet/outlet ports. **[vi]** The silicon nitride is selectively etched away with RIE and the remaining photoresist was stripped off. **[vii]** Then, the "top-side" of the wafer is spin-coated with photo-resist and the mask#3, which defines the inlet/outlet ports at the top-side and the final placement of the SiN membrane, is patterned and developed. **[viii]** RIE is used to etch the silicon-nitride at the ports and membrane at the top-side. After this step, the wafer is covered with silicon nitride except for the places where the channels, ports and membrane should come. **[ix]** The exposed silicon is then anisotropically etched in a KOH bath. After the etching process the wafer is cleaned with HCl and double- distilled water and dried. The chips are diced from the wafer using a diamond-cutter and cleaned using RCA1 and RCA2. The front and backside of the resulting chip are presented in (Figure 5.b). The fabricated chip is then clamped to an optically transparent substrate in a vacuum-tight holder (Figure 5.c). Standard PEEK tubing with 1/32" outside diameter and stainless steel vacuum feed-troughs (IDEX Health & Science, USA) welded in a custom made flange are used to connect the holder to the reservoirs outside the SEM vacuum chamber (Figure 5.d).

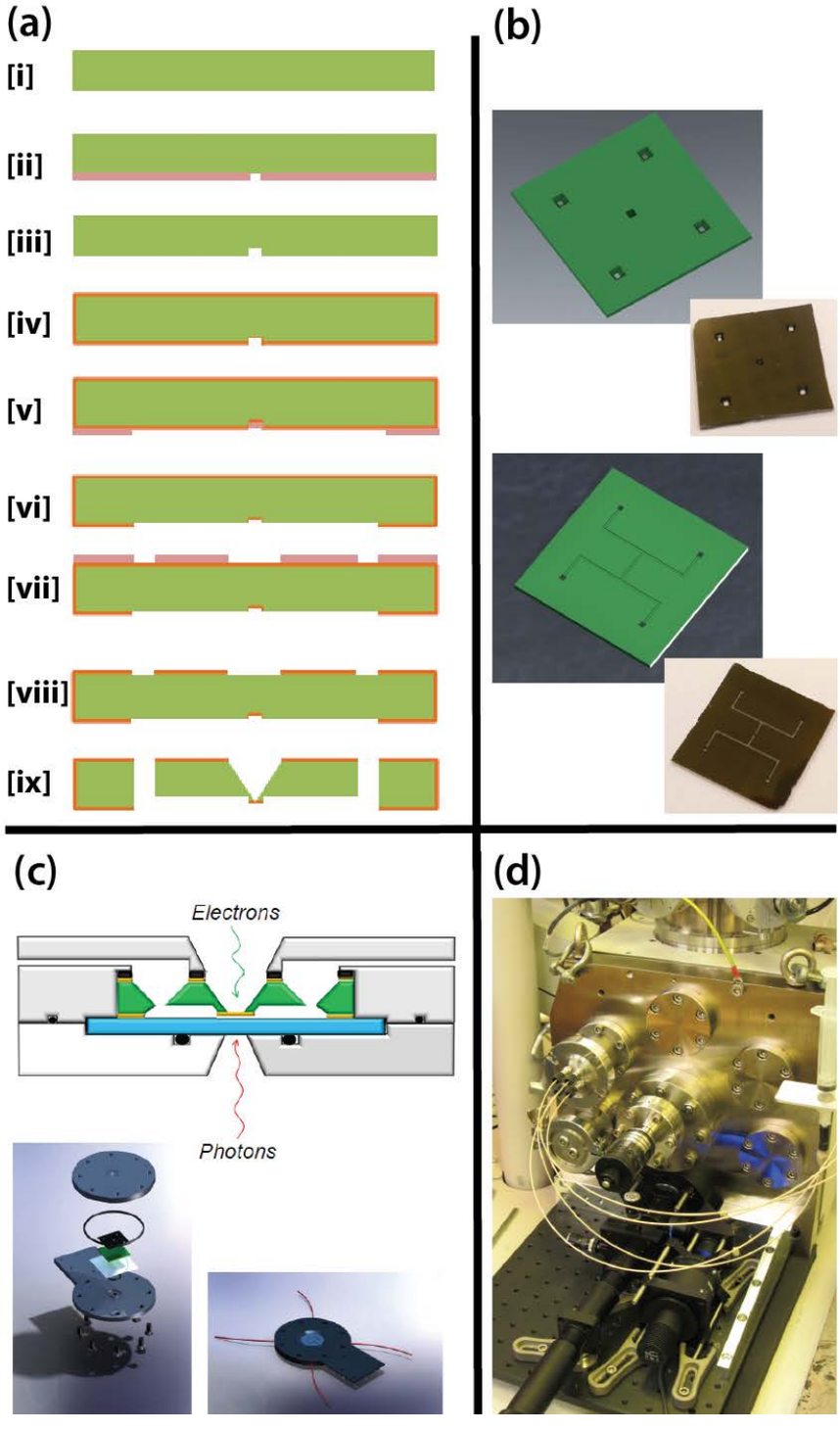

Figure 5. Integration of μ-fluidics in the liquid sample holder. (a) Microfabrication procedure for the chips with SiN membranes and flow channels. **(b)** Front and back side images of an individual chip, fabricated with the procedure shown in (a).**(c)** A vacuum-tight holder with tubing, is designed for clamping the fabricated chips and the optically transparent substrates. A cross-section view and an exploded view of the holder with the chip and the glass slide are presented. **(d)** The holder is mounted in the integrated microscope and connected to the liquid reservoirs outside the SEM vacuum chamber with standard tubing and vacuum feed-troughs.

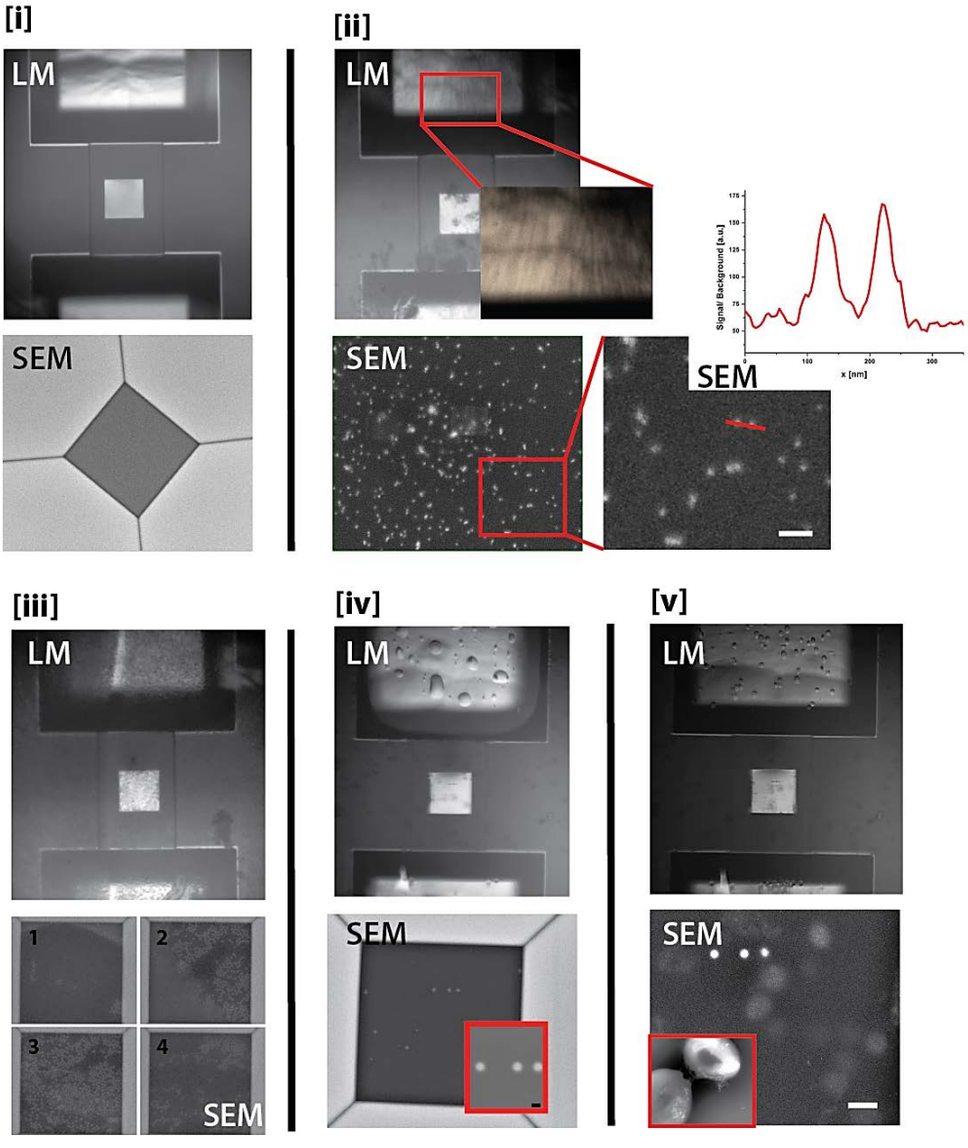

Figure 6. Consecutive flow in the µ-fluidic liquid holder.

[i] Optical image (top) and a SEM image (bottom) of the SiN membrane region in the µ-fluidic liquid holder which is filled with water in the integrated microscope. **[ii]** Optical image (top) and a SEM image (bottom) of 35nm Au NPs in water introduced in the µ-fluidic holder. A higher magnification image of the rectangled area in the SEM image is shown in right with a line profile taken over the depicted particles. Scalebar in the image is 200nm**. [iii]** Then, the reactor was flushed with water and filled with silica particles of 1 µm in size. An optical image (top) and instantaneous SEM images (bottom) during the flow of the particles are shown. **[iv]** After the reactor was flushed again with water, some particles remains fixed on the SiN membrane. Optical image (top) and a SEM image (bottom) of such a state are presented. Scalebar in the image is 1µm **[v]** Subsequently, *S. Cerevisiae* cells were introduced in the µ-fluidic holder. An optical image (top) and a SEM image (bottom) of the yeast cells are shown. Scalebar in the SEM image is 5µm. Inset shows a higher magnification image of the two yeast cells located next to the silica particles. The holder was not removed or opened in between the steps [i] to [iv].

To demonstrate the performance of the reactor, 35 nm Au NPs, 1μm SiO_2 particles and *S. Cerevisiae* cells in aqueous solutions were sequentially flushed and imaged in the integrated microscope. The liquid samples were introduced by manually applied pressure to the syringes attached at the end of the tubing. The microscope was operated in high vacuum mode and no change was observed in the chamber pressure while the liquids were introduced to the reactor. As all samples contain non-fluorescent materials, all band filters were removed from the light microscope set-up, thus operating it in a reflection mode. A LED with a wavelength of 470 nm is used as the light source (Thorlabs, USA) and the images are captured using a CCD camera (CoolSNAP, Photometrics, USA). It was possible to watch the flow of all the particles with the light microscope and observe them with the SEM when they come to close proximity with the SiN membrane.

Consecutive loading and imaging of samples in the reactor is demonstrated in Figure 6. Figure 6.**[i]** shows an optical image (top) and a SEM image (bottom) of the reactor after it is mounted in the integrated microscope and filled with water. Next, Au NPs in water, which are 35 nm in size, were introduced in the reactor Figure 6.**[ii]**. SEM image of the particles taken consecutively with the optical image can be seen in Figure 6.**[ii]**. As the NPs are far smaller than the resolution limit of the light optical system, it is not possible to identify single particles. However, upon close inspection and comparison with the image in Figure 6.**[i]**, streamlines of flowing particles can be discerned, especially in the upper channel. Also, large clusters and debris can be seen to have flushed in, mostly at the lower part of the image. Note that there is also some creep flow next to the thinner part of the channel with the membrane, which is due to the fact that both parts of the reactor are not bonded but clamped together. The SEM enables high resolution imaging of single particles as well as clusters. A magnified image of the area depicted with a rectangle, recorded with a 20 keV acceleration voltage and a 30 μs pixel dwell time, is shown to the right. The line profile taken over 2 Au NPs is also presented below the enlarged image and shows the achievable SEM resolution in the reactor is enough to identify single particles. Then, the reactor was flushed again with water until it was clean of Au NPs and filled with silica particles of 1 μm in size suspended in water. Although the Au NP tend to stick to the SiN membrane during electron beam exposure, they detach easily after flushing the reactor with water. Figure 6.**[iii]**shows an optical image together with four instantaneous SEM images(20 keV, 300 ns dwell time) from a recorded video of SiO_2 particle flow. During the flow of the particles, a small amount remains permanently fixed on the SiN membrane. This enables taking images of the fixed particles with longer dwell times (100 μs) as shown in Figure 6.**[iv]**. Lastly, the reactor was flushed again with water and *S. Cerevisiae* cells in PBS were introduced. Figure 6.**[v]**shows an optical image and a SEM image of these cells in the reactor. The three silica particles that were stuck on the SiN membrane are still present. A higher magnification SEM image (20 keV, 30 μs dwell time) of the two yeast cells located next to those particles is recorded with BSED and shown in the inset.

Discussion

With the presented holder, samples can be kept in liquid for correlative light and electron microscopy. The holder is designed to offer ease of handling during cell culturing and sample preparation procedures. Therefore, it provides an easy means to link functional FM observations with high resolution EM observations of the samples in their near native states. Presence of liquid eliminates the risk of structural deformation in the cells due to drying artefacts and makes it possible for visualization of native fine structures in the SEM.

The holder presented here has several assets compared with the other methods linking LM and EM of liquid samples. Firstly, it can be easily used on separate LM and EM's as well as integrated (S)CLEM microscopes. In means of attainable resolution in LM techniques, the presented holder can be favorable to the holder presented for FM and wet- STEM imaging, as the imaging for LM is also done through a SiN membrane in that configuration and that permits only the use of low NA and long working distance objective lenses. On the other hand, the light transparent window of the holder presented here consists of glass, and therefore enables light microscopy using glass corrected high NA objective lenses and (vacuum compatible) immersion oils. On the other hand, it should be noted that with the holder presented here only SEM imaging is possible, limiting the observable depth near the SiN membrane. Also the presented holder is less vulnerable to damage and rupture during sample preparation processes.

The SEM resolution with the presented holder is directly related with the thickness of the SiN membranes that constitute the electron transparent windows. Thicker membranes lead to loss of resolution due to the broadening of the primary electron beam while passing the membranes. Even though the expected FW50 size of the primary electron beam after passing a 40 nm membrane is less than 2 nm, thinner SiN membranes or membranes from graphene[109] can also be used if a higher resolution is required. Resolution will decrease for imaging labels located deeper inside the cells or in water. Therefore, culturing cells on the SiN membranes is important and actually makes this technique especially strong and promising for studies related with the cellular processes on the adherent surface of the cells.

Blurring in SEM imaging of particles was observed due to their movement and flow in liquid. Imaging of particles with longer dwell times was only possible for the immobilized particles on the SiN membrane (see, Figure 6.**[iv]**). Therefore, incorporating dielectrophoretic, and/or optical trapping methods can be a significant improvement for the presented holder. With trapping methods, dispersed samples like nanoparticle suspensions, viruses and bacteria in solution, can be sorted and pre-selected in liquid. And then they can be transported and brought in contact with the SiN membrane for high resolution SEM imaging.

The addition of flow capabilities to the designed holder facilitates simultaneous high resolution correlative imaging and manipulation of the environment of living cells in their natural hydrated state. This device can be applied to perform experiments that were basically not possible before. It would be also beneficial to combine a μ-fluidic design with a means to easily culture cells on SiN.

With the flowing liquid, the environment of which the cells are kept in can be manipulated, nutrients and pharmaceuticals can be introduced, and the response of the cells can be monitored not only with light microscopy but also with high resolution SEM. The resulting imaging would provide complementary structural and functional information of the sample in reaction to the introduced stimuli.

This technique is also promising in other fields like materials science and chemistry. e.g. for correlative imaging of catalytic reactions in liquid, visualizing crystal growth etc. In-situ EM studies have been previously reported where nucleation and growth kinetics[127] are analysed, diffusion characteristics of individual nanoparticles are investigated[128,129] , and catalytic reactions are visualized[130] . The surface reaction studies and/or studies with materials immobilized on the membranes can be easily coupled with LM observations with the presented holder. Especially placing the holder in an integrated CLEM platform provides novel capabilities for imaging electron beam-induced processes like beam-induced nanoparticle formation[114] , assembly[131] and quantitative radiation damage studies.

Ultimately, the possibility of imaging samples in liquid with FM and SEM in an integrated platform may well enable a way to combine the live-cell FM imaging with high resolution SEM. The samples can be imaged in liquid with live-cell FM, and SEM snapshots can be captured at selected regions and time-points on-demand, based on the dynamic FM observations. This will be the subject of the next chapter.

Conclusion

We have shown the design and fabrication process of a holder for correlative light and scanning electron microscopy of whole cells in liquid. The holder is designed to be light transparent below with a glass substrate for LM imaging and electron transparent above with a thin SiN membrane for SEM imaging. Cells can be cultured and processed on SiN membranes similar to fluorescent microscopy applications. We have presented the detailed sample preparation process for correlative imaging of whole cells in liquid, which brings new possibilities to study cells in their near native environment. By mounting the presented holder in an integrated microscope, we visualized the distribution of EGF-Qdot proteins in CV1 cells in their native liquid environment with SCLEM. We have also illustrated that the existing enclosure can be advanced to a microfluidic reactor and we have demonstrated consecutive filling and imaging in the reactor with Au NPs, SiO2 particles and yeast cells. We believe the presented method for correlative imaging of samples in liquid opens novel possibilities to study distribution of specific proteins in biological samples in near native environment.

Acknowledgements

We would like to thank Ruud van Tol, Frans Berwald, Ger Schotte, and Cor Barends for technical support.

Chapter VIII

On-Demand Electron Microscopy of Living Cells in Liquid

We present a novel approach towards dynamic bio-imaging wherein live-cell fluorescence microscopy (FM) is carried out in-situ in a scanning electron microscope (SEM). The FM observation of cellular dynamics allows the selection of region and time of interest capturing live-cell structural SEM snapshots. To illustrate this on-demand application of SEM, we study the uptake and retrograde transport of epidermal growth factor (EGF) conjugated quantum dots (QDots) in filopodium of fibroblasts. The cells are cultured on a thin, electron-transparent substrate, which is placed in a light-transparent sample holder containing the EGF-QDot solution. The on-demand SEM images reveal positions of individual QDots on the cytoskeleton transport tracks within filopodia from the position of uptake up to the docking region at the microtubules frontier where QDots accumulate before further transport in the cytoplasm.

This chapter is submitted for publication as:

Liv, N., van Oosten Slingeland, D. S. B., Baudoin, J. P., Kruit, P., Piston, D. W., Hoogenboom, J. P. (n.d.). On-Demand Electron Microscopy of Living Cells in Liquid. *Submitted.*

Introduction

One of the major strengths of light microscopy, and especially fluorescence microscopy (FM), is the ability to observe the dynamics of labelled biomolecules during live biological processes. Improved understanding of biomolecular activity, however, increasingly relies on the ability to image molecular positions with respect to cellular ultrastructure with a resolution beyond that of the light microscope. Super-resolution techniques surpass the diffraction limit, but the increased spatial resolution often comes at the expense of temporal resolution, e.g., due to the sequential nature of recording and switching individual fluorophores [15,16,132,133]. In addition, only labelled species are visualized and non-labelled structural components are not imaged with super-resolution. Cellular ultrastructure is traditionally imaged with electron microscopy (EM), where the samples are fixed, dehydrated, and even sectioned. EM of samples in a near-native environment has been recently shown possible by separating the liquid sample from the vacuum chamber of EM with an enclosure compromising one (for Scanning EM (SEM)) [40,42] or two (for (Scanning) Transmission EM ((S)TEM)) [38,39,107] thin electron transparent membranes. However, these methods can only image fixed cells as the destructive nature of EM imaging precludes observing cellular dynamics. Thus, microscopy techniques are needed that link the live cell imaging capabilities of FM with high resolution structural EM imaging.

Integrated microscopes combining FM and EM in a single apparatus have recently been developed [64–66]. Such systems can enable Simultaneous Correlative Light and Electron Microscopy (SCLEM) by which fluorescence measurements can be directly projected onto the structural detail measured in SEM[83]. The electron and optical axes are aligned to each other and therefore, the same region on the sample can be imaged with FM and SEM at the same time or sequentially. With an enclosure to hold samples in liquid in the vacuum environment which also has a light transparent window on one side and an electron transparent window on the other, SCLEM can be performed on fixed cells in liquid[121]. Specific protein labels consisting of nanoparticles can be used to study the locations of individual proteins in liquid.

Here we introduce the methodology of On-Demand EM (ODEM) and we show imaging of single nanoparticle biomarkers in live cells cultured on the electron transparent window. The integrated FM is used to monitor the sample and based on the observed dynamics, the region and time of interest for SEM snapshots are determined. These SEM snapshots are thus recorded without any additional preparation for EM.

We use this method to study the internalization and the cellular distribution of the Epidermal Growth Factor (EGF) in fibroblasts possessing EGF receptors (EGFR). EGF triggers several signalling cascades responsible for cellular motility, DNA replication, and cell proliferation[134]. EGF binding the EGFR leads to dimerization and activation of the EGFR[135]. EGFR then undergo retrograde transport on cell edge protrusions via the F-actin cytoskeleton[136]. Activated EGFR are internalized through clathrin-dependent endocytosis, and they are either sorted into the recycling endosomes and returned to the plasma membrane, or centripetally transported from peripheral

early endosomes to perinuclear multivesicular bodies (MVBs)/late endosomes[137]. EGFR that do not recycle follow the degradative trafficking pathway and are ultimately dumped into lysosomes. Microtubules are associated with the regulation of EGFR internalization, intracellular trafficking and targeting to lysosomes [138].

Complexes of streptavidin-conjugated quantum dots (QDs) with biotinylated EGF (EGF-QD) are biochemically competent ligands for EGFR. Their unique fluorescence properties (brightness, selectivity, and photo-stability) meet the requirements for prolonged in vivo imaging[139]. Also their visibility in electron microscopy makes them a good candidate for ODEM[81,140]. Therefore, EGF was conjugated with Quantum Dots (QDots) and their uptake and transport was monitored with FM. On-demand EM snapshots then revealed the positions and distribution of labelled EGFR molecules with respect to cellular ultrastructure.

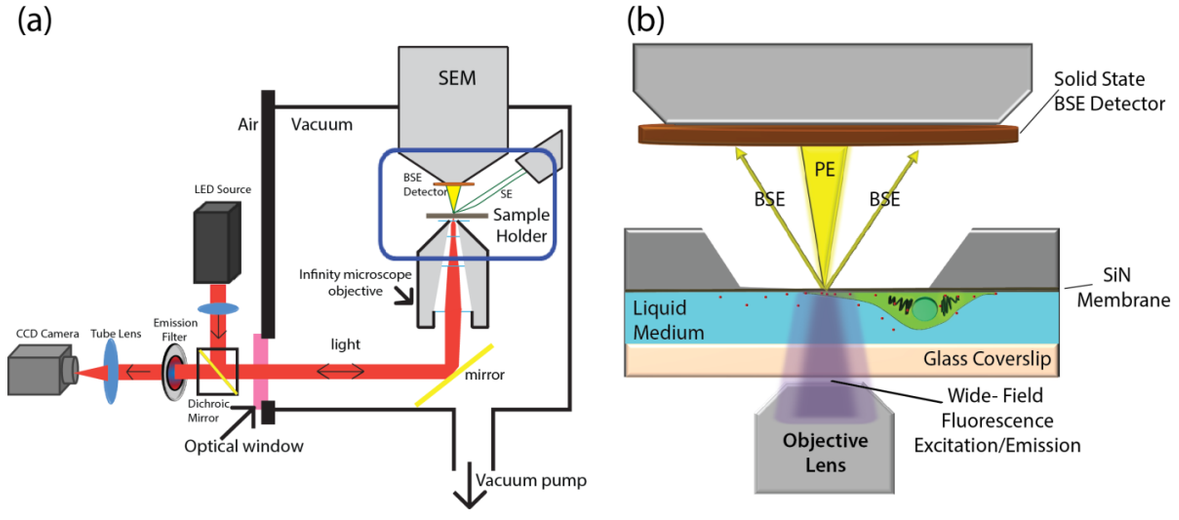

Figure 1. (a) ODEM of live samples is enabled by placing a liquid enclosure in an integrated light-electron microscope **(b)** Live-cell fluorescence microscopy is carried out from below through the light transparent substrate, while the high-resolution electron images can be taken on demand from above through the electron transparent membrane.

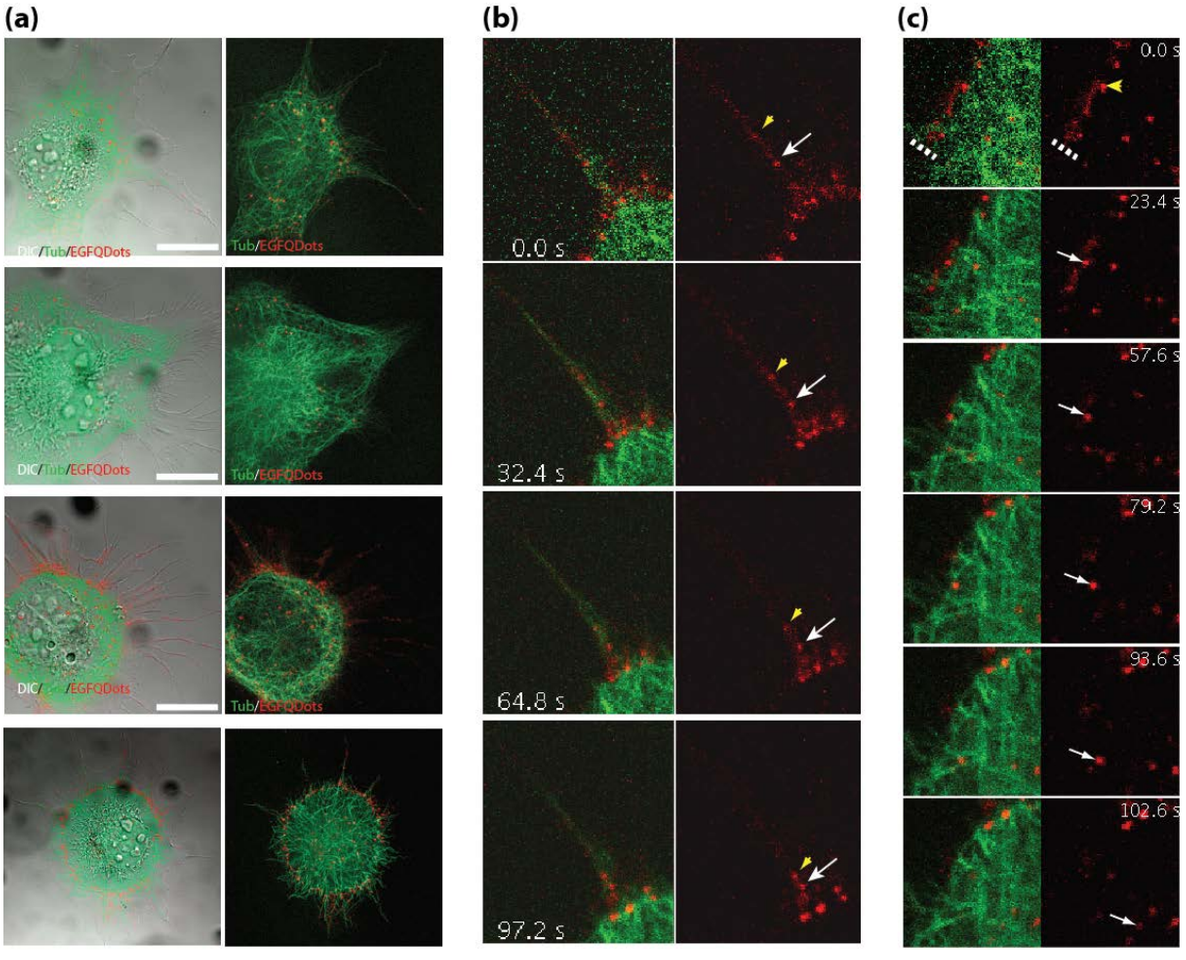

Figure 2. Various stages of EGF-QDot uptake and transport. (a) EGF-QDot uptake and transport in COS7 cells. The cells were grown for 1day in serum-free medium on glass slides. Live staining of microtubules was performed by Tubulin-Tracker and.the cells were further labelled with 10 nM EGF-QDots for 5 minutes, and imaged with a confocal scanning laser microscope. Scalebars are 20 μm. **(b)** Time-lapse imaging of a similarly labelled living Cos7 cell zoomed in a filopodial extension. Arrows depict QDOts filled vesicles which are uptaken in filopodia and being transported towards the cellular cortex. **(c)** Time-lapse imaging zoomed in cellular cortex and the microtubule frontier. Arrows depict EGF-QDot conjugates which await at the microtubule frontier before being further transported in the cytoplasm.

Results

Uptake and Transport of EGF bound QDots

Cos7 and CV1 cells were cultured on silicon nitride membranes that can serve as the electron-transparent window in an enclosure to hold liquids in the SEM (see Figure 1). First, the motion of EGF-QDot clusters during and after EGFR mediated internalization by Cos7 cells was characterized by imaging live cells cultured on glass bottom dishes with confocal fluorescence microscopy and DIC. We also labelled the microtubules with a live staining reagent and analyzed the respective cellular distribution of the EGF-QDot clusters and of the microtubule cytoskeleton, at different time points after labelling of the cells.

We observed that during the first 15 minutes following the labelling, EGF-QDots were gradually taken up at the filopodia and transported in clusters along filopodia in the direction of the cell (Figure 2), as also previously reported by Lidke *et al.*[136]. After 15 minutes, clusters transported from the filopodia towards the cell body were observed to assemble and remain in the cell periphery at the outline of the microtubule network before being internalized into the cell body. This so-called "docking region" forms a distinct boundary surrounding the microtubule network (Figure 2.b). After being internalized into the cell region containing the microtubule network, clusters followed the microtubules during transport towards the cell nucleus (Figure 2.c). Clusters moving along tubules show directionally consistent movement. Collisions between moving clusters result in temporary pauses in their transport, followed by either each cluster continuing its own path, or fusion into a larger cluster that also moves along the microtubule network[141]. For ODEM we focused on the uptake of EGF-QDots and their transport along filopodia to the docking region.

On Demand SEM of intracellular EGF-QDot Transport

The same culturing procedure was carried out with EGF-QDots added to a sample of CV1 cells that was then clamped in a holder and mounted in an integrated microscope (Figure 1) where they were first visualized with the wide-field fluorescence microscope. Figure 3.a shows an overlay of a fluorescent image and a reflection image of the cells inside the liquid enclosure. The image provides information about the position of the cells on the silicon nitride membrane and the distribution of QDot clusters. Live-cell dynamics were monitored with the fluorescence microscope to identify active transport regions. Figure 3.b shows a time-lapse series of such a region. At some locations, clusters of QDots seem temporarily trapped (denoted with an asterisk), whereas at other regions clusters continuously move along cellular structure. Based on these dynamics, we selected this region for a SEM snapshot. The corresponding snapshot is presented in Figure 3.c, in which the cellular structure and the cortex are clearly visible. Outside the area covered by the cell, large clusters of QDots attached to the bare window. The bright white spot visible within the cellular structure probably represents a lipid droplet. Individual QDots cannot be identified at this magnification, but inside the cell darker tracks can be seen reminiscent of the trajectories followed by internalized EGF-QDot conjugates. Figure 3.d and 3.e are enlarged images of the regions depicted with blue and green rectangles in Figure 3.c, respectively.

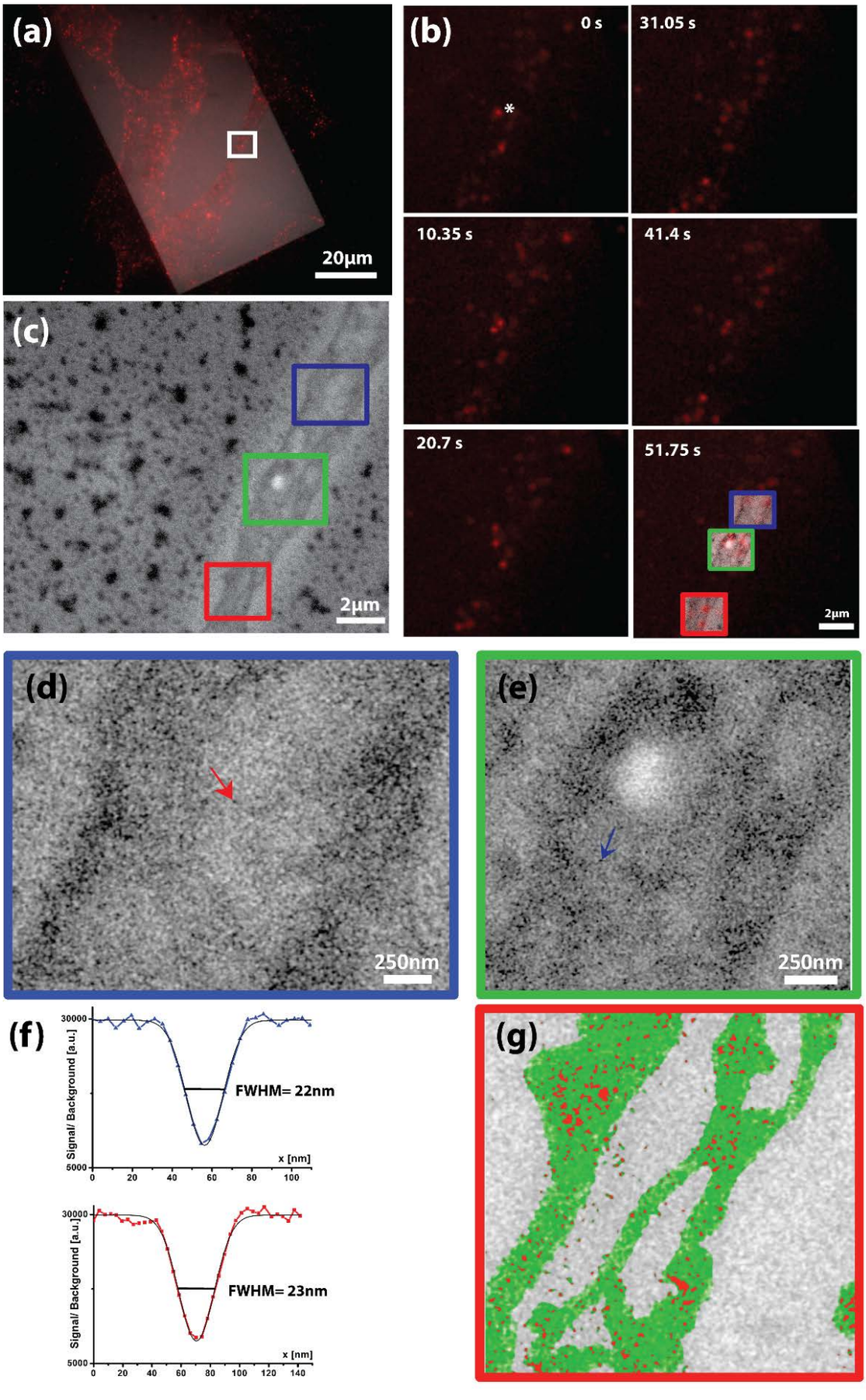
(a)
20µm
(b)
0 s
31.05 s
10.35 s
41.4 s
20.7 s
51.75 s
2µm
(c)
2µm
(d)
250nm
(e)
250nm
(f)
FWHM= 22nm
Signal/ Background [a.u.]
x [nm]
FWHM= 23nm
Signal/ Background [a.u.]
x [nm]
(g)

Figure 3. On-Demand Electron Microscopy of EGF-QDot transport in a CV1 cell.

(a) Overlay of reflection and fluorescence images of CV1 cells grown for 1day in serum-free medium on SiN membranes and labelled with 5 nM EGF-QDots for 15 minutes in the liquid enclosure.

(b) Time-lapse images of the white rectangular area in (a). Some clusters of QDots, like the one denoted with an asterisk, are static while some are rather dynamic. The last panel shows the overlay of the higher magnification SEM images with the fluorescent image of the same regions.

(c) SEM snapshot of the depicted area in (a) and (b).

(d) Higher magnification image of the area in (c) depicted with a blue rectangle.

(e) Higher magnification image of the area in (c) depicted with a green rectangle. A higher concentration of QDot clusters is visible around the cellular cortex and around the crossings of followed trajectories.

(f) Line profiles of the two rectangle QDots in (d) and (e), with FWHM of 22 and 23 nm, respectively.

(g) Render constructed from the area in (c) depicted with a red rectangle, where green illustrates the light grey tracks and the red shows the black particle clusters.

The smallest size of visible particles we encounter is 20 nm in FWHM, and therefore this size is attributed as the size of a single EGF-QDot. Here, these EGF-QDots as well as clusters of particles are clearly visible as dark spots on the tracks identified in Figure 3.c. To confirm that the single dark spots correspond to a single EGF-QDot particle, intensity profiles were taken over the two spots indicated in Figure 3.d and 3.e respectively. The full width at half maximum (FWHM) of these profiles were 22 nm and 23 nm, respectively (Figure 3.f). Considering the electron beam broadening [41] in the silicon nitride window, the poly-l-lysine layer and the cell membrane, these values are consistent with the producer mentioned size (15-20 nm) for the QDot particles. The calculated 25%-75% edge resolution values for 10 particles using both left and right side of the line profiles vary between 7 and 8.5 nm. This variation may well result from the presence of QDots at different depths inside the cell which alters the effective beam broadening per QDot.

In the last panel in Figure 3.b, we show the overlay of higher magnification SEM images with the fluorescent image of the same regions. The image clearly represents the resolution gap between fluorescence microscopy and SEM. The fluorescent signal mainly originates from dense clusters of QDots visualized in the SEM images. There is particular overlap between the fluorescence and SEM images for (quasi-)static clusters of QDots (Figure 3.e). The fact that mostly static clusters overlap results from the approximately 2 minutes of time difference between the last fluorescence and the SEM image. The localization of the (quasi-)static QDot clusters clearly coincides with structural components such as the intersections between trajectories and the lipid droplet indicated with an asterix (Figure 3.d & e & g). We note that the number of QDots visible in the SEM images is certainly higher than the amount that can be extrapolated from the fluorescence images. This suggests either a lot of QDot particles are in a non-fluorescent state or their fluorescence is too low to be detected in the current setup. We note that it is an important benefit that both fluorescent and non-fluorescent QDots are visualized, as each QDot depicts the position of an internalized EGF(R) molecule.

Our SEM results are consistent with our previous finding about the directional transport of EGF-QDot conjugates after their internalization. The tracks followed by internalized QDots can be clearly distinguished, and as an example Figure 3.g shows a segmented blow-up of the red boxed region in the last panel in Figure 3.b, where the light grey tracks are depicted in green and the black particle clusters in red (Figure 3.g). Again, a higher density of QDots is visible around the crossing points of segmented tracks and at the flattened extension around the cortex. These regions also predominantly co-localize with the strong and (quasi-)static fluorescence spots, suggesting an accumulation and slower transport of QDot clusters around these structural “bottlenecks”.

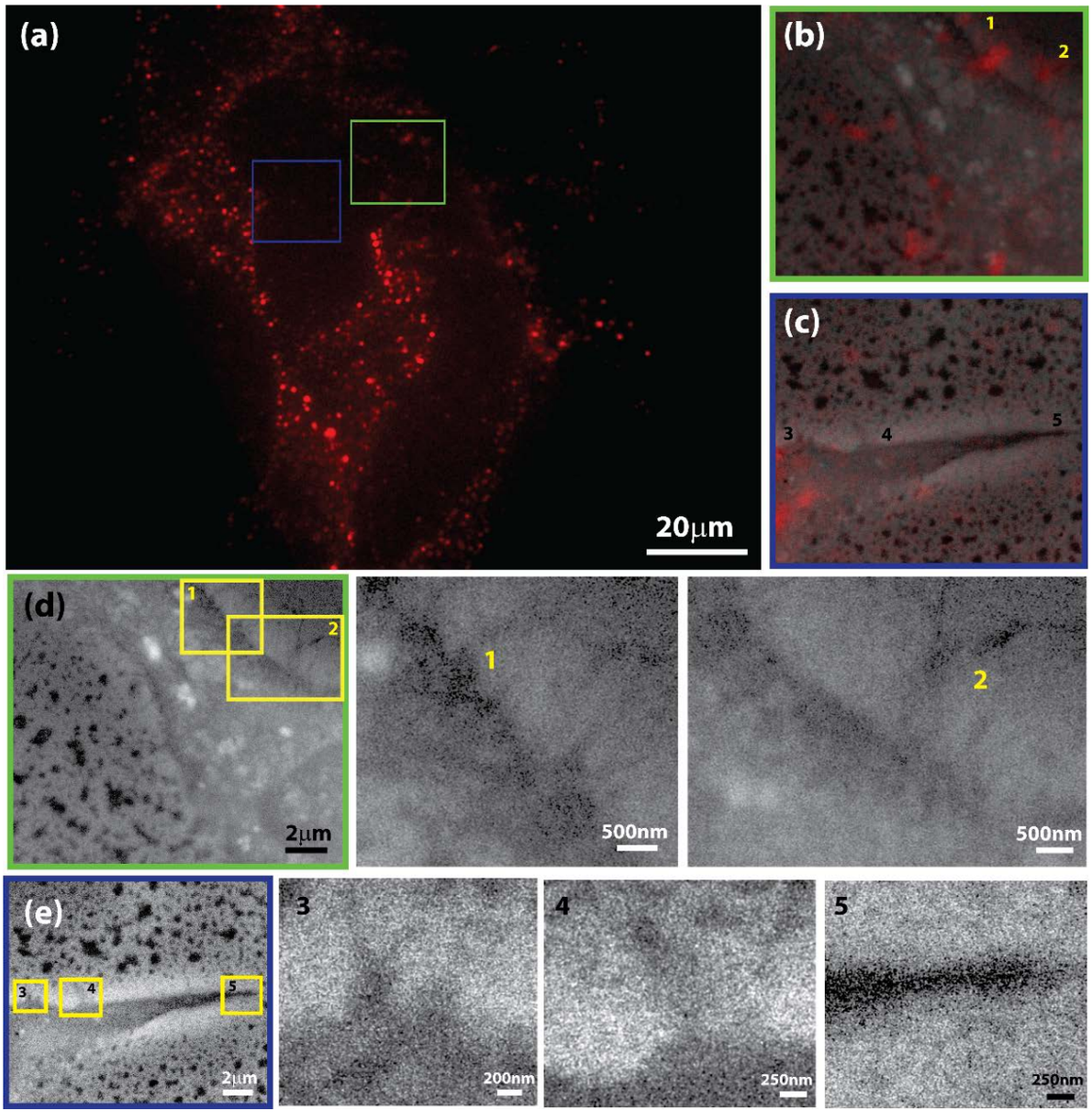

Figure 4. Uptake and transport in filopodia. (a) Fluorescent image showing EGF-QDot uptake in CV1 cells grown on the SiN membranes in the liquid enclosure. **(b)** Overlay of fluorescent image and the corresponding SEM image of the green rectangular area in (a). the regions depicted with circles appear as highly active uptake regions in dynamic observations. **(c)** Overlay of fluorescent image and the SEM image of the blue rectangular area in (a), showing a cellular extension. **(d)** Higher magnification images of the area in (a) depicted with a green rectangle. Encircled regions in the SEM images with high QDot concentrations co-localize with the encircled fluorescently intense sub-regions in (b) as anticipated. **(e)** Higher magnification images of the area in (a) depicted with a blue rectangle**.** A high density of QDots is observable at the filopodial structures present in (3) and (4), and especially at the tip of the cellular extension (5), suggestive of the tip as an active uptake site.

EGF-QDot uptake and transport in filopodia

Next, we focused our attention to the uptake of the EGF-QDots. This has been previously reported to take place at the filopodia[136], as was also observed in our confocal fluorescence experiments in Figure 2.b. We use ODEM to reveal the filopodia structure with the actual position of the EGF-QDot conjugates

We determined the positions of the cells and the QDot clusters using FM (Figure 4.a). The live cell fluorescence observations enable us to pinpoint the location of the uptake regions. We identified two regions as active uptake points, depicted with green and blue rectangles in Figure 4.a. At these positions, we took our SEM snapshots, shown in Figure 4.b and Figure 4.c overlaid with the fluorescence images. Figure 4.d and Figure 4.e show the SEM images alone. The contours of the cell and some intracellular structures, like lipid droplets and internal tracks, are readily visible. In Figure 4.b the fluorescently intense sub-regions, labelled 1 and 2, co-localize with the filopodial structures in the SEM images as expected. These regions were also apparent as active uptake regions in live fluorescence observations. Higher magnification images of these two selected regions are represented in Figure 4.d.1 and Figure 4.d.2. The mentioned regions with strong fluorescence signals are denoted with circles in the overlay (Figure 4.b) and enlarged SEM images. Corresponding to our fluorescence observations, a high density of QDot clusters is visible along the filopodia in Figure 4.d.1 and Figure 4.d.2, especially at the tip of the filopodial structure visible in Figure 4.d.2. The docking of EGF-QDot conjugates at the cell contour is visible in Figure 4.d.1, and is consistent with our previous observation that the conjugates wait at the microtubule frontier before being further transported into the cellular matrix. Three regions in Figure 4.c, marked as 3, 4, and 5 are also represented as higher magnification images in Figure 4.e.3, 4 and 5 respectively. The images shown in Figure 4.e.3 and 4 also show the QDots present along the filopodia, especially at the tip region. The region represented in Figure 4.e.5, which is the tip of the cellular extension, contains a high density of QDots suggesting the tip as an active uptake site for EGF-QDot conjugates.

Discussion

The above results demonstrate the SEM imaging of individual bio-marker positions in connection to the cellular structure during live processes. The achieved 25%-75% edge resolution in the presented data for ODEM is estimated to be ~7.5 nm, about a factor of 40 higher than of confocal microscopy. Super-resolution light microscopy techniques can provide images of fixed cells around 15-20 nm resolution, but live cell imaging is usually only possible at the expense of resolution. Additionally, ODEM does not require data post-processing, and the SEM image adds cellular structural detail to the FM images.

The achievable resolution in liquid SEM depends on the broadening of the electron beam before it reaches the sample. Therefore, the resolution is highest if the sample is placed directly beneath the electron transparent membrane[121]. Thus, cellular processes like adhesion, motility, cell to cell connections, and cellular signalling are well-suited for ODEM imaging. We used QDots as labels providing contrast both in FM and SEM, but other labels like FluoroNanoGold[53] and second harmonic generating nanoprobes[11] could also be used. For these applications, there is no need for dedicated or modified sample preparation protocols for ODEM compared to FM, but application may also be extended to recently emerging dedicated light-electron probes such as photo-conversion or metal-tagging proteins[23,24,54,58]. In the latter case, it is particularly interesting to note that live cells could be exposed to low concentrations of gold salt for tagging metallothionein without signs of morphological or viability changes for up to 1 hr[24]. Although temporal correlation between FM and EM images would be lost, the possibility to maintain the ROI in view and under FM monitoring throughout the EM labelling procedure could be an important benefit of ODEM.

In general, the capabilities of ODEM can be extended with microfluidic connections to the sample enclosure. This would enable sequential labelling, but also in-situ fixation or labelling of cells for different biomolecules with labels of different characteristics. In addition, the response of cells after external stimulus, e.g., pharmaceuticals, could be investigated with ODEM. A continuous liquid flow could also be beneficial for reducing beam damage by flushing with scavengers for free radical species and aqueous electrons formed by the e-beam.

The effects of radiation damage are critical for electron microscopy of cells. In our method as FM is used to monitor and select regions of interest, electron-beam exposure to the cells is intrinsically limited to the recorded SEM snapshots. Therefore, damage occurring after exposure would be more of a concern if repetitive SEM imaging is aimed at the same region. The typical electron dose used for the images in this study was ~1 x 10^3 e^-/nm^2 and we did not observe morphological changes in the cells with this dose. However, dissociation of the cells from the SiN membrane was observed after recording a series of consecutive images from the same region (see Figure 5). On the other hand, the possibility of repeated imaging of the same area in liquid STEM imaging of fixed cells without structural damage was previously reported for electron doses which are 2 magnitudes higher than used in this study[119]. It should be noted that radiation damage of biological samples in EM has mostly been addressed for fixed, dehydrated samples in conventional or environmental EM[142,143]. For samples in liquid, charge accumulation is prevented by grounding

through the conductive fluid, but on the other hand, radical species and aqueous electrons are generated in water by irradiation with electron energy higher than 10 eV, the bond energy of a valence electron in water[144]. Thus, damage to the sample can mostly be a secondary effect due to the radical species generated in the fluid. ODEM could provide an interesting, novel means to quantitatively study electron-beam induced radiation damage in the cells, e.g., by monitoring cell viability through fluorescence reporters. Ultimately, the effects of radiation damage could also be further minimised by using scanning strategies that keep the accumulation of radical species below a critical level, e.g., interlaced scanning or frame integration.

Finally, the presented implementation of ODEM is with a wide-field fluorescence microscope. The incorporation of optical sectioning in the FM observations, would improve imaging quality in the upper part of the sample that is observable with SEM, and thus lead to a more quantitative correlation between FM and SEM signals. This could then also allow decreasing the size of the SEM region of interest so that a snapshot *during* a dynamic event could be taken. We believe that ODEM will thus not only open entirely novel perspectives for imaging biological dynamics, but could in addition also be useful for studying other types of processes typically taking place in liquid, such as in soft matter science, nanoparticle synthesis and (self-)assembly, and (photo-) catalysis.

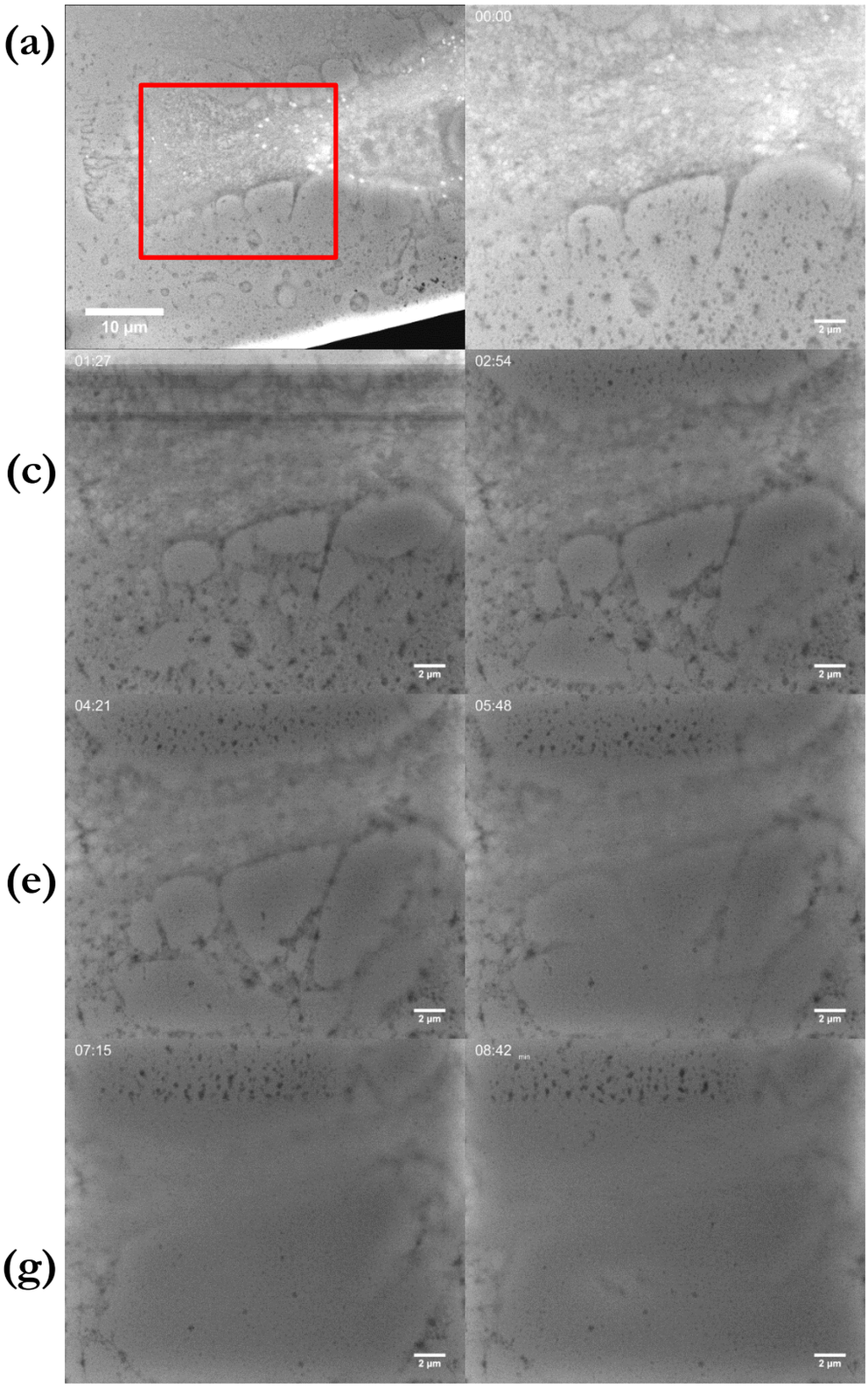

Figure 5. Detachment of cells from the SiN membrane upon long electron beam exposure. Consecutive SEM images (b to h) of the region depicted with a rectangle in (a) were recorded with a pixel size of 6.25 nm^2, and a pixel dwell time of 3 µs. The cell is totally dissociated from the SiN surface after 8 minutes of scanning with an electron dose of ~1 x 10^3 e^-/nm^2.

Material and Methods

SCLEM Set-Up

The experiments were performed on a home-built integrated high NA light-electron microscope where an inverted epi-fluorescence microscope is integrated into a commercial SEM (FEI Quanta FEG 200). The integrated microscope is explained in detail elsewhere[66]. The set-up is also schematically indicated in Figure 1.a.

For SEM imaging of the CV1 cells with QDots, the SEM was operated under High Vacuum with 14 keV primary beam energy and a working distance of 8 mm. The images were recorded with 4096x3775 pixels with a pixel dwell time of 100 μs. For the fluorescence imaging of QDot uptake in CV1 cell, the integrated microscope was equipped with a Nikon CFI PLAN APO, 40X, NA 0.95 dry objective lens and a Nikon 1.5x tube lens. A 470 nm Thorlabs LED source was used for illumination. A dichroic mirror (Semrock FF506-Di03), which has an edge wavelength of 506 nm, separates excitation and emission light. The detection path consisted of a 655 nm band-pass filter (Semrock 655/40 nm BrightLine®) and a CCD camera (Andor Clara). Images were recorded using μ- Manager1.2.

Preparation of Chips with SiN Membrane

The chips were manufactured by depositing low stress silicon nitride (30 nm) on silicon wafers (300 μm) by low-pressure chemical vapour deposition. Two windows (300x100 μm) were opened in each chip by anisotropic etching in a KOH heat bath. The wafers were then coated with photoresists and diced. To remove the chips from the wafers, they were first kept in 50°C acetone for approximately 15 minutes. The chips were then washed in 100% ethanol and finally rinsed with ddH_2O. They were cleaned with RCA1 (125ml ddH_2O; 50ml H_2O_2; 25ml NH_4; 15minutes) and rinsed with ddH_2O. Prior to seeding the chips were plasma cleaned for 15minutes (250Watt) and coated with poly-L -lysine.

Culturing CV1 cells

Monkey Kidney Fibroblast (CV1) cell line (Cell Lines Service, Germany), were maintained in DMEM supplemented with 10% Fetal Bovine Serum, Penicillin/Streptomycin and 2 mM Glutamine at 37° under 5% CO_2. The cells were washed with Phosphate Buffered Saline (PBS) (pH 7.4), trypsinized with 1X TrypLE™ Express (Invitrogen) and then seeded onto sterile, poly-L -lysine coated, 50 nm thick Si_3N_4 membranes and they were grown overnight. Prior to Quantum Dot (QDot) labeling, the cells were incubated in serum free medium for 4 hours at 37° under 5% CO_2.

EGF-QDot Labelling of CV1 cells

For QDot-EGF labeling, EGF-QDot conjugates were formed by incubating EGF-biotin (Invitrogen, USA) with streptavidin-QDot655 (Invitrogen, USA) for 2 h at room temperature in

50 mM borate buffer, pH 8.3. A microcentrifuge purification column (Ultracel-100YM, Millipore) was used to remove unbound EGF-biotin. Then the cells were incubated with 5 nM EGF-QDot655 in Tyrode's buffer (Sigma), supplemented with 0.1% BSA (Sigma) and 50 mM D-glucose (Sigma-Aldrich) for 5 min at room temperature[111]. After the staining, the cells were washed three times. 70 µl of previously stated Tyrode's Buffer was added in the enclosure, and the sample was imaged in liquid in the integrated microscope.

EGF-QDots and microtubules labeling of Cos7 cells

Cos7 cells were grown for one day in serum-free medium on glass slides (MatTek). Live staining of microtubules was performed by incubating the cells for 30 minutes in 100 nM Tubulin-Tracker solution (Invitrogen). Cells were then labelled with 10 nM EGF-QDots for 5 minutes, and imaged with a confocal scanning laser microscope (LSM510).

References

1. Chalfie, M., Tu, Y., Euskirchen, G., Ward, W. W. & Prasher, D. C. Green fluorescent protein as a marker for gene expression. *Science (80-.).* **263,** 802–5 (1994).
2. Cormack, B. P., Valdivia, R. H. & Falkow, S. FACS-optimized mutants of the green fluorescent protein (GFP). *Gene* **173,** 33–38 (1996).
3. Zhao, Y. *et al.* An expanded palette of genetically encoded Ca^{2+} indicators. *Science* **333,** 1888–91 (2011).
4. Pawley, J. *Handbook Of Biological Confocal Microscopy*. (Springer US, 2006). doi:10.1007/978-0-387-45524-2
5. Mertz, J. Optical sectioning microscopy with planar or structured illumination. *Nat. Methods* **8,** 811–9 (2011).
6. Dertinger, T., Xu, J., Naini, O. F., Vogel, R. & Weiss, S. SOFI-based 3D superresolution sectioning with a widefield microscope. *Opt. nanoscopy* **1,** 2 (2012).
7. Konig, K. Multiphoton microscopy in life sciences. *J. Microsc.* **200,** 83–104 (2000).
8. Zipfel, W. R., Williams, R. M. & Webb, W. W. Nonlinear magic: multiphoton microscopy in the biosciences. *Nat. Biotechnol.* **21,** 1369–77 (2003).
9. Sidani, M., Wyckoff, J., Xue, C., Segall, J. E. & Condeelis, J. Probing the microenvironment of mammary tumors using multiphoton microscopy. *J. Mammary Gland Biol. Neoplasia* **11,** 151–63 (2006).
10. Moreaux, L., Sandre, O. & Mertz, J. Membrane imaging by second-harmonic generation microscopy. *J. Opt. Soc. Am. B* **17,** 1685 (2000).
11. Pantazis, P., Maloney, J., Wu, D. & Fraser, S. E. Second harmonic generating (SHG) nanoprobes for in vivo imaging. *Proc. Natl. Acad. Sci. U. S. A.* **107,** 14535–40 (2010).
12. Rehman, S., Balla, N. K., Seng, E. Y. Y. & Sheppard, C. J. R. in *Opt. Fluoresc. Microsc.* (Diaspro, A.) 55–74 (Springer Berlin Heidelberg, 2011). doi:10.1007/978-3-642-15175-0
13. Abbe, E. Beiträge zur Theorie des Mikroskops und der mikroskopischen Wahrnehmung. *Arch. für Mikroskopische Anat.* **9,** 413–418 (1873).
14. Dyba, M., Jakobs, S. & Hell, S. W. Immunofluorescence stimulated emission depletion microscopy. *Nat. Biotechnol.* **21,** 1303–4 (2003).
15. Rust, M. J., Bates, M. & Zhuang, X. Sub-diffraction-limit imaging by stochastic optical reconstruction microscopy (STORM). *Nat. Methods* **3,** 793–5 (2006).
16. Shroff, H. *et al.* Dual-color superresolution imaging of genetically expressed probes within individual adhesion complexes. *Proc. Natl. Acad. Sci. U. S. A.* **104,** 20308–13 (2007).
17. Sahl, S. J. & Moerner, W. E. Super-resolution fluorescence imaging with single molecules. *Curr. Opin. Struct. Biol.* **23,** 778–87 (2013).
18. Knoll, M. & Ruska, E. Das Elektronenmikroskop. *Zeitschrift fur Phys.* **78,** 318–339 (1932).
19. Reimer, L. *Transmission electron microscopy - Physics of Image Formation and Microanalysis. Scanning* **12,** 547 (Springer, 1984).
20. Reimer, L. *Scanning Electron Microscopy — Physics of Image Formation and Microanalysis. J. Basic Microbiol.* **27,** 529 (Springer, 1985).
21. Koster, A. J. & Klumperman, J. Electron microscopy in cell biology: integrating structure and function. *Nat. Rev. Mol. Cell Biol.* **Suppl,** SS6–10 (2003).

22. Oorschot, V., de Wit, H., Annaert, W. G. & Klumperman, J. A novel flat-embedding method to prepare ultrathin cryosections from cultured cells in their in situ orientation. *J. Histochem. Cytochem.* **50,** 1067–80 (2002).
23. Diestra, E., Fontana, J., Guichard, P., Marco, S. & Risco, C. Visualization of proteins in intact cells with a clonable tag for electron microscopy. *J. Struct. Biol.* **165,** 157–68 (2009).
24. Risco, C. *et al.* Specific, sensitive, high-resolution detection of protein molecules in eukaryotic cells using metal-tagging transmission electron microscopy. *Structure* **20,** 759–66 (2012).
25. Dubochet, J. & Sartori Blanc, N. The cell in absence of aggregation artifacts. *Micron* **32,** 91–99 (2001).
26. Glaeser, R. M. Cryo-Electron Microscopy of Biological Nanostructures. *Phys. Today* **61,** 48 (2008).
27. Studer, D., Humbel, B. M. & Chiquet, M. Electron microscopy of high pressure frozen samples: bridging the gap between cellular ultrastructure and atomic resolution. *Histochem. Cell Biol.* **130,** 877–89 (2008).
28. Hoenger, A. & McIntosh, J. R. Probing the macromolecular organization of cells by electron tomography. *Curr. Opin. Cell Biol.* **21,** 89–96 (2009).
29. Micheva, K. D. & Smith, S. J. Array tomography: a new tool for imaging the molecular architecture and ultrastructure of neural circuits. *Neuron* **55,** 25–36 (2007).
30. Lichtman, J. W. & Denk, W. The big and the small: challenges of imaging the brain's circuits. *Science* **334,** 618–23 (2011).
31. Knott, G., Marchman, H., Wall, D. & Lich, B. Serial section scanning electron microscopy of adult brain tissue using focused ion beam milling. *J. Neurosci.* **28,** 2959–64 (2008).
32. Denk, W. & Horstmann, H. Serial block-face scanning electron microscopy to reconstruct three-dimensional tissue nanostructure. *PLoS Biol.* **2,** e329 (2004).
33. Briggman, K. L. & Bock, D. D. Volume electron microscopy for neuronal circuit reconstruction. *Curr. Opin. Neurobiol.* **22,** 154–61 (2012).
34. Stokes, D. J. Recent advances in electron imaging, image interpretation and applications: environmental scanning electron microscopy. *Philos. Trans. A. Math. Phys. Eng. Sci.* **361,** 2771–87 (2003).
35. Stokes, D. J. *Principles and Practice of Variable Pressure: Environmental Scanning Electron Microscopy (VP-ESEM).* (John Wiley & Sons, 2008).
36. Kirk, S. E., Skepper, J. N. & Donald, A. M. Application of environmental scanning electron microscopy to determine biological surface structure. *J. Microsc.* **233,** 205–24 (2009).
37. Liu, K.-L. *et al.* Novel microchip for in situ TEM imaging of living organisms and bio-reactions in aqueous conditions. *Lab Chip* **8,** 1915–21 (2008).
38. De Jonge, N., Peckys, D. B., Kremers, G. J. & Piston, D. W. Electron microscopy of whole cells in liquid with nanometer resolution. *Proc. Natl. Acad. Sci. U. S. A.* **106,** 2159–64 (2009).
39. Klein, K. L., Anderson, I. M. & de Jonge, N. Transmission electron microscopy with a liquid flow cell. *J. Microsc.* **242,** 117–23 (2011).
40. Thiberge, S. *et al.* Scanning electron microscopy of cells and tissues under fully hydrated conditions. *Proc. Natl. Acad. Sci. U. S. A.* **101,** 3346–51 (2004).
41. Thiberge, S., Zik, O. & Moses, E. An apparatus for imaging liquids, cells, and other wet samples in the scanning electron microscopy. *Rev. Sci. Instrum.* **75,** 2280 (2004).

42. Nishiyama, H. *et al.* Atmospheric scanning electron microscope observes cells and tissues in open medium through silicon nitride film. *J. Struct. Biol.* **169,** 438–449 (2010).
43. Van Rijnsoever, C., Oorschot, V. & Klumperman, J. Correlative light-electron microscopy (CLEM) combining live-cell imaging and immunolabeling of ultrathin cryosections. *Nat. Methods* **5,** 973–80 (2008).
44. Polishchuk, E. V, Polishchuk, R. S. & Luini, A. Correlative light-electron microscopy as a tool to study in vivo dynamics and ultrastructure of intracellular structures. *Methods Mol. Biol.* **931,** 413–22 (2013).
45. Spiegelhalter, C., Laporte, J. F. & Schwab, Y. Correlative light and electron microscopy: from live cell dynamic to 3D ultrastructure. *Methods Mol. Biol.* **1117,** 485–501 (2014).
46. Robinson, J. M. & Takizawa, T. Correlative fluorescence and electron microscopy in tissues: immunocytochemistry. *J. Microsc.* **235,** 259–72 (2009).
47. Kolotuev, I., Schwab, Y. & Labouesse, M. A precise and rapid mapping protocol for correlative light and electron microscopy of small invertebrate organisms. *Biol. Cell* **102,** 121–32 (2010).
48. Kukulski, W. *et al.* Correlated fluorescence and 3D electron microscopy with high sensitivity and spatial precision. *J. Cell Biol.* **192,** 111–9 (2011).
49. Watanabe, S. *et al.* Protein localization in electron micrographs using fluorescence nanoscopy. *Nat. Methods* **8,** 80–4 (2011).
50. Karreman, M. A. *et al.* Optimizing immuno-labeling for correlative fluorescence and electron microscopy on a single specimen. *J. Struct. Biol.* **180,** 382–6 (2012).
51. Karreman, M. A, Van Donselaar, E. G., Agronskaia, A. V, Verrips, C. T. & Gerritsen, H. C. Novel contrasting and labeling procedures for correlative microscopy of thawed cryosections. *J. Histochem. Cytochem.* **61,** 236–47 (2013).
52. Peddie, C. J. *et al.* Correlative and integrated light and electron microscopy of in-resin GFP fluorescence, used to localise diacylglycerol in mammalian cells. *Ultramicroscopy* (2014). doi:10.1016/j.ultramic.2014.02.001
53. Takizawa, T., Suzuki, K. & Robinson, J. M. Correlative Microscopy Using FluoroNanogold on Ultrathin Cryosections: Proof of Principle. *J. Histochem. Cytochem.* **46,** 1097–1102 (1998).
54. Grabenbauer, M. *et al.* Correlative microscopy and electron tomography of GFP through photooxidation. *Nat. Methods* **2,** 857–62 (2005).
55. Sosinsky, G. E., Giepmans, B. N. G., Deerinck, T. J., Gaietta, G. M. & Ellisman, M. H. Markers for correlated light and electron microscopy. *Methods Cell Biol.* **79,** 575–91 (2007).
56. Giepmans, B. N. G. Bridging fluorescence microscopy and electron microscopy. *Histochem. Cell Biol.* **130,** 211–7 (2008).
57. Brown, E. & Verkade, P. The use of markers for correlative light electron microscopy. *Protoplasma* **244,** 91–7 (2010).
58. Shu, X. *et al.* A genetically encoded tag for correlated light and electron microscopy of intact cells, tissues, and organisms. *PLoS Biol.* **9,** e1001041 (2011).
59. Verkade, P. Moving EM: the Rapid Transfer System as a new tool for correlative light and electron microscopy and high throughput for high-pressure freezing. *J. Microsc.* **230,** 317–28 (2008).
60. Koning, R. I. *et al.* MAVIS: An integrated system for live microscopy and vitrification. *Ultramicroscopy* (2013). doi:10.1016/j.ultramic.2013.10.007

61. Wouters, C. & Koerten, H. Combined light microscope and scanning electron microscope, a new instrument for cell biology. *Cell Biol. Int. Rep.* **6,** 955–959 (1982).
62. Agronskaia, A. V *et al.* Integrated fluorescence and transmission electron microscopy. *J. Struct. Biol.* **164,** 183–9 (2008).
63. Kanemaru, T. *et al.* A fluorescence scanning electron microscope. *Ultramicroscopy* **109,** 344–9 (2009).
64. Morrison, I. E. G. *et al.* Atmospheric scanning electron microscope for correlative microscopy. *Methods Cell Biol.* **111,** 307–24 (2012).
65. Maruyama, Y., Ebihara, T., Nishiyama, H., Suga, M. & Sato, C. Immuno EM-OM correlative microscopy in solution by atmospheric scanning electron microscopy (ASEM). *J. Struct. Biol.* **180,** 259–70 (2012).
66. Zonnevylle, A. C. *et al.* Integration of a high-NA light microscope in a scanning electron microscope. *J. Microsc.* (2013). doi:10.1111/jmi.12071
67. Giepmans, B. N. G., Adams, S. R., Ellisman, M. H. & Tsien, R. Y. The Fluorescent Toolbox for Assessing. *Science (80-.).* **312,** 217–224 (2006).
68. Hell, S. W. Far-field optical nanoscopy. *Science* **316,** 1153–8 (2007).
69. Biel, S. S., Kawaschinski, K., Wittern, K.-P., Hintze, U. & Wepf, R. From tissue to cellular ultrastructure: closing the gap between micro- and nanostructural imaging. *J. Microsc.* **212,** 91–9 (2003).
70. Gaietta, G. M. *et al.* Golgi twins in late mitosis revealed by genetically encoded tags for live cell imaging and correlated electron microscopy. *Proc. Natl. Acad. Sci. U. S. A.* **103,** 17777–82 (2006).
71. Pluk, H., Stokes, D. J., Lich, B., Wieringa, B. & Fransen, J. Advantages of indium-tin oxide-coated glass slides in correlative scanning electron microscopy applications of uncoated cultured cells. *J. Microsc.* **233,** 353–63 (2009).
72. Plitzko, J. M., Rigort, A. & Leis, A. Correlative cryo-light microscopy and cryo-electron tomography: from cellular territories to molecular landscapes. *Curr. Opin. Biotechnol.* **20,** 83–9 (2009).
73. Mironov, A. A. & Beznoussenko, G. V. Correlative microscopy: a potent tool for the study of rare or unique cellular and tissue events. *J. Microsc.* **235,** 308–21 (2009).
74. Spiegelhalter, C. *et al.* From dynamic live cell imaging to 3D ultrastructure: novel integrated methods for high pressure freezing and correlative light-electron microscopy. *PLoS One* **5,** e9014 (2010).
75. Caplan, J., Niethammer, M., Taylor, R. M. & Czymmek, K. J. The power of correlative microscopy: multi-modal, multi-scale, multi-dimensional. *Curr. Opin. Struct. Biol.* **21,** 686–93 (2011).
76. Kopek, B. G., Shtengel, G., Xu, C. S., Clayton, D. a & Hess, H. F. Correlative 3D superresolution fluorescence and electron microscopy reveal the relationship of mitochondrial nucleoids to membranes. *Proc. Natl. Acad. Sci. U. S. A.* **109,** 6136–41 (2012).
77. Lucas, M. S., Günthert, M., Gasser, P., Lucas, F. & Wepf, R. Bridging microscopes: 3D correlative light and scanning electron microscopy of complex biological structures. *Methods Cell Biol.* **111,** 325–56 (2012).
78. Wouters, C. H. Techniques for combining light microscopy and scanning electron microscopy: a survey of the literature. *J. Microsc.* **147,** 5–14 (1987).

79. Rushe, N. *et al.* Cytocompatibility of novel tin oxide thin films. *J. Mater. Sci. Mater. Med.* **16,** 247–52 (2005).
80. Niitsuma, J.-I., Oikawa, H., Kimura, E., Ushiki, T. & Sekiguchi, T. Cathodoluminescence investigation of organic materials. *J. Electron Microsc. (Tokyo).* **54,** 325–30 (2005).
81. Giepmans, B. N. G., Deerinck, T. J., Smarr, B. L., Jones, Y. Z. & Ellisman, M. H. Correlated light and electron microscopic imaging of multiple endogenous proteins using Quantum dots. *Nat. Methods* **2,** 743–9 (2005).
82. Cortese, K., Diaspro, A. & Tacchetti, C. Advanced correlative light/electron microscopy: current methods and new developments using Tokuyasu cryosections. *J. Histochem. Cytochem.* **57,** 1103–12 (2009).
83. Liv, N. *et al.* Simultaneous Correlative Scanning Electron and High-NA Fluorescence Microscopy. *PLoS One* **8,** e55707 (2013).
84. Haring, M. T. *et al.* Automated sub-5nm overlay accuracy in correlative light and electron microscopy. *Prep.*
85. Faas, F. G. A. *et al.* Localization of fluorescently labeled structures in frozen-hydrated samples using integrated light electron microscopy. *J. Struct. Biol.* **181,** 283–90 (2013).
86. Micheva, K. D., Rourke, N. O., Busse, B. & Smith, S. J. Array Tomography : High-Resolution Three-Dimensional Immunofluorescence Array Tomography : High-Resolution Three-Dimensional Immunofluorescence. *Cold Spring Harb. Protoc.* 697–719 (2010). doi:10.1101/pdb.top89
87. Jahn, K. A. *et al.* Correlative fluorescence and transmission electron microscopy: an elegant tool to study the actin cytoskeleton of whole-mount (breast) cancer cells. *J. Microsc.* **235,** 282–92 (2009).
88. Oberti, D., Kirschmann, M. A. & Hahnloser, R. H. R. Correlative microscopy of densely labeled projection neurons using neural tracers. *Front. Neuroanat.* **4,** 24 (2010).
89. Ravelli, R. B. G. *et al.* Destruction of tissue, cells and organelles in type 1 diabetic rats presented at macromolecular resolution. *Sci. Rep.* **3,** 1804 (2013).
90. Livet, J. *et al.* Transgenic strategies for combinatorial expression of fluorescent proteins in the nervous system. *Nature* **450,** 56–62 (2007).
91. Lacoste, T. D. *et al.* Ultrahigh-resolution multicolor colocalization of single fluorescent probes. *Proc. Natl. Acad. Sci. U. S. A.* **97,** 9461–6 (2000).
92. Michalet, X., Lacoste, T. D. & Weiss, S. Ultrahigh-resolution colocalization of spectrally separable point-like fluorescent probes. *Methods* **25,** 87–102 (2001).
93. Churchman, L. S., Okten, Z., Rock, R. S., Dawson, J. F. & Spudich, J. A. Single molecule high-resolution colocalization of Cy3 and Cy5 attached to macromolecules measures intramolecular distances through time. *Proc. Natl. Acad. Sci. U. S. A.* **102,** 1419–23 (2005).
94. Koyama-Honda, I. *et al.* Fluorescence imaging for monitoring the colocalization of two single molecules in living cells. *Biophys. J.* **88,** 2126–36 (2005).
95. Barlow, A. L., Macleod, A., Noppen, S., Sanderson, J. & Guérin, C. J. Colocalization analysis in fluorescence micrographs: verification of a more accurate calculation of pearson's correlation coefficient. *Microsc. Microanal.* **16,** 710–24 (2010).
96. Churchman, L. S. & Spudich, J. A. Colocalization of fluorescent probes: accurate and precise registration with nanometer resolution. *Cold Spring Harb. Protoc.* **2012,** 141–9 (2012).

97. Erdelyi, M. *et al.* Correcting chromatic offset in multicolor super- resolution localization microscopy. *Opt. Express* **21,** 12177–12183 (2013).
98. Schellenberger, P. *et al.* High-precision correlative fluorescence and electron cryo microscopy using two independent alignment markers. *Ultramicroscopy* (2013). doi:10.1016/j.ultramic.2013.10.011
99. Van den Born, E., Posthuma, C. C., Knoops, K. & Snijder, E. J. An infectious recombinant equine arteritis virus expressing green fluorescent protein from its replicase gene. *J. Gen. Virol.* **88,** 1196–205 (2007).
100. Knoops, K. *et al.* Ultrastructural characterization of arterivirus replication structures: reshaping the endoplasmic reticulum to accommodate viral RNA synthesis. *J. Virol.* **86,** 2474–87 (2012).
101. Narváez, A. C. *et al.* Cathodoluminescence Microscopy of nanostructures on glass substrates. *Opt. Express* **21,** 29968 (2013).
102. Parthasarathy, R. Rapid, accurate particle tracking by calculation of radial symmetry centers. *Nat. Methods* **9,** 724–6 (2012).
103. Zaidel-Bar, R., Milo, R., Kam, Z. & Geiger, B. A paxillin tyrosine phosphorylation switch regulates the assembly and form of cell-matrix adhesions. *J. Cell Sci.* **120,** 137–48 (2007).
104. Peddie, C. J. & Collinson, L. M. Exploring the third dimension: volume electron microscopy comes of age. *Micron* **61,** 9–19 (2014).
105. Edelstein, A., Amodaj, N., Hoover, K., Vale, R. & Stuurman, N. Computer control of microscopes using μManager. *Curr. Protoc. Mol. Biol.* **Chapter 14,** Unit14.20 (2010).
106. Kieft, E. & Bosch, E. Refinement of Monte Carlo simulations of electron–specimen interaction in low-voltage SEM. *J. Phys. D. Appl. Phys.* **41,** 215310 (2008).
107. De Jonge, N. & Ross, F. M. Electron microscopy of specimens in liquid. *Nat. Nanotechnol.* **6,** 695–704 (2011).
108. Park, J. *et al.* Direct observation of nanoparticle superlattice formation by using liquid cell transmission electron microscopy. *ACS Nano* **6,** 2078–85 (2012).
109. Yuk, J. M. *et al.* High-resolution EM of colloidal nanocrystal growth using graphene liquid cells. *Science* **336,** 61–4 (2012).
110. Creemer, J. F. *et al.* Atomic-scale electron microscopy at ambient pressure. *Ultramicroscopy* **108,** 993–8 (2008).
111. Ring, E. a, Peckys, D. B., Dukes, M. J., Baudoin, J. P. & de Jonge, N. Silicon nitride windows for electron microscopy of whole cells. *J. Microsc.* **243,** 273–83 (2011).
112. Mirsaidov, U. M., Zheng, H., Bhattacharya, D., Casana, Y. & Matsudaira, P. Direct observation of stick-slip movements of water nanodroplets induced by an electron beam. *Proc. Natl. Acad. Sci. U. S. A.* **109,** 7187–90 (2012).
113. Green, E. D. & Kino, G. S. Atmospheric scanning electron microscopy using silicon nitride thin film windows. *J. Vac. Sci. Technol. B Microelectron. Nanom. Struct.* **9,** 1557 (1991).
114. Zheng, H. *et al.* Observation of single colloidal platinum nanocrystal growth trajectories. *Science* **324,** 1309–12 (2009).
115. Zheng, H., Claridge, S. A., Minor, A. M., Alivisatos, A. P. & Dahmen, U. Nanocrystal diffusion in a liquid thin film observed by in situ transmission electron microscopy. *Nano Lett.* **9,** 2460–5 (2009).

116. Ramachandra, R., Demers, H. & de Jonge, N. Atomic-resolution scanning transmission electron microscopy through 50-nm-thick silicon nitride membranes. *Appl. Phys. Lett.* **98,** 93109 (2011).
117. Hyun, J. K., Ercius, P. & Muller, D. a. Beam spreading and spatial resolution in thick organic specimens. *Ultramicroscopy* **109,** 1–7 (2008).
118. Green, E. D. & Kino, G. S. Theoretical model for scanning electron microscopy through thin film windows. *J. Vac. Sci. Technol. B Microelectron. Nanom. Struct.* **9,** 3070 (1991).
119. Dukes, M. J., Peckys, D. B. & de Jonge, N. Correlative fluorescence microscopy and scanning transmission electron microscopy of quantum-dot-labeled proteins in whole cells in liquid. *ACS Nano* **4,** 4110–6 (2010).
120. Joy, D. C. & Joy, C. S. Scanning electron microscope imaging in liquids - some data on electron interactions in water. *J. Microsc.* **221,** 84–8 (2006).
121. Liv, N., Lazić, I., Kruit, P. & Hoogenboom, J. P. Scanning electron microscopy of individual nanoparticle bio-markers in liquid. *Ultramicroscopy* **143,** 93–99 (2013).
122. Da Silva, J. J. R. F. & Willimans, R. J. P. in *Biol. Chem. Elem. Inorg. Chem. Life* **20,** 7–12 (Oxford University Press,, 2001).
123. Koning, R. I. *et al.* Cryo electron tomography of vitrified fibroblasts: microtubule plus ends in situ. *J. Struct. Biol.* **161,** 459–68 (2008).
124. Rodenburg, C., Jepson, M. A. E., Inkson, B. J., Bosch, E. G. T. & Humphreys, C. J. Energy filtered scanning electron microscopy: applications to characterisation of semiconductors. *J. Phys. Conf. Ser.* **241,** 012074 (2010).
125. Peckys, D. B., Veith, G. M., Joy, D. C. & de Jonge, N. Nanoscale imaging of whole cells using a liquid enclosure and a scanning transmission electron microscope. *PLoS One* **4,** e8214 (2009).
126. Sato, T. *et al.* The New Atmospheric Scanning Electron Microscope observes cells in solution as an optical- and electron-correlative microscope . - The ASEM （Atmospheric Scanning Electron Microscope） is able to observe samples in atmospheric pressure at high resolution .
127. Radisic, A., Ross, F. M. & Searson, P. C. In situ study of the growth kinetics of individual island electrodeposition of copper. *J. Phys. Chem. B* **110,** 7862–8 (2006).
128. Franks, R. *et al.* A Study of Nanomaterial Dispersion in Solution by Wet-Cell Transmission Electron Microscopy. *J. Nanosci. Nanotechnol.* **8,** 4404–4407 (2008).
129. Creemer, J. F. *et al.* A MEMS Reactor for Atomic-Scale Microscopy of Nanomaterials Under Industrially Relevant Conditions. *J. Microelectromechanical Syst.* **19,** 254–264 (2010).
130. Gai, P. L. M icroscopy M icroanalysis Development of Wet Environmental TEM (Wet-ETEM) for In Situ Studies of Liquid-Catalyst Reactions on the Nanoscale. 21–28 (2002).
131. Grogan, J. M., Rotkina, L. & Bau, H. H. In situ liquid-cell electron microscopy of colloid aggregation and growth dynamics. *Phys. Rev. E* **83,** 061405 (2011).
132. Betzig, E. *et al.* Imaging intracellular fluorescent proteins at nanometer resolution. *Science* **313,** 1642–5 (2006).
133. Hell, S. W. Toward fluorescence nanoscopy. *Nat. Biotechnol.* **21,** 1347–55 (2003).
134. Cole, N. B. & Lippincott-Schwartz, J. Organization of organelles and membrane traffic by microtubules. *Curr. Opin. Cell Biol.* **7,** 55–64 (1995).

135. Schlessinger, J. Ligand-induced, receptor-mediated dimerization and activation of EGF receptor. *Cell* **110,** 669–72 (2002).
136. Lidke, D. S., Lidke, K. a, Rieger, B., Jovin, T. M. & Arndt-Jovin, D. J. Reaching out for signals: filopodia sense EGF and respond by directed retrograde transport of activated receptors. *J. Cell Biol.* **170,** 619–26 (2005).
137. Leonard, D. *et al.* Sorting of EGF and transferrin at the plasma membrane and by cargo-specific signaling to EEA1-enriched endosomes. *J. Cell Sci.* **121,** 3445–58 (2008).
138. Gao, Y., Hubbert, C. C. & Yao, T.-P. The microtubule-associated histone deacetylase 6 (HDAC6) regulates epidermal growth factor receptor (EGFR) endocytic trafficking and degradation. *J. Biol. Chem.* **285,** 11219–26 (2010).
139. Lidke, D. S. *et al.* Quantum dot ligands provide new insights into erbB/HER receptor-mediated signal transduction. *Nat. Biotechnol.* **22,** 198–203 (2004).
140. Gaietta, G. *et al.* Multicolor and electron microscopic imaging of connexin trafficking. *Science* **296,** 503–7 (2002).
141. Bálint, Š., Verdeny Vilanova, I., Sandoval Álvarez, Á. & Lakadamyali, M. Correlative live-cell and superresolution microscopy reveals cargo transport dynamics at microtubule intersections. *Proc. Natl. Acad. Sci. U. S. A.* **110,** 3375–80 (2013).
142. Egerton, R. F., Li, P. & Malac, M. Radiation damage in the TEM and SEM. *Micron* **35,** 399–409 (2004).
143. Royall, C. P., Thiel, B. L. & Donald, a M. Radiation damage of water in environmental scanning electron microscopy. *J. Microsc.* **204,** 185–95 (2001).
144. Swallow, A. J. *Radiation chemistry. An introduction.* (Wiley, 1973).

Summary

A combined use of fluorescence and light microscopy is a powerful approach to further increase our understanding in biological systems of structure-function relations at cellular and sub-cellular levels. The power of fluorescence microscopy (FM) is to spectrally resolve and visualize individual proteins with endogenous or immuno- fluorescent labeling. Additionally, super-resolution microscopy techniques have beaten the diffraction limit and improved the achievable resolution in FM down to sub 20 nm. However, inherent to FM, it is only the labelled components that are visible and FM cannot provide the ultrastuctural information. On the other hand, electron microscopy (EM) has the power to visualize the ultrastructure with nanometer scale resolution. Therefore, correlative light and electron microscopy (CLEM), which brings the complementary information from FM and EM together, has gained deep interest in recent years. CLEM studies are typically carried out sequentially, by transferring the sample between two separate microscopes, which makes the process considerably cumbersome and therefore constrain widespread CLEM applications. A solution is proposed by integrated strategies, in which a light microscope is mostly integrated in an EM. We have also recently presented an integrated microscope design which enables high-resolution FM inside a Scanning EM (SEM) without compromises in the capabilities of both microscopes.

This thesis aims to explore the potential of the integrated microscope for linking spectrally resolved and live-cell imaging capable FM with structural and high-resolution EM. The novel possibilities introduced by the integrated microscope are presented and discussed firstly for fixed and dehydrated samples, as typical samples in CLEM studies. Furthermore, CLEM of samples in hydrated conditions is realized, and a novel method, which enables on-demand SEM of living cells in liquid is demonstrated.

Chapter II. introduces the method of Simultaneous Correlative Light and Electron Microscopy (SCLEM), which is a novel approach to CLEM brought up by the integrated microscope. The method is based on the new possibility to carry out both high-resolution light and electron microscopy *simultaneously* to the same region of a sample. The method makes it possible for fast and accurate acquisition of large CLEM datasets, and therefore for quantitative investigations of large sample areas. The correlation of high-NA fluorescence imaging with cellular ultrastructure is demonstrated for fluorescently labelled whole cells, as well as tissue sections stained both fluorescently and for EM. The optimized protocol for SCLEM, which aims to help other researchers to adapt their workflows to integrated CLEM, is presented in *Chapter III.* The complete sample preparation protocols for whole cells expressing endogenous fluorophores, for whole cells with immuno-labelling, and for resin embedded cells and tissues are presented together with the mounting procedure for the prepared samples in the integrated microscope. Also the imaging steps required to assure high accuracy registration between the FM and SEM images are explained and

demonstrated comprehensively. *Chapter IV*. presents the enrichment of SCLEM with multi-color capabilities. Simultaneous dual-color FM and SEM is demonstrated by imaging cellular sections of Equine Arteritis Virus (EAV) infected cells, where EAV expresses GFP from its replicase gene and the nuclei/DNA of the infected cells are labelled with Hoechst. The chapter also shows that the method for FM-SEM image registration can also be used for chromatic distortion correction in between distinct FM color channels, which is crucial if the fluorescence information will be mapped onto high-resolution SEM images. The presented method is demonstrated by registering dual-color fluorescence images and a SEM images of paxillin and phospho-paxillin labelled cells into a single coordinate frame with a high precision.

The rest of this thesis focuses on CLEM of samples in liquid, encapsulated in the integrated FM and SEM. *Chapter V*. investigates the achievable resolution in SEM imaging of liquid-immersed nanoparticle bio-labels in detail. Simulations with the Geant4-based Monte Carlo scheme are directly compared to the experimental results for nanoparticles located directly beneath SiN membranes of different thicknesses. The beam broadening, resulting from the interaction of the electron beam with the membrane, and the contrast forming mechanism was discussed and characterized. Also in liquid- SCLEM imaging of single epidermal growth factor (EGF) conjugated quantum dots docked at filopodia during cellular uptake is presented. Furthermore, the resolution and contrast for imaging nanoparticle bio-labels located not directly beneath the membrane but at different depths are investigated in *Chapter VI*. Some initial simulation and experimental results are presented which already shows that imaging single nanoparticle bio-labels is still feasible with reasonable resolution even under these conditions.

The design and fabrication processes of the holder used for CLEM of liquid samples are presented in *Chapter VII*. The holder encapsulates liquid samples in the vacuum chamber of the integrated microscope and enables simultaneous correlative microscopy through the electron transparent and the light transparent windows it has. The detailed sample preparation process for correlative imaging of whole cells cultured directly on the electron transparent membranes, which brings new possibilities to study cells in their near native environment, is represented. Also the possibility of advancing the holder to a microfluidic reactor is discussed and proof-of concept experiments with consecutive filling and imaging in the reactor are demonstrated. Finally, *Chapter VIII*. presents the novel method of on-demand EM (ODEM), which merges the strengths of live-cell FM imaging with high resolution SEM. The cellular dynamics are monitored in liquid with live-cell FM, and SEM snapshots are captured at selected regions and time-points on-demand, based on the FM observations. ODEM is demonstrated by imaging the uptake and retrograde transport of EGF-conjugated quantum dots (QDots) in fibroblasts. ODEM is promising for opening up entirely novel perspectives for imaging biological dynamics by linking the live cell imaging capabilities of FM with high resolution structural EM imaging.

Samenvatting

Een gecombineerd gebruik van fluorescentie en elektronenmicroscopie is een krachtige manier om ons begrip van structuur-functie relaties op (sub-)cellulair niveau in biologische systemen verder te vergrootten. De kracht van fluorescentiemicroscopie (FM) is dat individuele eiwitten spectraal opgelost en gevisualiseerd kunnen worden door middel van aangehechte fluorescente moleculen (immuno-labels) of fluorescente eiwitten (endogene labels). Daarbij komt dat super-resolutie microscopietechnieken de diffractielimiet doorbroken hebben en de haalbare resolutie met FM verbeterd hebben tot kleiner dan 20 nm. Desalniettemin, en inherent aan FM, zijn het enkel de gelabelde componenten die zichtbaar zijn en kan FM geen ultrastructurele informatie opleveren. Aan de andere kant, elektronenmicroscopie (EM) heeft de mogelijkheid om de ultrastructuur weer te geven met een resolutie op de nanometer schaal. Daarom is de afgelopen jaren correlatieve licht- en elektronenmicroscopie (CLEM), wat de complementaire informatie van FM en EM samenbrengt, in sterk toenemende mate in de belangstelling komen te staan. Normaal gesproken worden CLEM-onderzoeken sequentieel uitgevoerd door het monster te verplaatsten tussen twee losstaande microscopen, wat het proces zeer lastig maakt en daardoor het wijdverspreid gebruik van CLEM-toepassingen verhindert. Een oplossing wordt [hier] aangedragen in de vorm van geïntegreerde strategieën, waarbij een lichtmicroscoop zo goed als geheel wordt geïntegreerd in een EM. Ook hebben we recent een ontwerp voor een geïntegreerde microscoop getoond welke hoge resolutie FM toestaat in een Scanning EM (SEM), zonder in te leveren op de mogelijkheden van één van beide microscopen.

Deze dissertatie beoogt het potentieel van de geïntegreerde microscoop in kaart te brengen om spectraal opgeloste FM, gecombineerd met beeldopnames van levende cellen, samen te brengen met hoge resolutie EM met structurele informatie. De nieuwe mogelijkheden die de geïntroduceerd worden door de geïntegreerde microscoop worden ten eerste voor een gefixeerd en gedehydrateerd monster, typisch voor CLEM onderzoeken, getoond en bediscussieerd. Verder is CLEM op samples in gehydrateerde toestand gerealiseerd, en wordt een nieuwe methode gedemonstreerd, waarmee het mogelijk is om op een willekeurig moment SEM op levende cellen in vloeistof uit te voeren.

Hoofdstuk II. introduceert de methode van Simultane Correlatieve Licht en Elektronenmiscroscopie (SCLEM), wat een nieuwe aanpak is van CLEM, mogelijk gemaakt door de geïntegreerde microscoop. De methode is gebaseerd op de nieuwe optie om simultaan zowel hoge-resolutie licht- en elektronenmicroscopie uit te voeren op hetzelfde gedeelte van een monster. De methode maakt een snelle en accurate acquisitie van grote CLEM datasets mogelijk, en daarmee kwantitatief onderzoek van grote monsteroppervlakken. De correlatie van hoge-NA fluorescentiebeeldopnames met cellulaire ultrastructuren wordt gedemonstreerd voor fluorescent gelabelde hele cellen, als ook weefselsecties die gemerkt zijn voor zowel fluorescentie als EM. Het

geoptimaliseerde protocol voor SCLEM, welke er op gericht is om andere onderzoekers te ondersteunen bij het aanpassen van hun werkplan voor geïntegreerde CLEM, wordt gepresenteerd in *Hoofdstuk III*. Complete monsterpreparatieprotocollen worden beschreven voor gehele cellen met expressie van endogene fluoroforen, voor hele immuno-gelabelde cellen, en voor cellen en weefsels ingebed in hars, samen met de procedure voor het plaatsen van de geprepareerde monsters in de geïntegreerde microscoop. Tevens worden de benodigde stappen om een hoge nauwkeurigheid te waarborgen tussen de FM en SEM beelden grondig uitgelegd en gedemonstreerd. *Hoofdstuk IV*. beschrijft de verrijking van SCLEM met meerkleuren mogelijkheden. Simultane tweekleuren FM en SEM wordt gedemonstreerd aan de hand van beeldopnames van cellulaire secties van door het Equine Arteritis Virus (EAV) geïnfecteerde cellen, waarbij de expressie van GFP gekoppeld is aan het replicasegen van EAV en de nuclei/DNA van de geïnfecteerde cellen gelabeld zijn met Hoechst. Het hoofdstuk toont ook dat de methode voor FM-EM beeldregistratie ook gebruikt kan worden om chromatische afwijkingen te corrigeren tussen verscheidene FM kleurkanalen, wat cruciaal is als de fluorescentie-informatie gerelateerd wordt aan hoge resolutie SEM beelden. De beschreven methode wordt gedemonstreerd aan de hand van de registratie van tweekleuren fluorescentiebeelden en SEM beelden van paxilin en phospho-paxilin-gelabelde cellen en de plaatsing daarvan in een enkel coördinatenstelsel met hoge precisie.

Het overige deel van deze dissertatie concentreert zich op CLEM op monsters in vloeistof, ingebed in de geïntegreerde FM en SEM. *Hoofdstuk V*. behandelt de haalbare resolutie met SEM beeldregistratie van in vloeistof ondergedompelde nanodeeltje-biolabels in detail. Simulaties met de op Geant4 gebaseerde Monte Carlo methode worden één op één vergeleken met de experimentele resultaten voor nanodeeltjes welke zich direct onder SiN membranen van verschillende diktes bevinden. De bundelverbreding, het resultaat van de interactie van de elektronenbundel met het membraan, en het mechanisme welke het contrast vormt worden besproken en gekarakteriseerd. Ook wordt het maken van SCLEM beeldopnames, in vloeistof, van enkele epidermale groeifactor (EGF)-geconjugeerde quantum dots, aangehecht aan filopodia tijdens opname door de cel, beschreven. Voorts behandelt *Hoofdstuk VI*. de resolutie en het contrast voor de beeldregistratie van nanodeeltje-biolabels welke zich niet direct onder het membraan bevinden, maar op verschillende dieptes. Enkele eerste simulaties en experimentele resultaten worden getoond, die nu al laten zien dat zelfs onder deze omstandigheden de beeldregistratie van enkele nanodeelte-biolabels nog haalbaar is met redelijke resolutie.

Het ontwerp- en fabricageproces van de houder die gebruikt wordt voor CLEM op monsters in vloeistof wordt beschreven in *Hoofdstuk VII*. De houder kapselt monsters in vloeistof in in de vacuümkamer van de geïntegreerde microscoop en maakt simultane correlatieve microscopie mogelijk door middel van de vensters die de houder bevat, welke transparant zijn voor elektronen dan wel licht. Een gedetailleerde beschrijving wordt gegeven van het monsterpreparatieproces voor correlatieve beeldregistratie van gehele cellen, welke direct op het elektronen-transparante membraan gegroeid worden, wat nieuwe mogelijkheden oplevert om cellen in nagenoeg natuurlijke

omstandigheden te bestuderen. Tevens wordt de optie besproken om de houder verder door te ontwikkelen tot een microfluïdische reactor en worden experimenten getoond welke bewijzen dat het concept werkt, namelijk het eerst vullen van en vervolgens beelden registreren in de reactor. Als laatste beschrijft *Hoofdstuk VIII*. de nieuwe methode van On Demand EM (ODEM), welke de sterke kanten van FM beeldregistratie van levende cellen samenvoegt met hoge resolutie SEM. De cellulaire dynamica wordt bijgehouden in een vloeistof met FM op levende cellen, en instantane SEM beelden worden op een willekeurig moment genomen van bepaalde gebieden op bepaalde tijdstippen, gebaseerd op de FM observaties. ODEM wordt aangetoond door de beeldregistratie van de uptake en het retrograde transport van EGF-geconjugeerde quantum dots in fibroblasten. ODEM is veelbelovend voor het ontsluiten van geheel nieuwe perspectieven op de beeldregistratie van biologische dynamica door het samenvoegen van de mogelijkheden met FM beeldregistratie van levende cellen en de EM beeldregistratie van structuurinformatie met hoge resolutie.

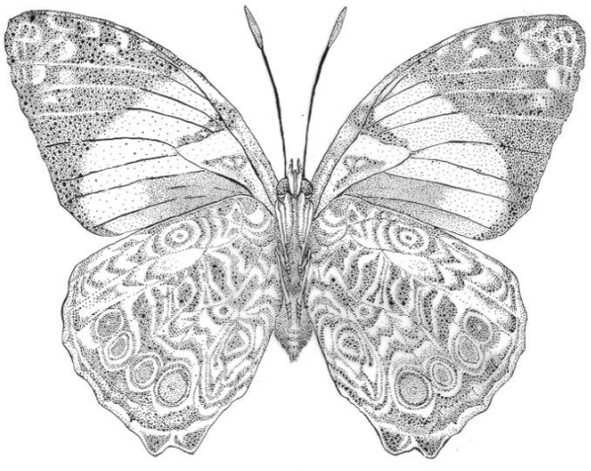

Publication List

THIS THESIS IS BASED ON THE FOLLOWING PUBLICATIONS:

- **N. Liv**, A. C. Zonnevylle, A. C. Narvaez, A. P. J. Effting, P. W. Voorneveld, M.S. Lucas, J. C. Hardwick, R. A. Wepf, P. Kruit, J. P. Hoogenboom. ***Simultaneous Correlative Scanning Electron and High-NA Fluorescence Microscopy***. PLoS ONE 01/2013; 8(2):e55707.
  (Chapter 2)

- C. J. Peddie, **N. Liv**, J. P. Hoogenboom, L. M. Collinson. ***Integrated light and scanning electron microscopy of GFP-expressing cells.*** Accepted for publication in the book Correlative Light and Electron Microscopy (Methods in Cell Biology, Volume 124)
  (Chapter 3)

- **N. Liv**, M.T. Haring, H.G.P. Peters, P. Kruit, J.P.Hoogenboom. ***Image Registration and Chromatic Distortion Correction in Multi-Color SCLEM.*** In preparation.
  (Chapter 4)

- **N. Liv**, I. Lazić, P. Kruit, J.P. Hoogenboom. ***Scanning electron microscopy of individual nanoparticle bio-markers in liquid.*** Ultramicroscopy; 10.1016/j.ultramic.2013.09.002
  (Chapter 5)

- **N. Liv**, A. C. Zonnevylle, A. P. J. Effting, D.S.B. van Oosten-Slingeland, P. Kruit, J. P. Hoogenboom. ***Preparation and Encapsulation of Whole Cells for in-situ Light and Scanning Electron Microscopy***. Submitted.
  (Chapter 7)

- **N. Liv**, D.S.B. van Oosten-Slingeland, J.P. Baudoin, P. Kruit, D. Piston, J.P.Hoogenboom. ***On-Demand Electron Microscopy of Samples in Liquid.*** Submitted.
  (Chapter 8)

OTHER PUBLICATIONS:

- P. W. Voorneveld, L. L. Kodach, R. J. Jacobs, **N. Liv**, A. C. Zonnevylle, J. P. Hoogenboom, I. Biemond, H. W. Verspaget, D.W. Hommes, K. de Rooij, C. van Noesel, H. Morreau, T. van Wezel, G. J. Offerhaus, G. R. van den Brink, M. P. Peppelenbosch, P. ten Dijke, & J. C. H. Hardwick. ***Loss of SMAD4 alters BMP signalling to promote colorectal cancer cell metastasis via activation of Rho and ROCK.*** Gastroenterology; 10.1053/j.gastro.2014.03.052.

- A. C. Narváez, I. G. C. Weppelman, R. J. Moerland, **N. Liv**, A. C. Zonnevylle, P. Kruit, J. P. Hoogenboom. ***Cathodoluminescence microscopy of nanostructures on glass substrates***. Optics Express 11/2013; 21(24):29968.

- A. C. Zonnevylle, R. F. C. van Tol, **N. Liv**, A. C. Narvaez, A. P. J. Effting, P. Kruit, J. P. Hoogenboom. ***Integration of a high-NA light microscope in a scanning electron microscope***. Journal of Microscopy 07/2013; 252(1), 58-70.

- M. T. Haring, **N. Liv**, A. C. Zonnevylle, A. C. Narvaez, P. Kruit, and J. P. Hoogenboom. ***Automated sub-5 nm Overlay Accuracy in Correlative Fluorescence and Electron Microscopy.*** In preparation.

- A. C. Narváez, **N. Liv**, I. G. C. Weppelman, A. C. Zonnevylle, P. Kruit, J. P. Hoogenboom. ***Cathodoluminescence microscopy of bio-conjugated quantum dots.*** In preparation.

PATENTS:

- J. P. Hoogenboom, P. Kruit, **N. Liv**, and A. C. Zonnevylle, ***Integrated Optical & Charged Particle Inspection Apparatus***. Patent number NLP193348A (granted, 2012), WO2013151421A8 (filed, 2013).

- *J.* .P. Hoogenboom, A.C. Narvaez, **N. Liv**, P. Kruit, ***Method for Focusing a Light Imaging Device on the Surface of a Sample.*** Patent number NLP192050A (pending).

- *J.* .P. Hoogenboom, **N. Liv**, P. Kruit, ***Method for One-Time Scanning Electron Microscopy Guided by in-situ Light Microscopy.*** Patent number NLP195269A (pending).

POPULAR SCIENCE JOURNALS:

- **N. Liv**, D.S.B. van Oosten-Slingeland, M.T. Haring, A. C. Zonnevylle, P. Kruit, J. P. Hoogenboom. ***Simultaneous correlative scanning electron and high-na fluorescence microscopy.*** Microscopy and Analysis; July 2013; pp.25.

- D.W. Morsink, A.C. Zonnevylle, D.S.B. van Oosten Slingeland, **N. Liv**, A.P.J. Effting, N. Liv, C.T.H. Heerkens, U. Staufer, P. Kruit, J.P. Hoogenboom. ***Design of a liquid flow cell for live cell observation in an integrated light and electron microscope***. NEVAC Blad; December 2013, 51/3; pp.6-9.

- J. P. Hoogenboom, **N. Liv**, A. C. Zonnevylle, P. Kruit***. Two Microscopes Integrated in One- Simultaneous Correlative Light and Electron Microscopy.*** G.I.T. Imaging & Microscopy; 2/2013; pp.30-32.

- A.C. Zonnevylle, R.F.C. van Tol, G.A. Schotte, C.A.N. Barends, A.C. Narvaez, **N. Liv**, P. Kruit, J. P. Hoogenboom***. Licht en elektronenmicroscopie geïntegreerd- "kleur geven aan de elektronenmicroscoop".*** NEVAC Blad; December 2012, 50/3; pp.7-13.

Acknowledgements

Coming for my PhD to the Netherlands was probably the most risky and luckily the most rewarding decision I have ever taken in my life. Perhaps, the best analogy for the last 5 years of my life would be to a rollercoaster ride. There were ups and downs during this period, it was challenging and very exciting. It felt like forever during this helter-skelter ride, but now when I look back, and I would be so eager to experience it again. A lot of people have contributed in different ways to my PhD and I would like to thank them all.

Firstly, I would like to express my gratitude to my promotor, Pieter. Thank you for your guidance and encouragement throughout these years. I have learned a lot from your experience and I consider myself really lucky for having this chance. You will always be a great example for me to follow. And Jacob. I am grateful for all the support, supervision, encouragement, all the ideas and also for the motivation you provided when I really needed. Thank you most importantly for the time you always kindly had for me.

CPO is one of the most pleasant groups I could actually imagine for doing a PhD. I would like to thank everyone who made me feel this way. Kees, thank you for always caring for us. I also learned a lot from your modest way of doing science. Frans, Ger, Cor, Wim, Han, Ruud, Vladimir, Carel and my dear Jan. I would like to thank you all, not only for the precise technical help you always provided, but also for being cheerful and always ready to help. Margaret, I thank you for everything, but mostly for always being there for me. You always said you are our Dutch stepmother, and you were right. Also Anjella, thank you for your sincerity and kindness. Bedankt allemaal voor de altijd fijne en gezellige samenwerking!

Angela, my compañero. You are the biggest present my PhD has provided me and your presence was a blessing throughout all these years. We shared a lot, almost everything possible. And I want you to know, you have the biggest share in the fact that I remember my PhD with a strong smile. Sangeetha, you joined us with a perfect timing and provided me a fresh point of view. And Gerward, thanks for all the pleasant times and nice discussions about almost anything. I always felt myself the luckiest for sharing my office with the three of you.

Everyone in CPO (Charged Particle Optics) felt more like friends than colleagues to me, since the very first day of my PhD. Ivan and Vincenzo, thank you guys for welcoming me to the group. You

two, together with Angela, made me feel at home starting from the very first week. I was also kindly welcomed to the group by Ben, Ali, David, and Willem. All the others, with whom I have met within CPO: Chris, Sander, Andries, Yan Ren, Leon, Thomas, Diederik, Marijke, Takashi, Minoru, Martin, Vidar, and Robert. Thanks for the friendly environment you have all contributed! Robert, I want to thank you one more time, not only for the translations you made for the thesis, but also for joining the group with such a great timing; when I needed your kind friendship, inspiration, and cheering up. I would also especially like to acknowledge Daan and Martijn here. Thank you guys not only for the great work, but also for accompanying me during the weekend, late night and Christmas experiments and for the fun during these occasions.

I have met a lot of great people in the Netherlands, and I would like to thank them all for the great time I had in the last 5 years: Ting, Nazli, Yunus, Narin, Ozge, Nihal, Burak, Vanya, Gozde, Sinan, Sertac, Engin, Ozgur, Ilhan, Merve, Jason, Esra, Olgu, Alper. Sevinc… Special words go to some of them. Nesli, you are my latest sister. You have been one of the best friends someone can actually hope for. Ahmet Koray and Anil, I really enjoyed spending the short breaks with you. Mine and Walter, although we met later, I feel there is a lot to be shared, and I will do my best to be a good aunty. Aleks and Maup, you are the smell of lilies in my life; relaxing and joyful. Nihal and Emre, your presence in the Netherlands have been more comforting for me than you can simply imagine, iyi ki varsiniz! And Berk, I would like you to know that every "simple" day we spent together, drinking, chatting, cycling, saving the world, was a really special happening for me. I would also like to thank my extended family and all my friends in Turkey for showing their support despite the distance in between. It is delightful to know all of you stand by me regardless of the circumstances.

Caner, my husband, my love, my best friend, my light house, and the only one to share my crowded loneliness. I can't even list the things that I want to thank you for. Every single day of life is a big pleasure with you by my side, and there is no current in this river we can't ride.

Finally, annecim! You have given me the greatest gifts of all; your endless love, a great education, and the freedom of choice. I would not be who I am and would never be where I stand today without you. Seni çok seviyorum!

Thank you all again.

NaLaN

About the Author

Nalan Liv was born in Uzunköprü, Turkey, on May 1, 1985. After receiving her high school diploma from Darüşşafaka High School in Istanbul in 2003, she studied Biological Sciences and Bioengineering at Sabanci University, where she received her BSc. degree in 2007 and her MSc. degree in 2009. Afterwards, she moved to the Netherlands and started her PhD studies in the Charged Particle Optics group at Delft University of Technology, under the supervision of Prof.dr.ir. Pieter Kruit and Dr.ir. Jacob Hoogenboom. The results of her PhD research are presented in this thesis. Her research interests include light & electron microscopy techniques and their applications in cell biology and structural biology. As of July 2014, she joined the group of Prof.dr. Judith Klumperman working as a post-doctoral researcher at the University Medical Center Utrecht.